EXPERIMENTAL STUDY ON THE CONTINUOUS WAVE LASER TREATMENT APPLIED TO CORRODED STEEL STRUCTURES

王, 啓迪

EXPERIMENTAL STUDY ON THE CONTINUOUS WAVE LASER TREATMENT APPLIED TO CORRODED STEEL STRUCTURES

Qidi WANG

EXPERIMENTAL STUDY ON THE CONTINUOUS WAVE LASER TREATMENT APPLIED TO CORRODED STEEL STRUCTURES

A Thesis Submitted

In Partial Fulfillment of the Requirements

For the Degree of

Doctor of Engineering

By

Qidi WANG

to the

DEPARTMENT OF URBAN AND ENVIRONMENTAL ENGINEERING

GRADUATE SCHOOL OF ENGINEERING

KYUSHU UNIVERSITY

Fukuoka, Japan

March, 2023

DEPARTMENT OF URBAN AND ENVIRONMENTAL ENGINEERING

GRADUATE SCHOOL OF ENGINEERING

KYUSHU UNIVERSITY

Fukuoka, Japan

CERTIFICATE

The undersigned hereby certify that they have read and recommended to the Graduate School of Engineering for the acceptance of this thesis entitled, "***Experimental Study on the Continuous Wave Laser Treatment Applied to Corroded Steel Structures***" by **Qidi WANG** in partial fulfillment of the requirements for the degree of **Doctor of Engineering**.

Dated: March, 2023

Thesis Supervisor:

_____

Prof. Shigenobu Kainuma, Dr. Eng.

Examining Committee:

_____

Prof. Hidenori Hamada, Dr. Eng.

_____

Prof. Kazuhisa Fujita, Dr. Eng.

ABSTRACT

Surface treatment is the necessary and key process in corrosion maintenance of steel structures before painting, and sufficient removal of rust and salt is important to ensure maintenance and coating quality. The traditional surface treatment flow was divided by two steps, pre-treatment with hand tools, power tools as the first step, and post-treatment by abrasive blasting as the final step. As the degree of corrosion increases, rust and salt removal will be much less effective in cleaning. Especially in cases of severe corrosion pits, the post-treatment will be repeated several times until the surface is visually cleaned. This undoubtedly increased the investment of manpower and financial resources, as well as prolonged the construction schedule. Even this visually cleaned surface treatment is insufficient, which will leave undetectable rust and salt embedded in the surface, and re-corrosion will occur under the coating for a period of time after painting. This not only reduces the protective performance of the coating, shortens the maintenance cycle and greatly improves the cost, but also reduces the safety and reliability of the structure.

To obtain a sufficiently cleaned surface and carry out effective coating maintenance engineering, it is crucial to select a suitable flow of surface treatment and then painting for steel components with different corrosion degrees. A new surface treatment flow is presented in this dissertation, which innovatively applies continuous wave laser (CWL) treatment technology to corrosion cleaning. CWL treatment as the intermediate step between pre-treatment and post-treatment, which with high energy density can help efficiently remove the rust and salt that are difficult to remove in corrosion pits. On this basis, not only can raise the efficiency of the entire surface treatment process and improve the treatment effect of abrasive blasting, but also reduce the construction period and cost. Even solved the problems of structural damage caused by excessive surface treatment and the corrosion caused by inadequate surface treatment. Which is especially noteworthy for the treatment of severely corroded steel components.

Up to now, research about corrosion cleaning technology mainly focus on general corrosion, and there are few reports on the treatment of severely corroded steel components with more than 20 years of service. Guidelines for the treatment of severely corroded components were still incomplete, and the quantitative criteria for salt removal were still deficient. In addition, corrosion cleaning

research also focuses on steel plates but ignores the connecting members, especially the bolts, which are vulnerable to corrosion. To solve the above problems, this dissertation investigated and summarized various degrees of corrosion from common steel and weathering steel specimens and bridge components, summed up the shape of corrosion pits and surface treatment difficulties. The effect and necessity of the new surface treatment flow were compared by experimental analysis, and the cleaning attempts were made for steel specimens with different corrosion degrees. In order to evaluate the salt removal effect directly, a time-lapse based test method called turning time test was proposed, which could evaluate the salt removal effect through the frequency and area rate of re-corrosion in corrosion pits. The turning time test also helped proved a quantitative evaluation method based on photometric analysis for 3 kW CWL surface treatment on weathering steel. Based on this quantitative evaluation method, a proper 3kW CWL cleaning process for weathering steel was proposed and suggested. Besides, CWL treatment was used in corrosion cleaning for salt removal for the first time in engineering. Through an engineering case attempt, the possibility of CWL treatment in humid and underwater environments was also considered. Verified the help of water vapor explosive effect on salt removal and the feasibility of CWL surface treatment in humid environments. In addition, it is the first time to use CWL surface treatment to clean high-strength bolts, and the axial force loss due to the thermal effects of CWL is also considered.

The results show that the corrosion pits have a conical spatial shape, and the severe corrosion accompanied by the appearance of secondary corrosion pits is the difficulty of surface treatment. The cleaning test of artificial corrosion pit specimens with different corrosion degrees proves that abrasive blasting is mainly suitable for general corrosion cleaning. In the case of severe corrosion, the treatment flow of power tool pre-treatment and then CWL surface treatment can efficiently clean rust and salt from severely corroded surfaces and provide a guarantee for high-quality abrasive blasting and coating. The turning time test revealed the effect of the hybrid methods on rust and salt removal and helped verify the reliability of the photometric analysis method based on CIE LAB color space for quantitative evaluation of the cleanliness of 3 kW CWL. The applicability of CWL treatment severely corroded steel components is proved by engineering cases, that verified the better salt removal effect of CWL under humid conditions. This provides the possibility for corrosion cleaning in a humid environment. In addition, laser treatment of the high-strength bolts was

attempted to ensure that the axial force loss of the bolts was within the allowable range after the 3 kW CWL treatment.

Keywords: steel structure, corrosion, surface treatment technology, continuous wave laser, photometric analysis, high-strength bolts

Highlights:

1. It was investigated and generalized the corrosion status of coated common steel bridges and uncoated weathering steel bridges used for more than 20 years and summarized the three-dimensional shape of severe corrosion pits.
2. The 3 kW CWL treated severe corrosion surface of weathering steel can obtain a turning time of more than one week in high temperature and humidity environments, confirming the effectiveness of laser salt removal.
3. It was proposed a quantitative evaluation method for 3 kW CWL treatment on weathering steel based on CIE LAB color space and photometric analysis.
4. It was verified the effect of hand-held 3 kW CWL treatment severely corroded steel components by an engineering case and confirmed the better salt removal effect of water supplied CWL treatment by SEM/EDX.
5. It was implemented the 3 kW CWL treatment on high-strength bolt and verified the feasibility of laser cleaning on bolts, ensured the axial force loss during the laser treatment process within an acceptable range by real-time monitoring and numerical simulation.

GRAPHICAL ABSTRACT

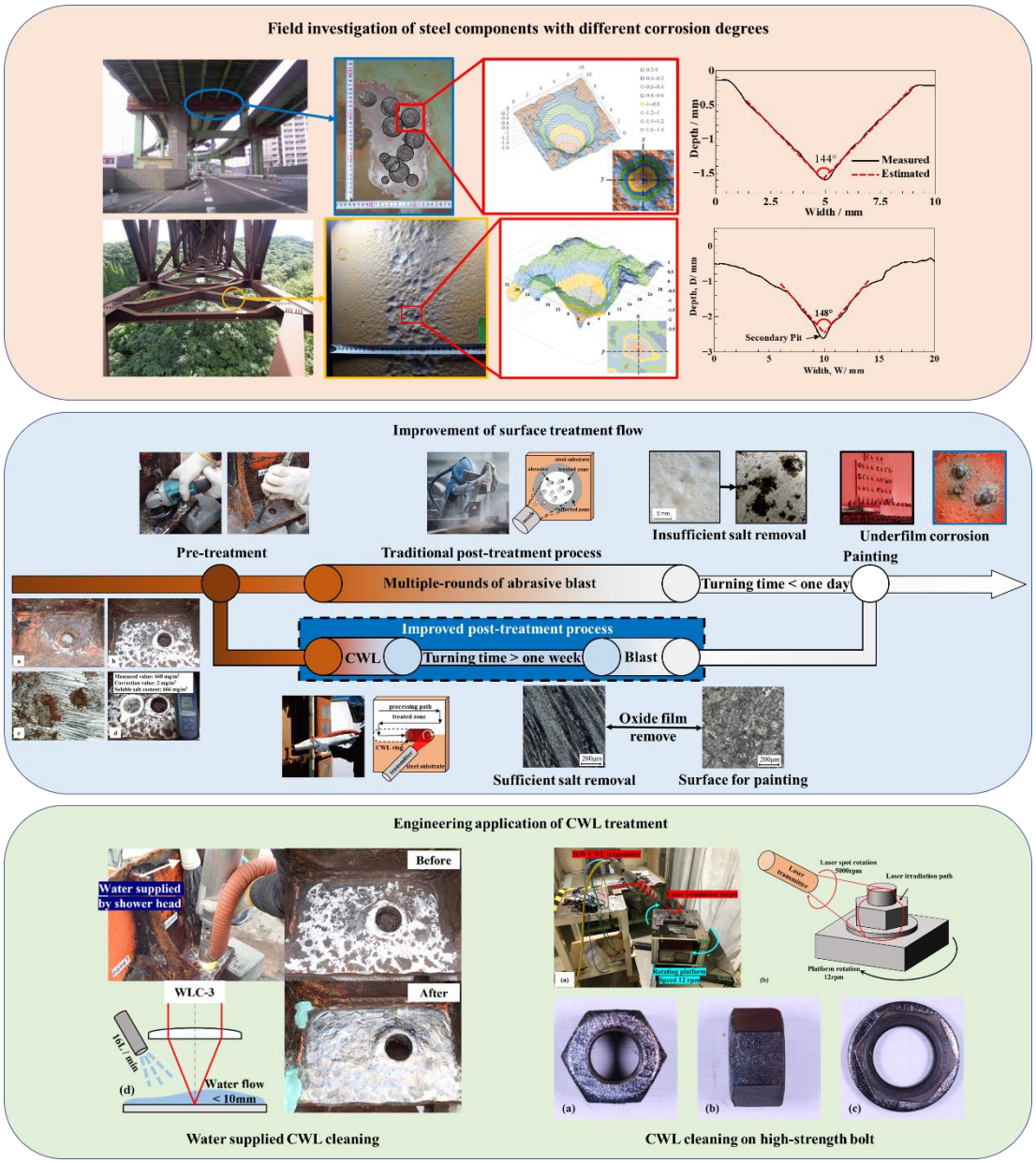

TABLE OF CONTENTS

ABSTRACT ..... **i**

GRAPHICAL ABSTRACT ..... **iv**

TABLE OF CONTENTS ..... **v**

LIST OF TABLES ..... **ix**

LIST OF FIGURES ..... **x**

CHAPTER 1 INTRODUCTION **1**

1.1 Research background 1

1.2 Research Objectives and Scope 3

1.3 Literature Review 5

1.3.1 Development of pre-treatment 5

1.3.2 Development of post-treatment 6

1.3.3 Development of high-strength bolt cleaning 9

1.4 Organization and outline 10

CHAPTER 2 INVESTIGATION OF THE CHARACTERISTICS AND RELATIONSHIP BETWEEN RUST LAYER AND CORROSION PIT **14**

2.1 Introduction 14

2.2 Investigation and analysis method of corrosion pits 15

2.2.1 Atmosphere Exposure Test 15

2.2.2 Measurement of Corroded Component 17

2.2.3 Analysis of Rust Layer and Corrosion Pits 18

2.3 Relationship and characteristics of corrosion pit and rust layer 19

2.3.1 Relationship between rust thickness and corrosion pit depth 19

2.3.2 Characteristics of rust layer and corrosion pits 22
2.4 Summary 25

CHAPTER 3 CLEANLINESS ANALYSIS OF CORRODED WEATHERING STEEL BY DIFFERENT SURFACE TREATMENT METHODS 28

3.1 Introduction 28
3.2 Preparation of corroded specimens with artificial pit 29
3.2.1 Specimens preparation 29
3.2.2 Accelerating corrosion 30
3.2.3 Pre-treatment and post-treatment 30
3.3 Surface characteristics of corroded specimens after surface treatment 35
3.3.1 Surface characteristics before and after pre-treatment 35
3.3.2 Surface characteristics after abrasive blasting surface treatment 41
3.3.3 Surface characteristics after laser surface treatment 42
3.4 Turning time test 44
3.4.1 Turning time test of blasted specimens 46
3.4.2 Turning time test of laser ablated specimens 51
3.5 Summary 55

CHAPTER 4 QUANTITATIVE EVALUATION OF SURFACE CLEANLINESS OF WEATHERING STEEL TREATED BY CONTINUOUS WAVE LASER 57

4.1 Introduction 57
4.2 Photometric Analysis method 58
4.3 Photographic analysis with CIE L*A*B* color space 59
4.3.1 Luminance and color 59
4.3.2 Comparison of the color difference 63
4.4 CWL surface treatment procedure 65

4.5 Summary 67

CHAPTER 5 SURFACE TREATMENT AND CLEANLINESS EVALUATION OF SEVERELY CORRODED STEEL COMPONENTS IN ENGINEERING 68

5.1 Introduction 68

5.2 Experimental 69

5.2.1 Samples 69

5.2.2 Abrasive blast cleaning 70

5.2.3 Laser cleaning 71

5.2.4 Observation and characterization 73

5.3 Macroscopic and microscopic characteristics of surface after cleaning 73

5.3.1 Processing efficiency 73

5.3.2 Macroscopic observation 75

5.3.3 Microscopic observation 82

5.3.4 Observation of heat-affected layer after laser cleaning 88

5.4 Mechanism analysis of surface cleaning 90

5.5 Summary 94

CHAPTER 6 CWL SURFACE CLEANING OF HIGH STRENGTH BOLTS: ANALYSIS OF BOLT AXIAL FORCE LOSS 96

6.1 Introduction 96

6.2 Preparation of high force bolt specimens 97

6.2.1 Specimen design 97

6.2.2 Specimen assembly 99

6.2.3 Laser Surface Treatment 99

6.2.4 Finite-element temperature simulation 101

6.3 Analysis and mechanism of axial force change during CWL cleaning 102

6.3.1 Axial force loss related to continuous irradiation of laser 103

6.3.2 Axial force loss related to multiple rounds irradiation of laser 105
6.3.3 Evaluation of the axial force loss ratio as a result of the laser irradiation..... 107
6.3.4 Evaluation of the temperature change during laser irradiation 111
6.3.5 Mechanism of the axial force change during laser irradiation 113
6.4 Summary 115

CHAPTER 7 CONCLUSIONS AND FUTURE WORKS 117
7.1 Summary and conclusions 117
7.2 Recommendations for future work..... 119

REFERENCES..... 121

ACKNOWLEDGEMENT..... 136

LIST OF TABLES

Table 2-1 Chemical compositions 15

Table 2-2 Atmospheric environment at exposure sites 16

Table 3-1 Chemical composition of the carbon steel plate 29

Table 3-2 Composition of garnet abrasive 32

Table 3-3 Laser processing parameters 32

Table 3-4 Composition ratio of corrosion products 40

Table 3-5 Calculated protective ability index 40

Table 5-1 Composition of garnet abrasive 70

Table 5-2 Laser processing parameters 71

Table 5-3 Surface roughness values of blasted surface of garnet 76

Table 5-4 Surface roughness of laser-irradiated surface 79

Table 5-5 Characteristics of cleaned surface 91

Table 6-1 Laser treatment specimens' irradiation duration 98

Table 6-2 CWL parameters 100

Table 6-3 Materials properties of FE model 101

Table 6-4 Initial strain and axial force of measured bolts 102

Table 6-5 Changes in axial force after continuous irradiation 103

Table 6-6 Changes in axial force after multiple rounds of irradiation 106

Table 6-7 Changes in axial force after two rounds of irradiation 108

LIST OF FIGURES

Figure 1-1 Flowchart of the dissertation 13

Figure 2-1 Exposure sites in (a) Kyushu University, (b) Momochi, (c) University of the Ryukyus and (d) Kyoda 16

Figure 2-2 Severe corrosion pits on common steel beam 17

Figure 2-3 Location of the severely corroded weathering steel bridge 18

Figure 2-4 Severe corrosion pits on weathering steel flange 18

Figure 2-5 Atmospheric exposure specimen and measure points 18

Figure 2-6 Thickness of rust layer and corrosion depth 21

Figure 2-7 Relationship between rust layer thickness and corrosion depth 22

Figure 2-8 Corrosion bud and pits 23

Figure 2-9 Characteristics of corrosion pit 26

Figure 2-10 Relationship between corrosion pit depth and cone angle 27

Figure 3-1 Specimens with artificial corrosion pits: (a) Schematic of manufacturing process and 29

Figure 3-2 Accelerated corrosion test data from Okinawa in the summer (August 16-30, 2019): (a) daily temperature change, (b) daily humidity change, (c) daily dew point change, and (d) wet and dry cycle used for accelerated corrosion 33

Figure 3-3 Schematic of abrasive blasting 34

Figure 3-4 Schematic of a rotating CWL: (a) formation of a laser ring by rotating prism refraction, (b) sweep path of laser ring, and (c) overlap rate of laser ring 34

Figure 3-5 Macroscopic characteristics of the surface of three specimens whose pits were exposed to salt deposits conditions of (a)10 mg/m2, (b)100 mg/m2, and (c)1000 mg/m2 37

Figure 3-6 Macroscopic characteristics of the surface of three different corrosion grades specimens after pre-treatment with salt deposit amounts of (a)10 mg/m^2, (b)100 mg/m^2, and (c)1000 mg/m^2 38

Figure 3-7 3D contour of severely corroded specimen (a) before pre-treatment and after pre-treatment with a (b) steel brush, (c) cup wire, and (D) diamond disc 39

Figure 3-8 Comparison of the rust layer profile before and after pre-treatment of three different

corrosion degree with salt deposit amounts of (a)10 mg/m^2, (b)100 mg/m^2, and (c)1000 mg/m^2 ..39
Figure 3-9 Corrosion product powders' (a) XRD spectrum and (b) the ratio of product composition 41
Figure 3-10 Macroscopic characteristics of the surface after abrasive blast treatment of (a, b) 1st round with garnet blasting, (c, d) 2nd round with alumina blasting, and (e–h) 3rd round with alumina blasting.....43
Figure 3-11 Macroscopic characteristics of the surface after laser treatment, with salt deposited amount of (a, b)10 mg/m2, (c, d)100 mg/m2, and (e–h)1000 mg/m2.....43
Figure 3-12 Turning time test specimens of (a) general corrosion and (b) severe corrosion 48
Figure 3-13 Turning time test of severely corroded specimens after different abrasive blast treatment 49
Figure 3-14 Ultrasonic salt spray device and the characteristic of surface adhesion salt 49
Figure 3-15 Schematic representation of the re-rusted area extracted using ImageJ 50
Figure 3-16 The ratio of the re-rusted area to the total area in the turning time test.....51
Figure 3-17 Macroscopic characteristics of the laser-cleaned surface of a specimen subjected to salt deposit amounts of (a) 10 mg/m^2 and (b) 100 mg/m^2 after the turning time test 53
Figure 3-18 Macroscopic characteristics of the laser-cleaned surface of severely corroded specimen after the turning time test 54
Figure 3-19 Occurrence rate of artificial pits re-corrosion on the surface of different treatment conditions.....55
Figure 4-1 Photograph conditions of an (a) indoor environment with low natural light, (b) device settings (c), and the pickup position of the color information.....58
Figure 4-2 Variation diagram of color information at different surface treatment stages 60
Figure 4-3 Color information of the surface in the pre-treatment stage: (a) a*b* plane, (b) and (c) L*C* plane.....61
Figure 4-4 Color information of laser treatment surface: (a) a^*b^* plane and L^*C^* plane of (b)100 mg/m^2, and (c) 1000 mg/m^2 62
Figure 4-5 Surface color difference change of laser treatment with different benchmarks: (a) standard surface and (b) surface after pre-treatment.....64

Figure 4-6 Flow chart of CWL surface treatment procedure 66
Figure 5-1 Location and surface conditions of severely corroded steel member: (a) Location of rock shed, (b) corroded columns of rock shed, (c) foot of corroded columns, (d) surface treatment target, and (e) used power tools with diamond grinding disc. 69
Figure 5-2 Garnet particle size distribution.....70
Figure 5-3 Surface conditions of severely corroded steel member treated via laser cleaning: (a) DLC, (b) WLC-1 of drench method, (c) WLC-2 of soak method, and (d) WLC-3 of rinse method. 72
Figure 5-4 Specimens of laser-treated surfaces (a) cut by hole saw and (d) surface condition before transportation. 72
Figure 5-5 Schematic illustration of rotating CWL treatment.....75
Figure 5-6 Morphologies of target surface: (a) Before cleaning and (b) after pretreatment; (c) local morphology after pretreatment; (d) soluble salt content after pretreatment.....76
Figure 5-7 OM images showing blasted surface of garnet.....77
Figure 5-8 Surface and cross-section profile of blasted surface of garnet. 77
Figure 5-9 Surface morphologies of (a) DLC, (b) WLC-1, (c) WLC-2, and (d) WLC-3 specimens. 80
Figure 5-10 Surface profile of laser-treated surfaces. 81
Figure 5-11 Cross-section profile of laser-treated specimens. 81
Figure 5-12 SEM–EDX micrographs showing pretreated surface of diamond disc power tool. 82
Figure 5-13 OM and SEM–EDX images showing cross-section of pretreated sample. 82
Figure 5-14 SEM–EDX micrographs showing blasted surface of garnet. 83
Figure 5-15 SEM–EDX images showing blasted surface of garnet.....84
Figure 5-16 SEM–EDX micrographs of DLC. 85
Figure 5-17 SEM–EDX micrographs of WLC-1. 86
Figure 5-18 SEM–EDX micrographs of WLC-2. 86
Figure 5-19 SEM–EDX micrographs of WLC-3. 86
Figure 5-20 OM and SEM–EDX images showing cross section of laser-cleaned sample.....88
Figure 5-21 Thickness of MZ and HAZ on laser-cleaned specimens: (a) DLC-1, (b) WLC-1, (c) WLC-2, and (d) WLC-3 specimens. 89

Figure 5-22 Mechanism of laser surface cleaning with water supply. 94
Figure 6-1 (a) High-strength bolt with strain gage and (b) dimensions of the friction connection specimen 98
Figure 6-2 Schematic diagram of rotating CWL transmitter.....100
Figure 6-3 Laser transmitter and rotating platform of (a) setting of laser treatment device and (b) schematic diagram of laser cleaning on nut side.....100
Figure 6-4 FE model of friction-type bolt components.....102
Figure 6-5 Time-dependent change in bolt axial force during laser processing of (a)15s in specimen S1, (b) 15 s in specimen S2, (c) 15 s in specimen S3, (d) 30 s in specimen S4, (e) 45 s in specimen S5 and (f) 1 min in specimen S6 105
Figure 6-6 Time-dependent change in the axial force during four rounds of 15 s irradiation.....106
Figure 6-7 Time dependence of axial force during two rounds of irradiation.....108
Figure 6-8 Relationship between the axial force and irradiation duration of (a) continuous irradiation, (b) four rounds of 15 s irradiation, and (c) two-round irradiation with first 15 s irradiation followed by additional irradiation for 15 s, 30 s and 45 s 110
Figure 6-9 Surface after laser irradiation of (a, b) top and side surface of nut and (c)top surface of washer 112
Figure 6-10 Temperature distribution during laser irradiation at (a) the position of the thermocouple and (b) center axial and column surface of the bolt 113
Figure 6-11 Schematic representation of the three stages of a bolt during laser cleaning 115

INTRODUCTION

1.1 Research background

Carbon steel material is widely used in a structure such as bridge, building and tower. In a highly corrosive atmospheric environments, steel members are often affected by corrosion problems, particularly in marine environments, as well as painted steel and weathering steel[1–4]. Without protection and timely maintenance, the corroded components will fail in a few years and destroy the structure. Therefore, it is necessary to carry out regular and timely maintenance of steel components. The global cost of corrosion is estimated to be in the trillions of dollars a year, 3% to 4% of global GDP[1,5]. The engineering structures can be safe and for long-term use to achieve economic benefits. Finding a suitable, economical, efficient, and environmentally friendly steel structure maintenance method is necessary.

Currently, the most effective corrosion protection strategy is still the coating process[6–8]. For existing structures, corrosion cleaning, maintenance, reinforcement, and re-painting are the most economical methods to extend the structural life. Generally speaking, surface treatment is the first step necessary for corrosion cleaning and maintenance. Surface treatment should make the rust layer completely removed, does not contain residual contaminates and salt, and the surface characteristics which is suitable for painting[9,10]. On this basis, painting operation can ensure long time protection performance. General surface treatment is divided into two steps, pre-treatment and post-treatment. The pre-treatment is an incomplete cleaning that removes the rust layer, which is easy to peel off using hand tools and power tools. The pre-treated surface is generally not directly usable for painting maintenance operations. After pre-treatment, the target surface still remains a lot of rust layer on the surface, which is usually closely integrated with the steel substrate and difficult to remove. These rust layer also contains a large amount of salt[11–13]. A strong surface treatment method must be carried out to achieve the ideal coating benchmark. The most common method is abrasive blasting[9,10,14]. As a high-efficiency surface treatment technology, abrasive blasting can clean a large area of corroded steel surface in a short time. Abrasives are accelerated by compressed air and

high-pressure water flow to impact the target surface at subsonic speed, extrude and cut the rust layer or even the substrate surface, and achieve the effect of rust removal and surface configuration. However, surface treatment still faces many problems. The stubborn and thick rust layer is the difficulty of surface cleaning, especially in cleaning severely corroded steel components. Deep corrosion pits usually accompany the position of severe corrosion. The pits are accompanied by secondary corrosion, where the residual rust remains after repeated cleaning[5]. In addition, even if the surface is cleaned to a visually clean level, re-corrosion still happens under the coating after painting[15]. indetectable rust, abrasive and salt residue lead to re-corrosion, which is a major cause of premature failure of the coating[16]. To solve the problem of incomplete cleaning, multiple rounds of repeated cleaning will inevitably result in longer cycles and higher costs. Besides rust removal, salt removal has become one of the most important goals in developing surface cleaning technologies, especially for the surface cleaning of the high salt environment and severely corroded steel components. To improve the effect of salt removal, wet abrasive blasting technology and abrasive water jet technology have been proposed to seek the way of water and abrasive work together, while rust removal and cleaning the soluble salt achieved good results[17,18]. However, in the process of rust removal, the secondary corrosion in the corrosion pits is often difficult to clean completely. The abrasive is sprayed at an angle to the target surface. Affected by the pit's shape, part of the surface will be obscured to form a shadow area. The rust hidden in these areas is often difficult to clean. In addition, the surface is affected by impact deformation. The rust and salt are buried in steel substrate, which is difficult to be distinguished by the naked eye. All these are the reasons for the re-corrosion and the corrosion under the coating. This situation is very common in severely corroded steel components.

Laser surface cleaning technology based on ablative mechanism has been proposed to solve this problem to clean severely corroded steel components[19–21]. In the past few decades, pulsed laser (PL) and continuous wave laser (CWL) have significantly developed. In particular, PL has been widely used in cultural relic cleaning, microscopic cleaning, paint removal and other industrial conditions[22–26]. As a cleaning technology, the PL can instantaneously excite a laser beam with ultra-high energy density, which is sufficient to cause surface impurities to vibrate, ablate, evaporate, and ionize, achieving the effect of action[19]. However, there are still some shortcomings in the

application of PL. For civil engineering structures, limited by the size of equipment, output power, and other influences, PL cleaning hundreds of micron thickness of the rust layer appears to be inadequate, although it has the ability to remove rust, in a short time can only remove tens of microns of rust layer in large structure rust removal application is still insufficient. CWL has developed rapidly in recent years[27,28]. High-power emission equipment has been developed, enabling CWL to continuously and stably form thermal energy output continuously and stably. The laser beam forms an instantaneous high temperature enough to ablate the rust layer or even melt metal materials on the target surface. This capability allows the CWL to remove a thicker layer of rust in the same amount of time[29,30]. Because of the precision of the laser, the CWL beam can accurately clean any part of the target surface and can melt the substrate to smooth the target surface, which is not abrasive blasting technology can do[31]. For severely corroded steel components, especially those with secondary corrosion, CWL rust removal will be a suitable alternative. There is still a lack of systematic experiments for this new technology to verify the scope of CWL cleaning. Lack of evaluation criteria to evaluate the degree of laser cleaning and no engineering application as a reference. Therefore, the research on laser surface treatment is of great significance. In addition, laser cleaning technology is suitable for local efficient cleaning methods, but it also can be applied to the cleaning and maintenance of narrow areas, such as complex joints and bolts cleaning. During the cleaning process, if these parts are not maintained, the overall safety of the structure will be threatened. The current research on the maintenance of these parts is also blank and needs to be solved urgently.

1.2 Research Objectives and Scope

In this study, we expect to find suitable cleaning methods for steel members with different corrosion degrees through the combination of different pre-treatment methods and post-treatment methods. We hope to propose a new surface treatment flow to solve the problem of incomplete corrosion cleaning by innovatively using CWL treatment for rust and salt removal between pre-treatment and abrasive-blasting post-treatment. The aim is to reduce the time of the surface post-treatment process, improve the rust removal, especially the salt removal effect, and obtain a surface

suitable for painting. At the same time, we expect to get the range of CWL cleaning of rust layer through experiments. Then put forward quantitative evaluation criteria and apply CWL cleaning treatment to practical projects. In addition to rust removal, laser treatment of high strength bolt joints is also considered in this study. For the sake of safety, the influence of thermal effect on the axial force of high-strength bolts during laser cleaning is studied and analyzed, and the suggestion of using CWL to clean bolts is put forward.

The main objectives of the dissertation are as follows:

(1) Summarize the corrosion problems in engineering and clarify the corrosion location and the corresponding corrosion grade. In addition, the morphology of the corrosion pit cannot be ignored. The geometric shape of the corrosion pit will have a direct impact on the surface treatment. The research data are obtained through atmospheric exposure test and field investigation, which includes general corrosion within four years, corrosion of coated ordinary steel, and weathering steel with a service life of more than 20 years. The results of the survey will help in the evaluation of corrosion grade and the preparation of experimental materials.

(2) Make corrosion test specimens with artificial corrosion pits for quantitative research and discuss the range of processing capacity of various pre-and post-treatments and the applicability of the different surface treatment flow. It is expected that propose an evaluation method which can be easily implemented in the engineering field. And using this method, obtain the cleanliness evaluation conclusion of different surface treatment flow for different corrosion degree specimens.

(3) Propose real-time evaluation methods and standards suitable for engineering, especially for CWL cleaning technology. Immediate assessment allows for quick determination of cleanliness and quick planning for re-cleaning, which can shorten construction time and improve construction quality. Image analysis technology is proposed as a technical means of quantitative evaluation to address the problem of the lack of standard laser cleaning evaluation.

(4) Discuss the possibility and feasibility of CWL treatment in engineering by case analysis. Verify the salt removal effect of CWL by scientific analysis. Considering the influence of humid environment, design test and reveal the salt removal effect of CWL treatment with water supply. For high-strength bolted connection members, test the axial force loss during treatment and the CWL irradiation duration safety range.

1.3 Literature Review

1.3.1 Development of pre-treatment

Pre-treatment is a kind of in-completed cleaning. Including the type of physical, chemical and electrochemical treatment.

Chemical surface treatment is a commonly used method in rust removal[32–34]. Due to the serious environmental impact of acidic and alkaline solutions, pickling is often used in industrial equipment, boilers and metal parts, and in civil engineering structures it is mainly used to clean thin plates[35]. Chemical cleaning has limited effectiveness and requires sufficient time to dissolve oxides and oil. However, if the time is not properly controlled, even if the corrosion inhibitor is added, the steel components will inevitably be excessively corroded[36,37]. For civil engineering steel structure, chemical residue after chemical cleaning in the narrow part and gap, will cause hidden dangers to the structure. Although the research on pickling is still going on, the main material is stainless steel, and the research is mainly focused on the development of corrosion inhibitors[38]. Because chemical methods are not commonly used in civil engineering, they will not be discussed in this study.

Electrochemical cleaning is a new pre-treatment method. Its mechanism is to use the applied current to make rust layer reduction reaction and then remove the rust layer, to achieve the effect of rust layer volume shrinkage and fall off[34,39]. Using this method, Iio applied a current of 1 V to the surface of severely corroded weathering steel for 12 hours and successfully stripped the rust layer from the corrosion pit[40]. This method can specifically remove the rust layer inside the corrosion pit, and it will be a suitable pretreatment method for severe corrosion in the future. However, in view of the current immature research and the lack of engineering application as a guide, this method will not be discussed in this study.

The mechanism of physical pre-treatment is removing the weak adhesion of the coating and rust layer by tapping, abrasion, and scraping principle of pashing and peeling of pre-treatment tools[41,42]. This is efficient and practical at the beginning of the cleaning project. Still, as the loose layer of rust flakes off, it will be inefficient to continue with the pre-treatment cleaning. The

underlying layer of rust is often hard and tight, and the secondary corrosion pits also limit the tools' efficiency. Pre-treatment can be used by various tools, corresponding to different working conditions, such as narrow parts, corrosion pits, etc. But due to the tool operation's complexity, the pre-treatment is a contact processing method, so the workspace is greatly limited. Physical pre-treatment has not developed much in the past decades as an artificial-dominated incomplete cleaning method. One of the reasons is that the commonly used tools are sufficient to meet the specification requirements. On the other hand, the development of tools has focused more on ergonomic improvements, with little reported improvement in functional aspects. Existing standard power and hand tools specifications are usually referred to as ISO 8501-1 (St 2 and St 3) and SSPC (SP-2 and SP-3). Both define treatment grades based on text and photographs, so the assessment method is often subjective. In these two specifications, the purpose of hand tools and power tools is only to remove the loosely attached oxide layer, rust layer, paint, and contaminants rather than completely remove them. Because of this, the range of each evaluation level of surface pre-treatment will be very large, and the efficiency and ability of different pre-treatment tools are different.

Therefore, in this study, we expect to discuss the working scope of different pre-treatment tools and match the best pre-treatment tools for post-treatment methods to improve the efficiency and quality of surface treatment.

1.3.2 Development of post-treatment

1.3.2.1 Abrasive blast cleaning

The same as the pre-treatment, abrasive blasting surface treatment is also a surface treatment method based on physical-mechanical cutting. It uses compressed air, high-pressure water flow, and other accelerated abrasive media. Abrasive media impact the target surface with high speed and energy to achieve extrusion and cutting of coating, rust layer, and even steel substrate and achieve the purpose of cleaning[43]. Abrasive blasting is not only to obtain a clean surface. The abrasive impact can form an appropriate surface shape on the surface, improve the surface roughness, and help achieve a good anchoring effect between the coating and the surface[44–46]. In addition, the repeated impact of abrasives on the surface strengthens the steel surface to eliminate residual

stresses and enhance the fatigue strength of components[47–49]. Abrasive blasting technology has strong cleaning ability, efficiency, and economic benefits. So, it has become the most commonly used high-quality surface treatment method preparation.

Abrasive blasting technology development mainly concentrated on the use of abrasives[50,51]. According to the different usage scenarios, abrasive applications include non-metallic media (such as corundum and glass) and metallic media (such as iron slag and fused alumina) used in dry blasting. In addition, media such as baking soda are used for wet blasting[17]. New blasting techniques are developed, such as dry ice blasting[52,53]. The choice of abrasives is varied according to the purpose of use. When performing blasting surface cleaning, considerations include but are not limited to cost-effectiveness and targeted surface quality, the convenience of processing, environmental friendliness, etc. Considering the wear resistance, durability, high hardness, and ability to remove the coating and rust layer of metal abrasives, the most commonly used blasting method in civil engineering is still metal abrasive dry blasting.

In the evaluation of abrasive blasting clean, the current focus is mainly on the ability to remove the rust layer or coating layer[54–57]. Complete surface cleaning by abrasive blasting is often difficult to achieve. The required engineering time and cost will increase exponentially to achieve the complete cleaning goal. Therefore, even some insignificant impurities can be tolerated in the evaluation criteria. ISO 8501-1 defines four levels of sandblasted surfaces (defined using the Sa level). These evaluation criteria are still based on verbal and visual control. Generally speaking, the blasted surface is controlled above the Sa 2.5 level before painting to avoid corrosion underpainting. Still, this phenomenon is often difficult to control because the visual evaluation criteria usually do not identify residual salt[16]. After blasting, the surface will often remain part of the abrasive, especially hard abrasive powder, resulting in a kind of secondary pollution[55,58]. These abrasives embedded in the surface will also bury tiny rust and salt in the shallow layer of the steel substrate, which is the main reason for flash rust and re-corrosion in a short time after blasting. The re-corrosion phenomenon is particularly significant in severely corroded steel members[15,16]. When the coating is carried out on this surface, the corrosion problem undercoating will inevitably appear, leading to the coating failure in advance. At present, engineers are still seeking solutions to this problem. The combination of blasting and high-pressure water washing, as well as wet blasting

technology and abrasive water jet technology, can solve the problem of abrasive embedding and rust/salt residue to a certain extent.

1.3.2.2 Laser cleaning

The mechanism of laser surface treatment is different from the mechanical cutting mechanism of abrasive blasting. The high energy density of the laser can cause instantaneous vibration, ablation, expansion, melting, and evaporation of coating, corrosion products, and impurities[20,21,59–62]. Due to the mechanism of the difference, the laser has broad prospects for development in corrosion maintenance engineering. It can be used as an alternative technology for abrasive blasting cleaning in some specific conditions. During laser cleaning, there is no need for additional abrasive media. The consumption is limited to electric energy when laser cleaning so that it avoids secondary pollution and the generation and recycling of by-products. Laser cleaning has a better economic benefit to a certain extent and is friendlier to the operator and the environment.

In the past decades, the development of laser cleaning technology has been mainly focused on PL[63–68]. Nanosecond laser or even picosecond laser emitter has been developed. The PL beam has a very high peak intensity, which can ablate, evaporate and ionized the coating and rust layer. The PL can sufficiently clean the coating and rust layer. Due to the accuracy and stability of PL, laser cleaning technology has been widely used in cultural relics cleaning, precision instrument manufacturing, and other industries. However, the PL still has some engineering limitations. The cleaning ability of the PL on the rust layer is limited. Under the short pulse effect, the rust layer can be removed from only a few microns to tens of microns. The treatment efficiency will be limited to the thick rust coating and rust layer commonly seen in civil engineering. Secondly, PL transmitters are usually not very large, making them difficult to clean for large-scale structures. Therefore, the development and application of CWL are more suitable for large structure laser cleaning applications. Unlike the PL, the output of CWL is continuous. The output power is usually dozens of times that of the PL, and the processing ability of the coating and rust layer will be higher[29,69–73]. With the development of high-power CWL emitter in recent years, stable CWL has been widely used. It has been proved that the high-power CWL emitter can instantly form high temperatures on

the irradiated surface, which is sufficient to ablate the coating and rust layer. The cleaning ability of the swept CWL is significantly better than that of the PL.

Currently, the evaluation of laser cleaning corroded steel components is still blank[74]. There are still many differences among different laser emitting devices in terms of laser type, irradiation mode, and output power. Laser cleaning on the metal surface will inevitably remelt the steel substrate, and the remelt layer and oxide layer will be formed. The surface characteristics formed by the different lasers will be totally different, and texture and luster are one of the reasons why it is difficult to form a unified evaluation standard. In addition, there is still a sound indicating that the oxide layer formed by laser cleaning will affect the quality of the coating to a certain extent. Therefore, laser cleaning technology still needs engineering practice to determine its applicability and scope of application.

1.3.3 Development of high-strength bolt cleaning

Bolts are the most common connector and are widely used in bridges and building structures. Most of the bolts used have hexagonal head and nut, due to the influence of edges and corners, the coating at the corners of bolt will be significantly thinner than other positions. This is where coating failure and corrosion most often occur. In addition, the geometric structure of the bolt joint is convex, where becomes the part where dust, impurities and rain-water most easily to gather, which also aggravates the speed of bolt corrosion[75]. According to the research, bolt corrosion will lead to the reduction of the volume of bolt head and nut, directly resulting in the loss of bolt clamping force[76–79]. In the current work on the surface treatment and coating maintenance of bridges and building structures, the cleaning of bolts is often neglected, and there are few researches on the cleaning and corrosion maintenance of bolts. The only bolt maintenance related research has been limited to coating removal using hand tools, power tools, or IH techniques[80]. In the corrosion maintenance engineering, the bolt joint is only simply cleaned by abrasive blast, and the narrow part around the bolt cannot be cleaned enough. The bolts with corrosion products and salt residue on the surface will suffer faster under film corrosion after coating, and even with the crevice corrosion between the bolts, washers and steel plates, resulting in faster damage of the bolt joint. In order to solve the

problem of axial force decline caused by corrosion of bolts, it is necessary to maintain the bolts at the same time during the process of surface treatment and maintenance of the structure.

At present, there have been a lot of studies focusing on the loss of bolt axial force[81–83]. PL can be used to test and obtain the vibration frequency of bolts without damage, and to know the residual clamping force of bolts[84,85]. This will help screen for bolts that need cleaning and maintenance. It is also proved that laser irradiation has little effect on the bolt and laser cleaning is a feasible method[86]. On the other hand, PL coating removal is also a mature technology capable of ablating both the organic and inorganic layers of the coating through ablation. The IH technique, which heats steel substrates to high temperatures to cause coating removal, has also been used to remove coating on bolts [24,25,65,87]. Referring to the above studies, CWL treatment can not only provide an ablative mechanism to clean organic and inorganic coatings, but also form a high temperature in the irradiation area to promote coating peeling, which will be a suitable method for cleaning bolt coatings.

1.4 Organization and outline

The main content of this dissertation is divided into five chapters, which are introduced in detail in chapters 2-6:

Chapter 2 discussed the correlation between rust layer characteristics and corrosion depth after atmospheric exposure. The measurement was carried from the 4-year atmospheric exposed test specimens and severely corroded bridge components of ordinary steel bridges protected by coating in urban highways and weathering steel bridges in the mountain area. The study revealed the strong influence of the rain effects on the rust layer thickness, also the relationship between the rust bud and the range of corrosion pit. It also discussed the unique profile of corrosion pit after a long time of exposure. It shows that both the thickness of the rust layer and corrosion bud range could be used for easy assessment of the atmosphere corrosion degree and applied to maintenance method selection in real structure.

Chapter 3 introduced the design and manufacture of artificial corrosion pits tests with different corrosion degrees. After one year of constant dew point cyclic corrosion acceleration, weathering

steel specimens with three different corrosion degrees were prepared. The rust layer in the corrosion pit of the specimens was observed and counted. An electromagnetic film thickness meter was used to count the thickness of the rust layer in different corrosion degrees' corrosion pits. XRD was used to analyze the oxide composition of the rust layer with varying degrees of corrosion. Three different pre-treatments tools were carried out on the specimens, and the thickness of the rust layer after pre-treatment was determined by three-dimensional contour scanning of a digital microscope. Abrasive blasting and CWL were used to clean the surface of the pre-treated specimens. A turning time test measured the corrosion frequency and area of the cleaned surface. The necessary cleaning times of abrasive blasting and CWL for different corrosion degrees were discussed. The results show that abrasive blasting cleaning has more advantages than laser cleaning for general corrosion. For severe corrosion, CWL cleaning can get better effects. The results can provide a reference for site cleaning engineering.

Chapter 4 introduced a quantitative evaluation method of CWL cleaning based on image analysis. Digital cameras were used to shoot the specimens cleaned by laser in different rounds. The color information of the corrosion pit area was captured by the software Photoshop 2022 to obtain the digital information based on the CIE LAB color space. The trend of color information in different cleaning stages was discussed. By calculating the color difference and combining it with the cleanliness evaluation conclusion obtained by the conversion time method in Chapter 3, the corresponding relationship between color difference and cleanliness is determined, and the quantitative evaluation standard based on image analysis and color analysis is proposed.

Chapter 5 introduced an engineering use of CWL cleaning. Treatment conditions of dry laser cleaning (DLC) and wet laser cleaning (WLC) of the drench, soak, and rinse methods are adopted, and SEM/EDX evaluates the cleanliness effect. The morphologies and chemical compositions of untreated and treated surfaces are analyzed using three-dimensional digital microscopy, laser confocal microscopy, and scanning electron microscopy–energy dispersive X-ray spectrometry. The results show that laser cleaning can efficiently remove corrosion products and salts that severely corrode steel members and prolong the cleaned surfaces' re-corrosion time. WLC can achieve excellent microscopic cleaning and reduce the effect of high-temperature inputs on the surface via laser irradiation. Further mechanistic analysis indicates that ablation, melting, and evaporation

during laser cleaning primarily contribute to removing corrosion products and salts. As a result, the WLC drench method yields the best surface cleanliness and is suitable for practical engineering applications. This study provides a basis for maintaining severely corroded structures via laser-cleaning techniques.

Chapter 6 introduced the use of CWL cleaning on high-strength bolts. This study examined the axial force loss of high-strength bolts after a 3 kW CWL treatment. Friction connection specimens with M22 high-strength bolt were prepared, and a fixed-angle CWL transmitter and rotating platform were used for high-strength bolt rotary cleaning. The change in the axial force of the bolts was examined during the laser treatment based on the irradiation duration on the nut surface. The experimental results indicated that the axial force's minimum and final stable values during CWL cleaning are affected by the total irradiation duration. The loss of the axial force for multiple rounds of irradiation is smaller than that of continuous irradiation for the same total irradiation duration. And CWL cleaning will not cause axial force loss to adjacent bolts. The distribution of bolt temperature when CWL cleans the bolt is stimulated by a FE model, which proves the overall temperature of the bolt does not exceed 300°C and is kept in a safe condition when the continuous irradiation duration is less than 45 s. From the relationship between the axial force change and the treatment duration, axial force loss equations were suggested, which can aid in estimating the axial force loss and creating a maintenance plan.

Chapter 7 summarized the work presented in this dissertation and also proposed further research topics emerged from this work.

The flowchart of work in this dissertation as shown in Figure 0-1.

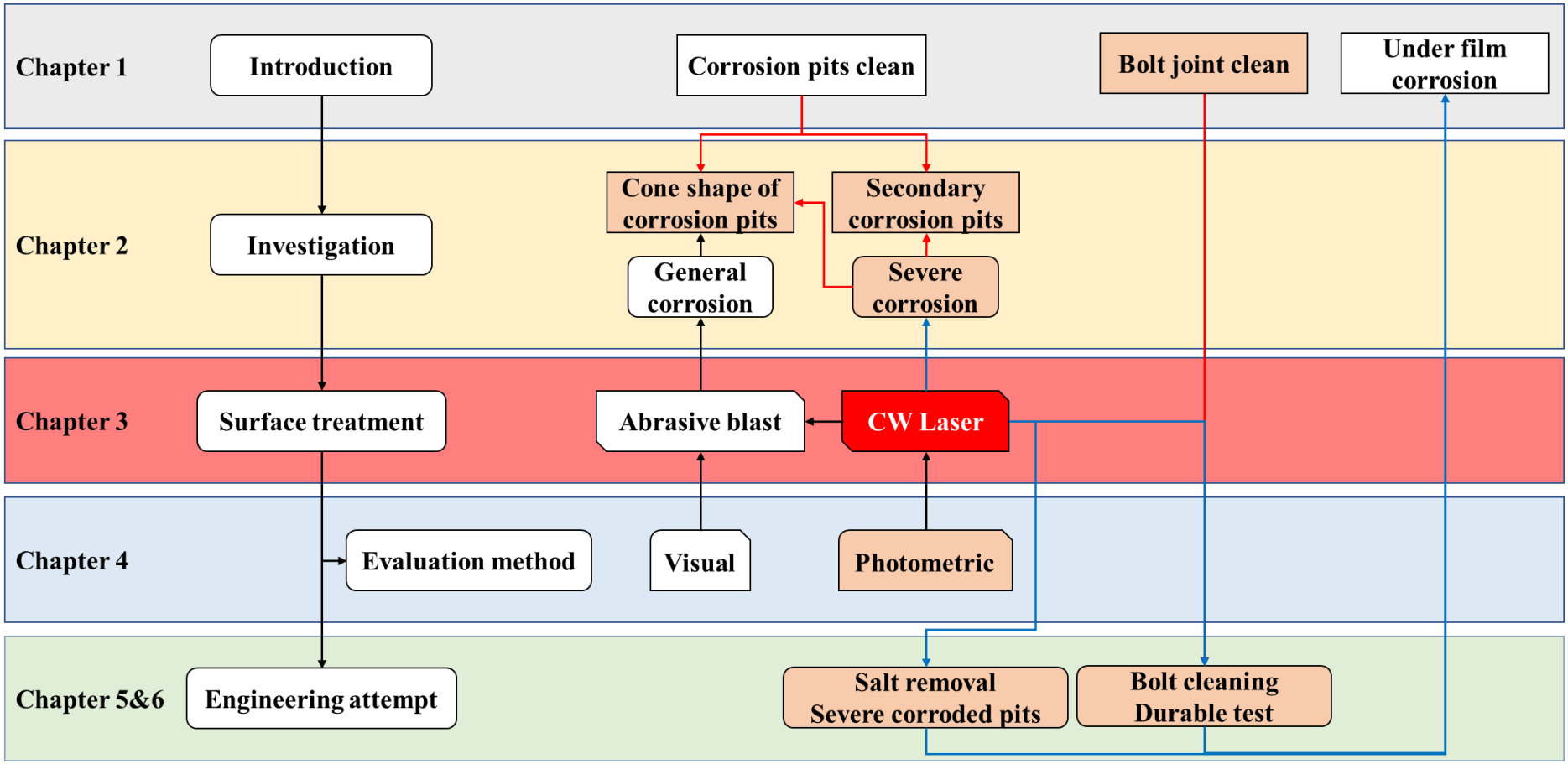

Figure 0-1 Flowchart of the dissertation

INVESTIGATION OF THE CHARACTERISTICS AND RELATIONSHIP BETWEEN RUST LAYER AND CORROSION PIT

1.5 Introduction

Evaluate the corrosion degree before corrosion maintenance is the first step, and the most common ways are based on the measurement of average corrosion depth and the maximum corrosion depth. However, this method is difficult to use in structural, especially with severe corrosion, the reason includes the hard inspection environment and limited instrument range of the sensor. So, there is needed to find easy and direct evaluation methods.

The mechanism of atmospheric exposure corrosion shows that the composition of the rust layer phases is commonly consistent, usually composed of Lepidocrocite (γ-FeOOH), Goethite (α-FeOOH) and Magnetite (Fe_3O_4) also with Akaganeite (β-FeOOH) in a high salt environment[88–93]. In the case of the corrosion mechanism, the thicken of steel is directly correlated with the weight loss of steel, which has been revealed by a large amount of atmospheric exposure test of carbon steel in the short and mid-term exposure. However, the information on long-term exposure for more than 20 years is considerably less abundant.

In order to find an easy way to evaluate the corrosion degree, carried out a short time exposure test from 0.5 to 4 years and also measured corroded components from two steel bridge more than 20 years of service to obtain the spatial information of corrosion products and the corroded surface of steel. In this chapter discussed the relationship between rust characteristics and corrosion degree. Besides, the features of corrosion pits are also analyzed.

1.6 Investigation and analysis method of corrosion pits

1.6.1 Atmosphere Exposure Test

The steel plates used in atmosphere exposure tests are uncoated JIS G 3106 SM490A with a size of 400 mm in length, 60 mm in width, and 9 mm in thick. The specimens are treated by grid blast to Sa 3 based on ISO standard. The chemical composition of specimens listed in Table 0-1.

Atmospheric environment and airborne salt amount are the main factors that affect the steel corrosion rate[1]. Besides, the effect of rainwater will directly affect the amount of salt attached to the surface: stagnate water will increase the amount of salt attached to the surface of the structure, and the rain wash effect will reduce the amount attached salt.

In order to avoid the influence of the atmospheric environment, and to consider the different airborne salt amount and rain wash effect, the test was set up in four exposure sites in Fukuoka and Okinawa, Kyushu, Japan, as shown in Table 0-2 with three setting angles as 0°, 45°, and 90°. In this study, define the specimens' surface into skyward and groundward. Define the 90° settled specimens' south-facing as skyward and north-facing as groundward.

As listed in Table 0-2, the specimen in Momochi and Kyoda coastline were placed in the site under bridge where are hardly affected by rainwater, so that define these specimens as without rain wash effect condition. The sites in Kyushu University and University of the Ryukyus are under open-air and directly affected by rain. Among them, the horizontally placed specimens are defined as the rainwater stagnation condition and the others as with rain wash condition.

The exposure time of all exposure sites are 0.5, 1, 2, 3 and 4 years. After the test, the thickness of the rust layer and the surface characteristics of the corroded surface were detected from both skyward and groundward surface. A total of 116 valid data were collected from atmosphere exposure test, including 39 at University of the Ryukyus, 32 at Kyushu University, 35 at Momochi, and 10 at Kyoda.

Table 0-1 Chemical compositions

Material	C	Si	Mn	P	S
Composition (wt%)	0.16	0.36	1.45	0.014	0.007

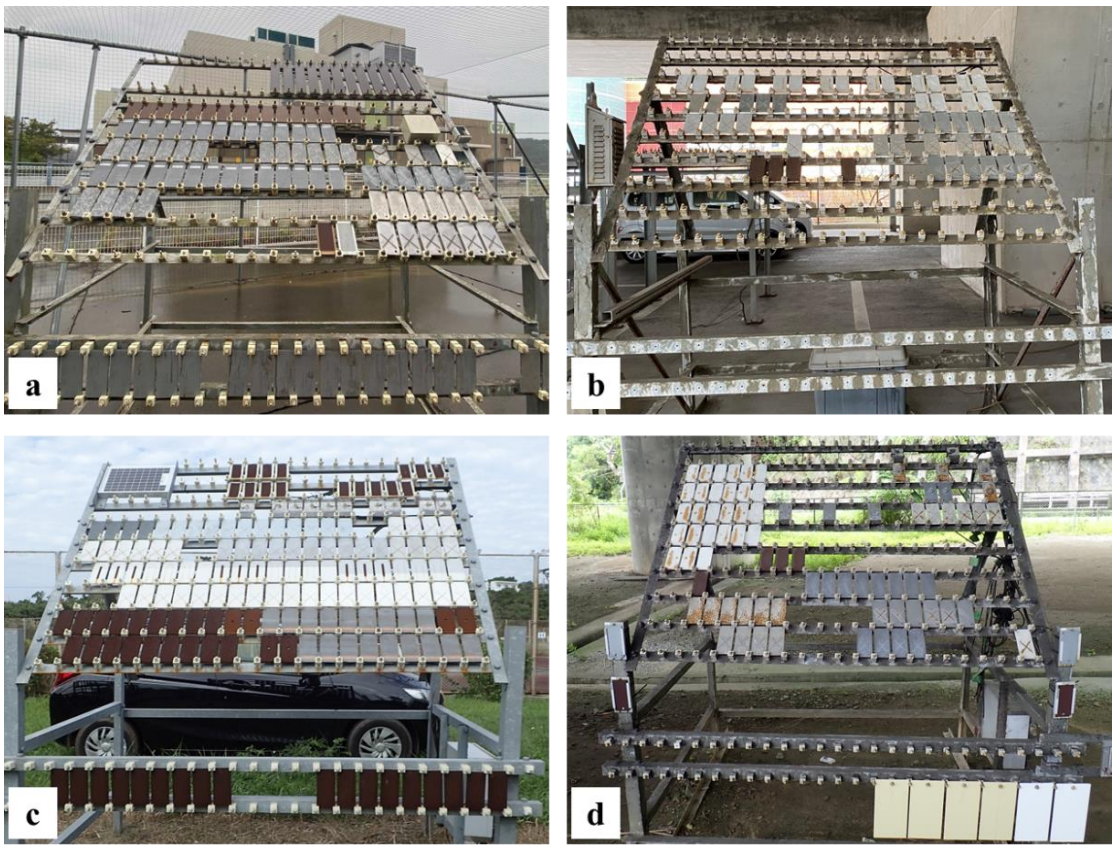

Figure 0-1 Exposure sites in (a) Kyushu University, (b) Momochi, (c) University of the Ryukyus and (d) Kyoda

Table 0-2 Atmospheric environment at exposure sites

Exposure site	Temperature (℃)	Relative humidity (%)	Precipitation (mm/yr.)	Offshore distance (km)	Amount of airborne salt (mdd)	Rain wash
University of the Ryukyus	23	75	2,064	2.3	0.30	Yes
Kyushu University	17	75	1,776	2.5	0.07	Yes
Kyoda	18	66	1,763	0.03	0.52	No
Momochi	23	73	2,196	0.07	0.78	No

1.6.2 Measurement of Corroded Component

The measured corroded component of coating protected common steel is from the top plate of a steel pier in Kitakyushu No.1 Expressway, which have been completed in 1980. The steel grade is JIS G3106 SM50YA. The structure is coated with rust rubber when it builds and were maintained in 1992 with the same coating. Severe corrosion occurred on the top of the steel beam, whose coating had failed, and large size deep corrosion pits appeared locally, as shown in Figure 0-2.

Another investigation is from a weathering steel bridge located at Kagoshima in the mountainous area which have been completed in 2001. The straight-line distance from the bridge to the west coastline is about 5 km. All target steel components used the weathering steel according to JIS G3106 SMA490AW without coating. Weathering steel components are seriously corroded by salt influence, the airborne sea salt coming from both north and south along the valley from the coast, as shown in Figure 0-3. Besides, affected by the influence of precipitation, fog and condensation, the wetting time of steel components more than 80%. Because of the high humidity environment, the dense oxide film of weathering steel cannot form, significant corrosion damage has occurred about 10 years after construction. Besides, the stagnant rainwater after heavy rainfall and the use of antifreeze during winter also help the causes of pitting corrosion. The analyzed corrosion data are from the corrosion pits on the upper flange, the web, and the lower flange, where the most prone to condensation, as shown in Figure 0-4.

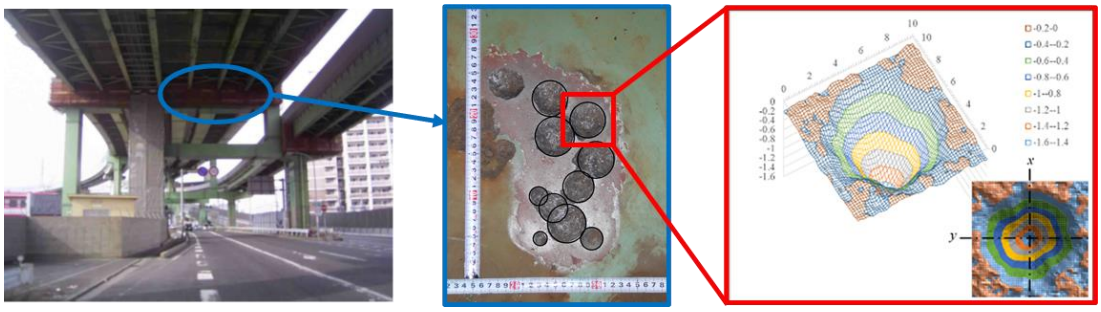

Figure 0-2 Severe corrosion pits on common steel beam

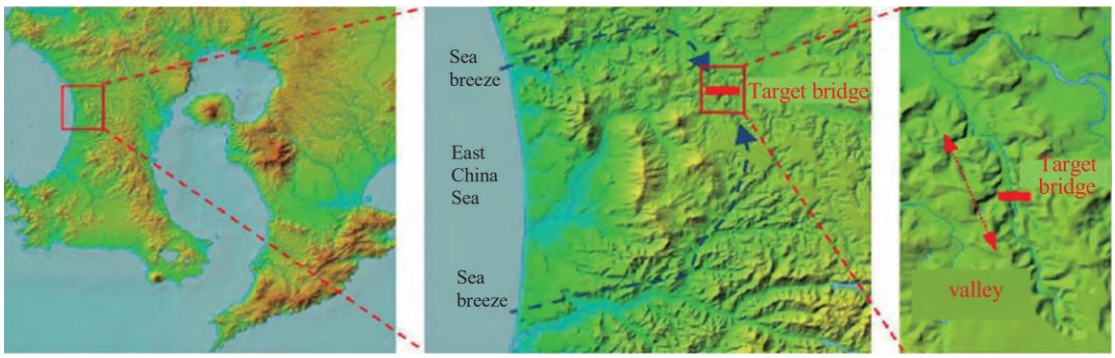

Figure 0-3 Location of the severely corroded weathering steel bridge

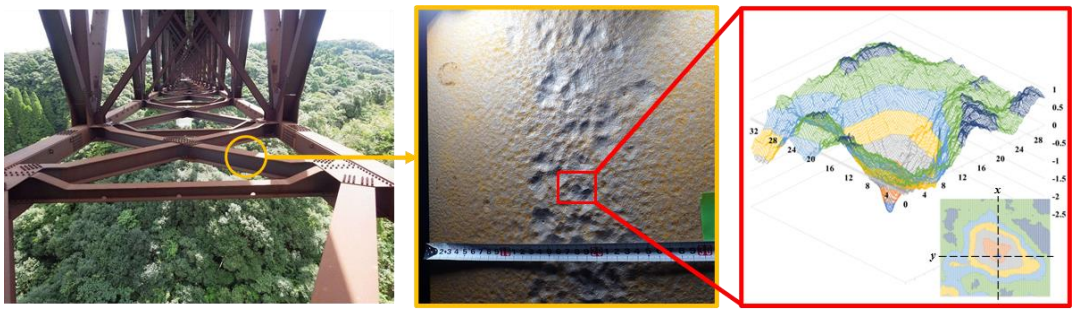

Figure 0-4 Severe corrosion pits on weathering steel flange

1.6.3 Analysis of Rust Layer and Corrosion Pits

Use the electromagnetic film thickness sensor with measurement accuracy: 1μm, decomposition energy: 1 μm (0~999 μm), 10 μm (1~8 mm) for the measurement of the average thickness of atmosphere exposure test specimens. During the measurement, choose 6 points on the specimen surface and measure 11 times at every point, as shown in Figure 0-5, and the average value was defined as the average thickness of the rust layer.

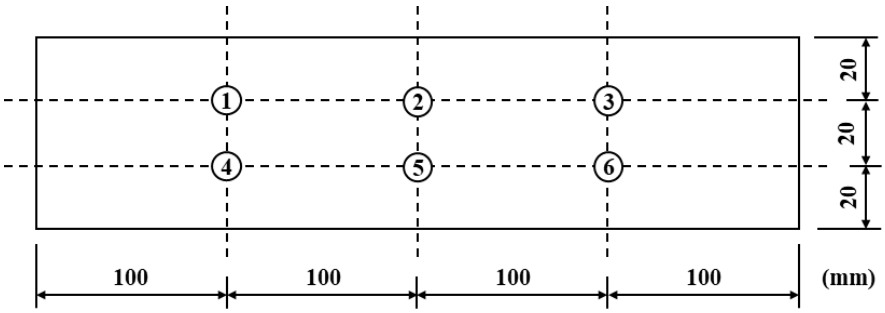

Figure 0-5 Atmospheric exposure specimen and measure points

The surface parameters of the atmospheric exposure test specimens are measured by the laser-focus scanner with laser diameter of 30 μm, decomposition energy of 0.05 μm. The measured scanning step is 0.2 mm. The measured data is 3D coordinates of the metal surface, and the depth of the corrosion pit can be obtained through the vertical coordinates. The surface parameters of the corrosion pit are measured by the 3D LED scanner (decomposition energy as 0.01 mm) based on the structured projection phase shift method. The measured scanning step is 0.2 mm. The collected data are 1:1 spatial coordinate, which are used to draw the three-dimensional contour map, plane elevation difference map and section contour map of the corrosion pit.

1.7 Relationship and characteristics of corrosion pit and rust layer

1.7.1 Relationship between rust thickness and corrosion pit depth

The specimens without rain wash effect have a notable feature that the rust layer does not peel off. From Figure 0-6(a)~(d), the specimen in the Momochi coastline show that the corrosion rate and the degree of corrosion of the skyward surface are higher than those of groundward, and the specimens with 45° sitting angle have the highest corrosion rate. The maximum corrosion depth reaches 0.1 mm, and the thickness of the rust layer reaches 0.5 mm.

Under the effect of rain wash, the specimens had significant rust peeling off during 2~3 years of exposure. As shown in Figure 0-6(e)~(h), the retained rust layer is around 0.15 mm. Contrasting with the case without rain wash, the specimen with rainwater stagnation is the most corroded, especially at University of the Ryukyus. After 4 years of exposure, some local corrosion pits happened at the groundward surface, and the maximum pit depth can reach to 2 mm.

In the corrosion process, the main corrosion products are γ-FeOOH, α-FeOOH, and Fe_3O_4, and contain β-FeOOH in a high-salt environment. Under the years' dry-wet cycle, the rust layer will delaminate. The bottom layer mainly consists of α-FeOOH and Fe_3O_4, while the surface layer contains more with γ-FeOOH [1]. Although the rust layer often delamination and peeling, the remained rust layer after a long period of circulation is very dense and firmly adheres to the steel surface. The research has shown that the volume of α-FeOOH produced by Fe corrosion will expand twice, and the volume of Fe_3O_4 increased by 1.4 times [1]. Therefore, the depth of corrosion can be

estimated to a certain extent through the thickness of the rust layer to determine the current degree of corrosion.

The thickness of the rust layer and the average corrosion depth are listed separately according to the stagnation condition, with rain washing and without rain washing conditions. In reference to previous research[5] drawing as Figure 0-7(a), not considering the peeling of the rust layer, the rust layer thickness and corrosion depth ratio of the three cases are slightly different, but all have a good error range. Among them, the corrosion depth to rust layer thickness ratio α is about 0.5 under stagnation conditions, 0.3 under rain washing conditions, and 0.2 under no rain-washing conditions.

To verify the applicability of analyzing the corrosion depth by the thickness of the rust layer, take an independent corrosion pit from the top plate of a steel pier in Kitakyushu No.1 Expressway for analysis, the relationship between the rust layer thickness and the corrosion depth chart shows in the Figure 0-7(b). Because the corroded part is from the top plate of steel beam, which can suffer from the rainwater flows down from the expansion joints, so it belongs to a stagnation condition. The analysis shows that α is 0.508 and has a relatively high correlation coefficient R of 0.980. The conclusion shows that the method of obtaining the depth of corrosion by the thickness of the rust layer is feasible, consistent with the research results of atmospheric exposure corrosion.

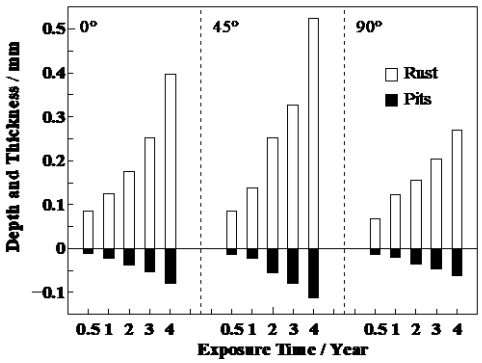

(a) Momochi (skyward)

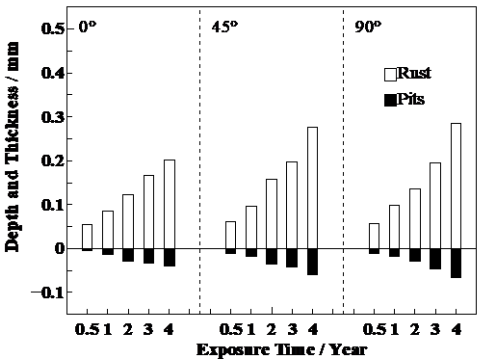

(b) Momochi (groundward)

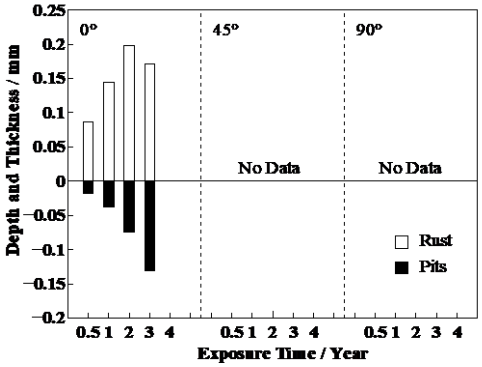

(c) Kyoda (skyward)

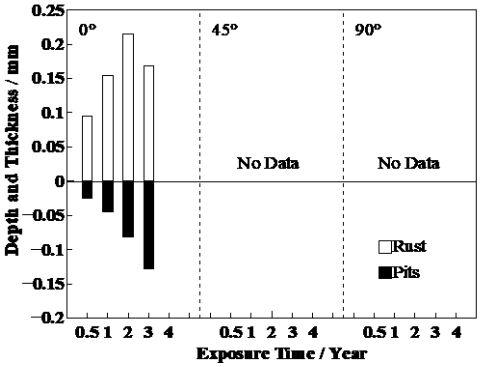

(d) Kyoda (groundward)

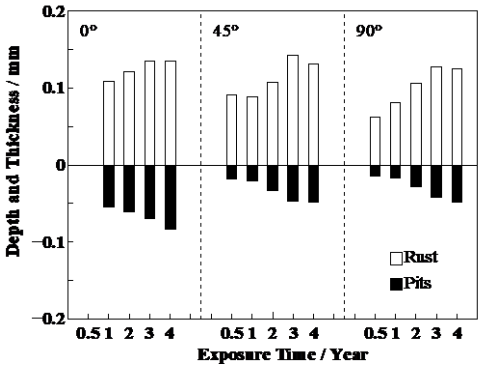

(e) Kyushu University (skyward)

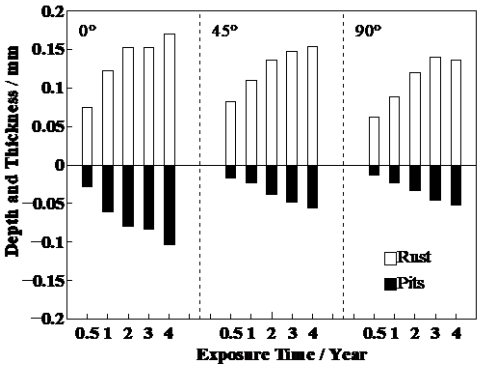

(f) Kyushu University (groundward)

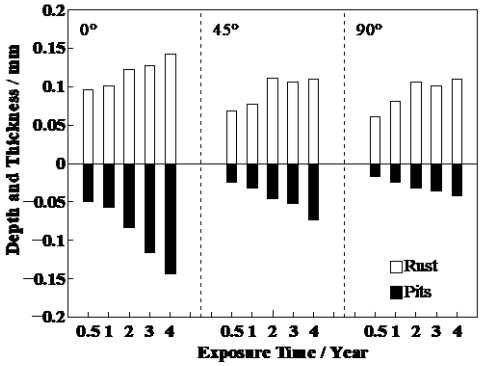

(g) University of the Ryukyus (skyward)

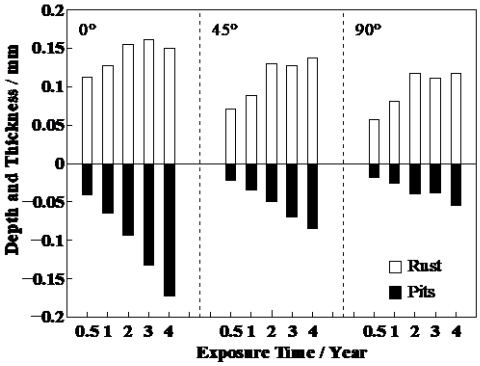

(h) University of the Ryukyus (groundward)

Figure 0-6 Thickness of rust layer and corrosion depth

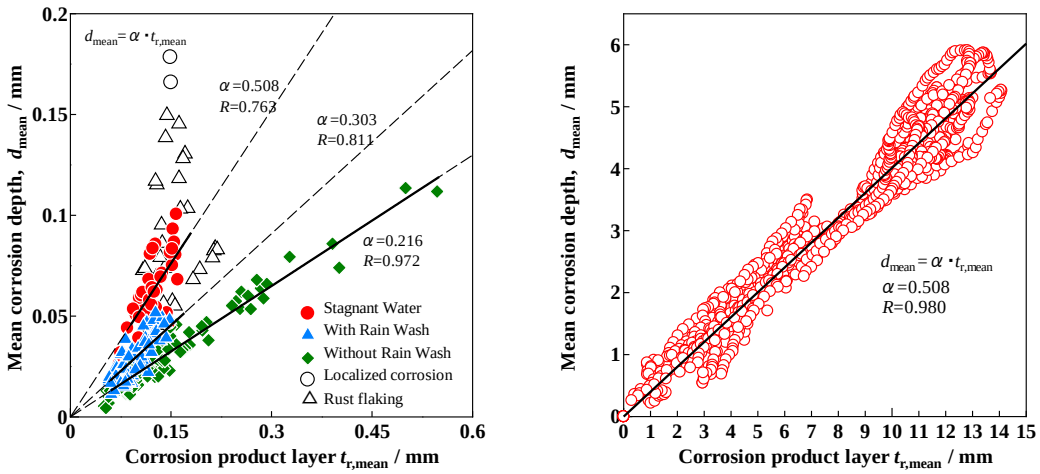

(a) Atmosphere exposure test (b) Corroded component measurement

Figure 0-7 Relationship between rust layer thickness and corrosion depth

1.7.2 Characteristics of rust layer and corrosion pits

During the atmosphere exposure test, pitting corrosion happened on the 4-year exposed specimens at University of the Ryukyus at the groundward surface set angle is 0°. The reason why corrosion pits occur is because of water droplets that contain salt attached at that side. And at the same position as the corrosion pit, one rust buds can be found on the rust layer as shown in Figure 0-8(a). This phenomenon is natural to see especially in severely corroded steel components. Therefore, taking the independent corrosion pits on the corroded components from the top plate of a steel pier in Kitakyushu No.1 Expressway as an example as shown in Figure 0-8(b), the cross-sectional profile of the rust layer and the corrosion pit are drawled, and it is found that the range of the corrosion pit corresponds to the scale of the rust bud.

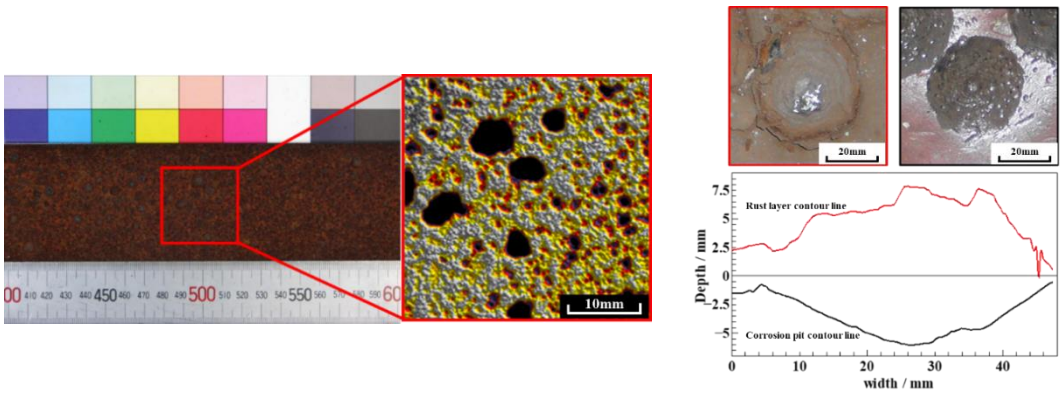

(a) Corrosion bud in pitting corrosion (b) Corrosion bud in server corrosion

Figure 0-8 Corrosion bud and pits

Besides, the shape of the corrosion pit under atmospheric exposure is not a part of the sphere generally considered but a cone, which can be seen from the cross-section of the independent corrosion pit. We found a similar phenomenon in our investigation of the corrosion pits.

During the test, found 22 independent pits from the pitting corrosion specimens at University of the Ryukyus, with an average depth of 1.58 mm. The three-dimensional diagram and the cross-sectional view of a typical corrosion pit as shown in Figure 0-9(a). The red dotted line shows the cross-section outline of the corrosion pit. The average corrosion pit diameter is about 10 mm and the average cone angle is 144°.

Corrosion pits of severely corroded steel components are more significant. The analysis obtained data of a total of 27 corrosion pits from two corroded components of coating protected common steel components. The average diameter of the independent corrosion pit is about 42 mm, and the depth is around 5 mm, and the average cone angle is also around 145°. By analyzing the corrosion pits of the atmospheric exposure specimen and the corroded compounds, founding that the width and depth of the corrosion pit are directly proportional, whether the corrosion pit overlaps or independent. Figure 0-9(b) and (c) shows the profile information of the independent and overlapping pits.

The corrosion pits of weathering steel are almost independent pit and do not overlap with each other. The most severe corrosion occurred at the bottom of the lower flange plate, mainly in the middle of the flange, where rain and dew are always concentrated. The width of the lower flange plate of the steel bridge is 360 mm, and the width of the corroded area is about 120 mm, accounting for 1/3 of the entire lower flange plate. The corrosion degree of the inner side of the upper flange plate of the lateral bracing is lower only by the bottom of the lower flange plate, and the corrosion pits are also in the middle part of the flange, but more concentrated in the area close to the web, which is caused by the flowing tendency of water. On the web, obvious corrosion pits only be found in the upper part. The corrosion pits at the web should be formed by the rainwater and dew condensation water flowing down from the upper flange and web plate. In the investigation of the lower flange, scanned the middle part of the bottom side of the lateral bracing, where the corrosion pit mainly concentrated, and chose 19 independent corrosion pits for analysis. The depth of these

corrosion pits ranged from 0.85 mm to 4.15 mm. Secondary corrosion is found at the bottom of eight corrosion pits, and the corrosion depth of these corrosion pits all over 2 mm. As shown in Figure 0-9(e), it is a corrosion pit with a secondary pit and has a cone shape like the corrosion pit of ordinary steel. It is found that the cone angle of the weathering steel corrosion pit has no relationship with the corrosion depth, and the average cone angle is 156°. In the investigation of the upper flange, scanned the surface of the inner side of the upper flange of the lateral bracing, chose 16 corrosion pits from this area for analysis. The corrosion depth of these pits is from 1.10 mm to 3.39 mm, smaller than the pits on the lower flange. Among these corrosion pits, only five of them have secondary corrosion pit. The corrosion depth of these corrosion pits also exceeds 2 mm. As shown in Figure 0-9(f), corrosion pits of the top flange are also cone shape, and their average corrosion angle is the same as that of the bottom flange, which is 156°. The corrosion pits on the web are significantly smaller than the flange. Scanned the upper part of the web and chose 14 corrosion pits for analysis, the maximum corrosion depth the chosen pits is 1.14 mm, and no secondary corrosion pits in them. As shown in Figure 0-9(g), the corrosion pits on the web are also cone shape. The average angle of the corrosion pits on the web is 166°, larger than the pits on the flange.

What more, it should be noted that at the bottom of the severely corroded pits, seven of them have secondary corrosion pits, all of which occurred in the independent corrosion pits', and the frequency of occurrence reach to 50%. The appearance of secondary corrosion pits may be due to the accumulation of water and salt. As shown in Figure 0-9(b) and (e), it is a typical secondary corrosion pit. Secondary corrosion pits will significantly affect the maximum corrosion depth of components. Therefore, when evaluating independent corrosion pits, after determining the approximate range of corrosion pits by the rust bud, there is necessary to use a layer thickness sensor to detect the maximum depth of the corrosion pits for corrosion degree evaluate.

All the corrosion pits investigated were classified according to the type of steel and the location where corrosion occurred, and the relationship between the depth of corrosion pits and the corn angle of corrosion pits was statistically analyzed, as shown in Figure 0-10. Based on the surface profile analysis, we know that the shape of the corrosion pit is conical rather than hemispherical as is commonly understood. This special shape may cause some difficulties for the surface treatment. For ordinary steel, the conical angle of corrosion pit is about 145°. For weathering steel, the conical

angle of corrosion pit is slightly larger than that of ordinary steel. The average cone angle of the corrosion pit at the flange is about 156°, while at the web is about 166°. From the investigation, the corrosion degree of weathering steel web is lower than that of flange. With the increase of corrosion degree, the cone angle of the corrosion pit decreases while the corrosion pit becomes deeper. This is due to the passivation of weathering steel and the formation of dense oxide layer. For ordinary steel, without the protection of dense oxide layer, the cone angle of corrosion pit is relatively concentrated around 145° at any corrosion stage. It can be predicted that after severe corrosion occurs to a certain extent, the cone angle of the corrosion pit will be close to 145°.

1.8 Summary

In this chapter, discussed the relationship between the thickness of the rust layer and the depth of corrosion pits, also summarized the shape of corrosion pits. Besides, proposed an easy detect method for corrosion depth assessment. The conclusions are as follows:

1) The thickness of the rust layer has a linear relationship with the mean corrosion depth. Without rain washing effect, the depth-to-thickness ratio is about 0.2, with rain washing the ratio up to 0.3, and in the case of rainwater stagnant, the ratio is 0.5.

2) Pitting corrosion, especially severely corrosion pits, will show as rust buds over the pit, and the size of the rust buds is the same as the size of the corrosion pits, which can be used for corrosion pit size analysis.

3) The shape of the corrosion pit cross-section is conical. The cone angle is around 145° to all of the common steel corrosion pits. The severe corrosion pits' shape of weathering steel is the cone, and its cone angle is larger than common steel corrosion pits, on the flange is about 156° and on the web is about 166°. With the increase of corrosion degree, the cone angle of corrosion pit decreases gradually. It can be predicted that the final cone Angle of the corrosion pit will be close to 145°.

4) Secondary corrosion appears at the bottom of the severely corroded pits. The conical angle of the secondary corrosion pit is much smaller than the corrosion pit itself, which will be the difficulty of surface treatment.

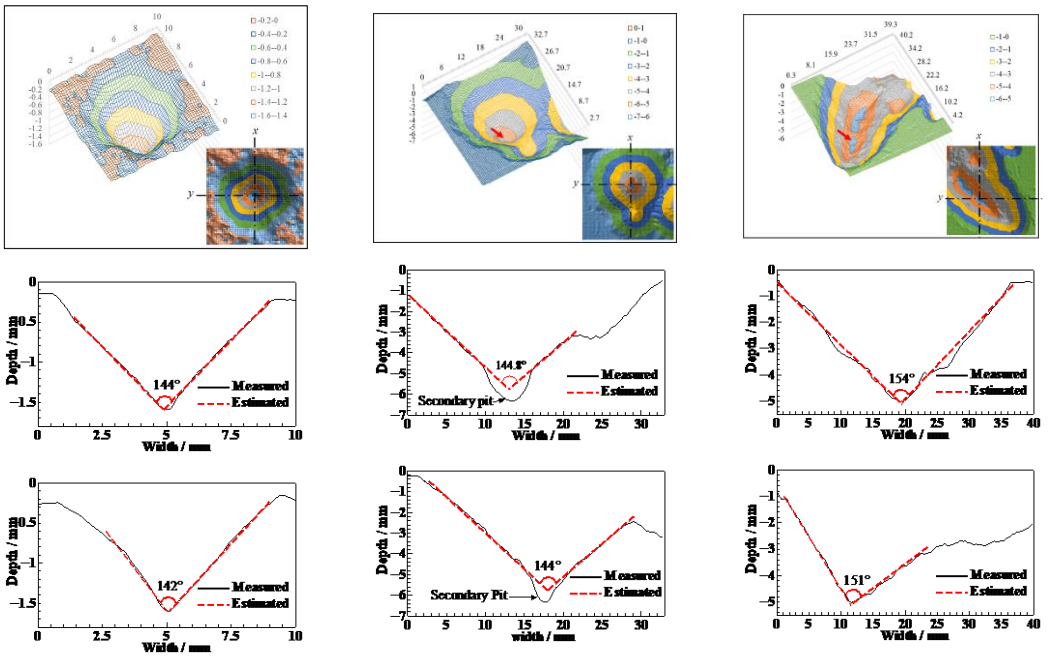

(a) Pitting corrosion (b) Independent corrosion pit (c) Overlapped corrosion pit

(d) Corrosion pits of the lower flange plate (e) Corrosion pits of the upper flange plate (f) Corrosion pits of the web

Figure 0-9 Characteristics of corrosion pit

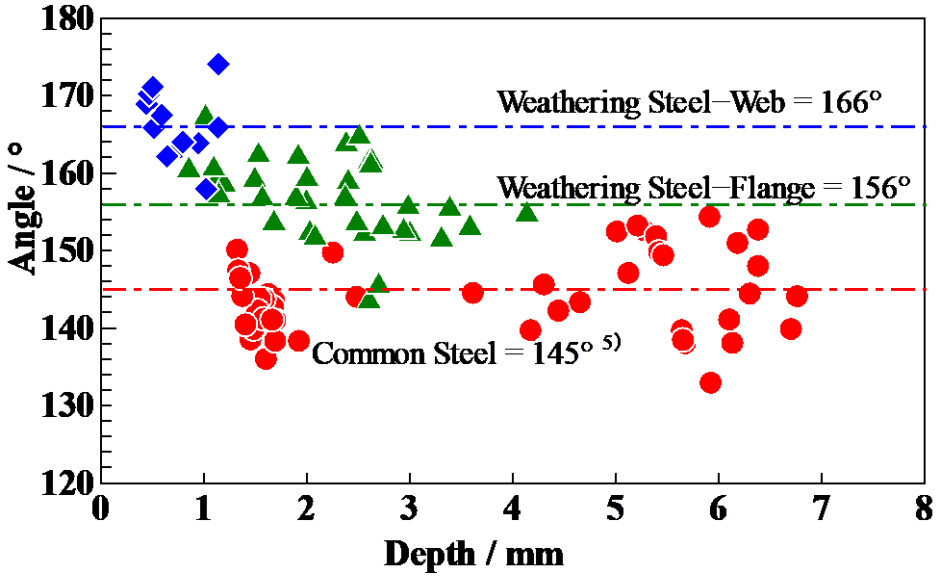

Figure 0-10 Relationship between corrosion pit depth and cone angle

CLEANLINESS ANALYSIS OF CORRODED WEATHERING STEEL BY DIFFERENT SURFACE TREATMENT METHODS

1.9 Introduction

The conical corrosion pit makes the surface treatment difficult. Especially severe corrosion, usually accompanied by the emergence of secondary corrosion pits. The attachment of a large amount of salt is the direct cause of severe corrosion, especially in weathering steel structures. In low air-borne salt environment, a dense protective layer can be formed to inhibit the further corrosion of the structure. However, in high salt and high temperature and humidity environment, the dense oxide layer cannot be formed, and the corrosion rate of the weathering steel is significantly increased. As described in Chapter 2, corrosion pits of weathering steel structures can also be several millimeters deep with secondary corrosion pits. In the study of abrasive blasting cleaning seriously corroded steel components, it is found that even if the surface is cleaned to the degree of no rust and no impurities visually, that is, the level of Sa2.5 or Sa3, in the atmospheric environment within a day, the corrosion pit will occur serious re-rust phenomenon. This phenomenon is due to inadequate salt removal. In addition, in the abrasive blasting cleaning project of the investigated weathering steel bridge, also faced the problem that the interior of the secondary corrosion pit could not be cleaned, and the problem of re-corrosion in a short time. The current solution method is still multiple rounds of cleaning, or even the use of waterjet to remove salt, but this undoubtedly increases the construction cycle and cost several times.

In order to discuss the hybrid surface treatment methods, and the applicability of laser cleaning, in this section we make three kinds of weathering steel specimens with different corrosion levels. Discussed the effectiveness of pre-treatment to rust removal and the relationship between post-treatment duration and cleanliness. Finally, a qualitative evaluation method, named turning time method, is proposed to evaluate the cleaning effect of hybrid treatment methods under different corrosion states.

1.10 Preparation of corroded specimens with artificial pit

1.10.1 Specimens preparation

Specimens with artificial corrosion pits were prepared, and accelerating corrosion tests were performed. As shown in Figure 0-1(a), 6 mm thick SMA490AW specified in Japanese Industrial Standard (JIS) weathering steel plates were drilled using a 142° cone angle drill to make corrosion pits of depth 2 mm and width 12 mm[94,95]. The chemical compositions of the SMA490AW steel are listed in Table 0-1. All specimens were blasted by garnet before accelerating corrosion, as shown in Figure 0-1(b). To prepare specimens with different degrees of corrosion, a NaCl solution was injected into each artificial corrosion pit with a pipette, resulting in salt deposits of 10 mg/m^2, 100 mg/m^2, and 1000 mg/m^2 in the artificial pits of the three groups of specimens[96,97]. All specimens were placed in the same constant temperature and humidity oven and subjected to accelerated corrosion with a constant dew point dry and wet cycle for one year.

Table 0-1 Chemical composition of the carbon steel plate

Material	C	Si	Mn	P	S	Cu	Ni	Cr	Fe
Composition (wt%)	0.12	0.22	1.14	0.01	0.002	0.31	0.09	0.49	bal

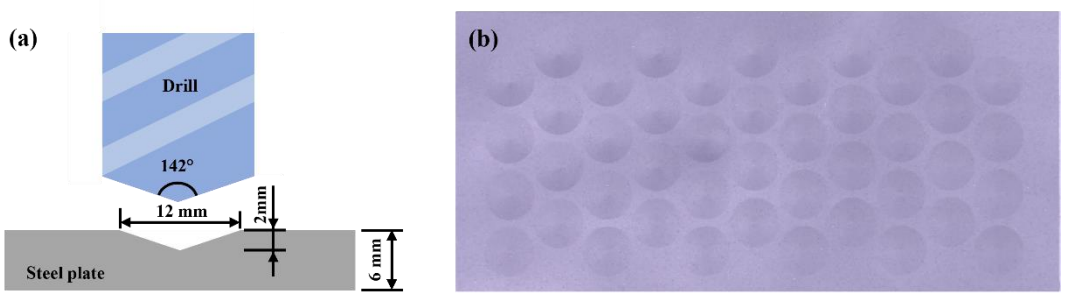

Figure 0-1 Specimens with artificial corrosion pits: (a) Schematic of manufacturing process and (b) the surface characteristics after abrasive blasting

1.10.2 Accelerating corrosion

The constant dew point dry and wet cycle was obtained based on the atmospheric data from the exposure site at the University of the Ryukyus. As shown in Figure 0-2, the atmospheric data in summer of Okinawa Island which has a sub-tropical climate was collected and analyzed. In two weeks, with the highest dew point temperature in the non-rainy season, the dew point reaches the range 25–30°C, and the daily dry and wet time accounts for 50% of each day. Under these conditions, accelerated corrosion can obtain a fast corrosion rate. The lowest temperature and humidity for the accelerated corrosion cycle are based on the average temperature and humidity at night. The highest temperature is the actual highest temperature plus 10°C. The dry and wet cycle curve is required to envelop the measured temperature and humidity[98–101]. The established constant dew point corrosion cycle curve is shown in Figure 0-2(d), and the fixed dew point is 27°C.

1.10.3 Pre-treatment and post-treatment

Before the laser treatment, the surfaces of each specimen were manually scrubbed with steel brushes and power tools with cup wire and diamond grinding discs. Before pre-treatment, an electromagnetic film thickness meter (SWT-9000, SANKO Inc., Japan) was used to determine the thickness of the rust layer in the corrosion pit, and a digital microscope (HRX-01, HIROX CO., LTD., Japan) was used to scan the surface before and after pre-treatment to obtain contour information.

Abrasive blasting was performed using a dry blasting system. The abrasive is ejected from a nozzle with a diameter of 10 mm, and the air pressure at the nozzle reaches 0.7 MPa. The distance between the nozzle mouth and the target surface was fixed at 30 cm, and the angle between the target surface and the nozzle was set at 60°. The abrasive shot on the target surface at high speed, which were enough squeezes and cuts the rust layer and steel substrate, and achieves the purpose of cleaning. As shown in Figure 0-3, when the nozzle is not moved, the surface within a certain range of the nozzle center is efficiently impacted and cleaned by abrasive, and this part is called the treated area. Although the outer area is impacted by some abrasives, the treatment effect is very poor, which is called the affected area. Under the blasting parameters settle as above mentioned, the radius of

the treated area is about 10 cm. The abrasives used in this study were garnet and fused alumina, all the abrasives are sieved identically with the same particle size of about 430 μm. Garnet was used as the abrasive for the beginning of blasting cleaning, and fused alumina was used as an additional abrasive for blasting due to its high price. The compositions of the two abrasives is shown in Table 0-2. The new Mohs hardness of garnet and fused alumina is 7.5 and 12 of 15, respectively. To control the uniformity of abrasive blasting for different specimens, the same blast duration was used for each 150 mm x 70 mm specimens. Among them, garnet blasting lasted for 15-20 s, and the actual blasting efficiency was about 2 m^2/h, which was equivalent to 4-5 rounds of blasting in actual engineering. While the alumina blasting lasts for 5-10 s, and the efficiency is about 5 m^2/h, which is comparable to the two rounds of blasting in engineering.

Laser cleaning was performed using a 3 kW rotary CWL. The laser beam is refracted by a high-speed rotating prism and strikes the target surface in a circular trace, as shown in Figure 0-4(a). The laser ring moves on the target surface to achieve the laser cleaning by moving the laser transmitter, as shown in Figure 0-4(b). The basic parameters are shown in Table 0-3. The laser parameters were determined to ensure that the laser transmitter was safe, stable, and easy to use in engineering, and to ensure that the inside and outside of all corrosion pits on the target surface could be similarly treated for quality control purposes. In this study, the focal depth and focal length were 20 and 200 mm, respectively, and the rotation speed of the prism was controlled at 5000 rpm. The diameter of the laser ring was controlled at 26 mm, which was sufficient to cover commonly sized corrosion pits. Under this setting, the moving speed of the laser spot could reach 680 cm/s. The interaction time was defined as the time when the laser spot moved out of its diameter, which was 63.2 μs. The average energy density of 3 kW CWL spot can reach 2070 kW/cm^2, which is sufficient to ablate a thin rust layer and even remelt the shallow steel substrate during the interaction time. To make the laser energy density and thermal density uniform across all irradiated areas of the cleaned surface, the overlap ratio of the laser spot and laser ring was set to 50%[29,71], as shown in Figure 0-4(c). Under this setting condition, the efficiency of 3 kW CWL cleaning was 0.84 m^2/h every round. For the specimens with different degrees of corrosion, one to four rounds of laser irradiation were carried out to determine the number of irradiation rounds required to clean the corrosion products under different degrees.

Table 0-2 Composition of garnet abrasive

Composition (%)	SiO_2	Al_2O_3	Fe_2O_3	CaO	MgO	TiO_2
Garnet	35–40	20–25	30–35	1–2	5–7	0.1–1
Fused alumina	<1	>95	<0.3	-	-	2-4

Table 0-3 Laser processing parameters

Parameter	Value	Units
Output	3	kW
Spot diameter	430	μm
Focal depth	20	mm
Focal length	200	mm
Motor speed	5000	rpm
Irradiation ring diameter	26	mm
Spot irradiation speed	680	cm/s
Interaction time	63.2	μs
Power density	2070	kW/cm^2
Cleaning efficiency	0.84	m^2/h

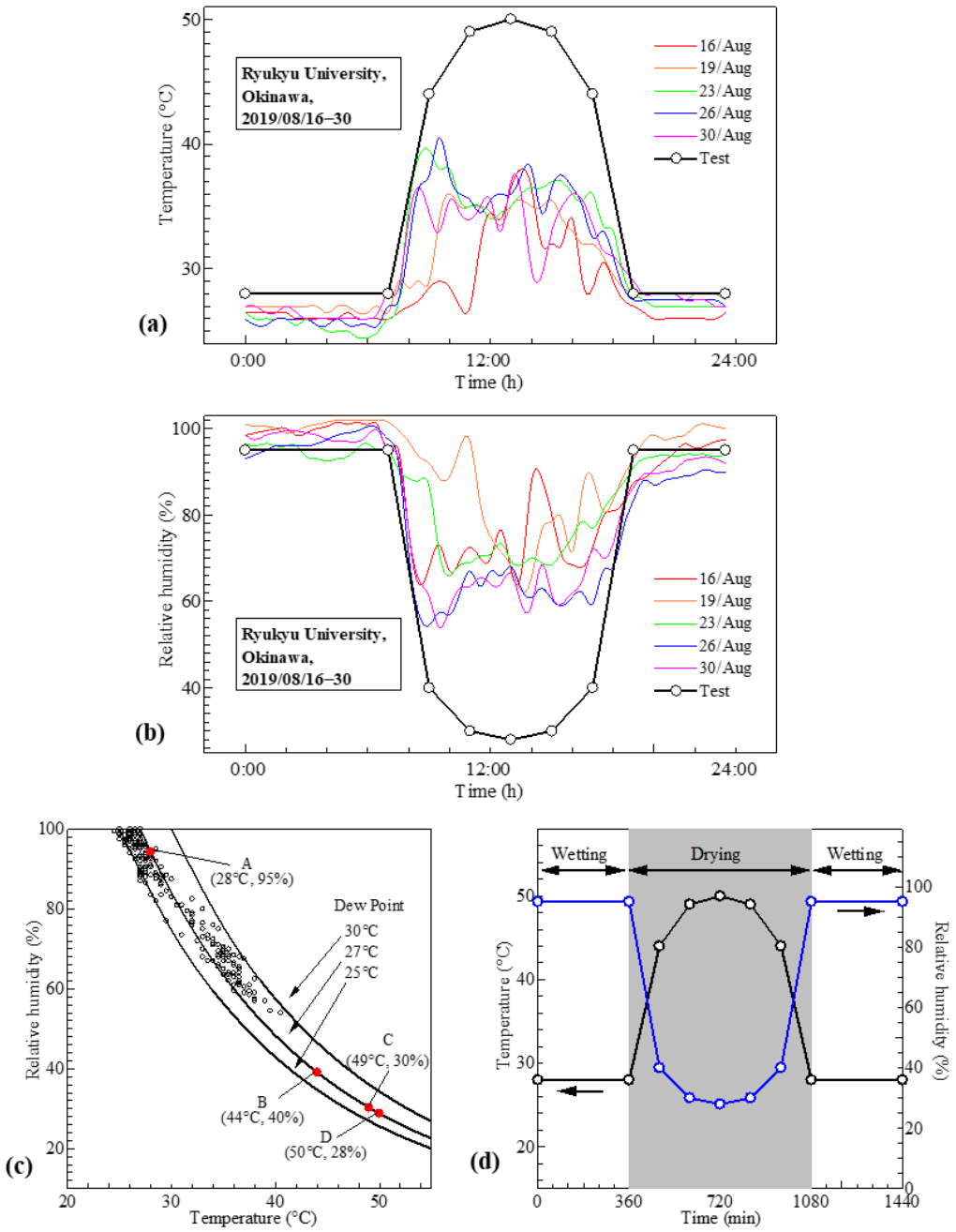

Figure 0-2 Accelerated corrosion test data from Okinawa in the summer (August 16-30, 2019): (a) daily temperature change, (b) daily humidity change, (c) daily dew point change, and (d) wet and dry cycle used for accelerated corrosion

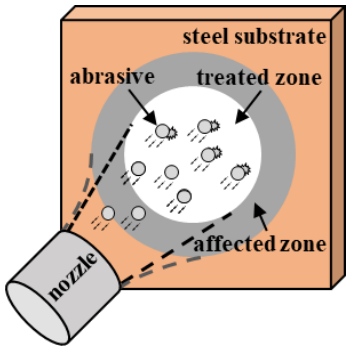

Figure 0-3 Schematic of abrasive blasting

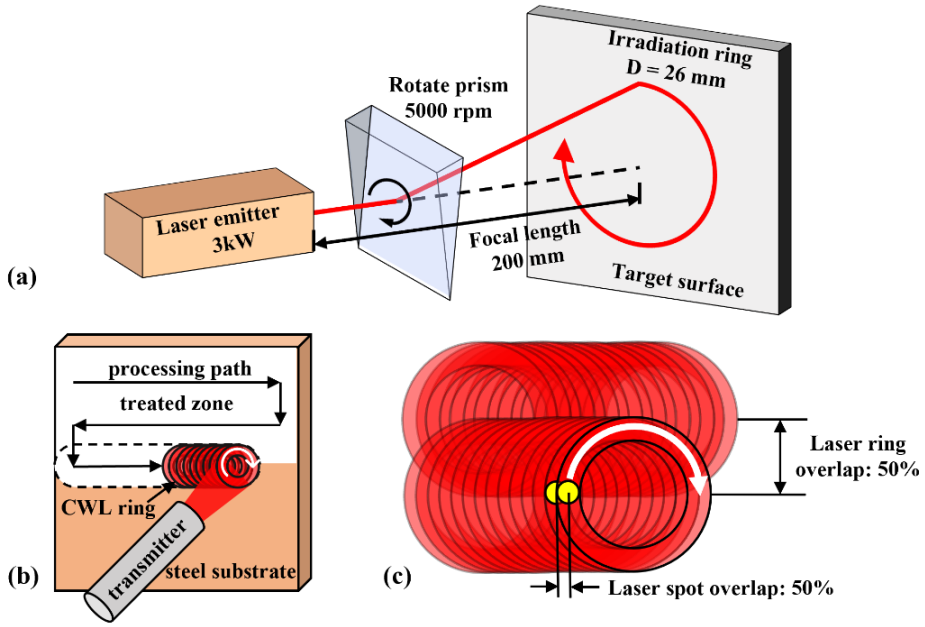

Figure 0-4 Schematic of a rotating CWL: (a) formation of a laser ring by rotating prism refraction, (b) sweep path of laser ring, and (c) overlap rate of laser ring

1.11 Surface characteristics of corroded specimens after surface treatment

1.11.1 Surface characteristics before and after pre-treatment

After one year of constant dew point corrosion acceleration, the specimens with three different salt deposit amounts have been corroded to different degrees and with different macroscopic characteristics, as shown in Figure 0-5. In the 10 mg/m^2 and 100 mg/m^2 salt deposition conditions, almost all corrosion surfaces showed brown and red granular corrosion products on the surface, but no apparent rust stratification. This corrosion condition can be defined as general corrosion. These two kinds of salt deposit ranges naturally occur in urban and coastline environments[97]. In the 1000 mg/m^2 salt deposited condition, the surface rust has a large orange-red and brown-red rust area. Moreover, there are apparent corrosion layers that are loose and easy to peel off. The corrosion degree has reached severe corrosion. This high concentration of salt deposits often occurs in coastal structures that are hard to wash by rain and structures where deicing salts are often used. The thicknesses of the rust layers in the corrosion pits for the 10 mg/m^2 and 100 mg/m^2 and 1000 mg/m^2 salt deposits conditions were 78 (±18), 120 (±29), and 816 (±230) μm, respectively. The measurements were performed in 10 artificial pits using an electromagnetic film thickness meter.

Figure 0-6 shows the surface state after pre-treatment. It can be seen that the cleaning ranges of the three pre-treatment methods are different. The ability of steel brush pre-treatment (left area) to remove rust is very limited. The steel brush can only remove the loose rust layer and granules from the outermost layer. The rust removal effect of electric tools was more effective than that of hand tools. The cup wire can remove the rust layer outside most of the corrosion pits (middle area), exposing a relatively smooth steel substrate. However, because of the size and shape of the cup wire, the innermost rust layer at the bottom of the corrosion pits could not be completely removed. In particular, for severely corroded steel components, conical corrosion pits are often deep and accompanied by secondary corrosion pits. The power tool with a diamond grinding disc has several times the pre-treatment efficiency compared to cup wire; however, limited by the shape of the diamond grinding disc, the rust inside the corrosion pit can hardly be removed (right area). Moreover, it can have a polishing effect on the steel substrate surface. According to Hashimoto, more than 70% of the corroded areas can be polished by a diamond disc[102,103]. The remaining part is the

corrosion pit, which contains many corrosion products and salts and is the main target cleaning area in this study. In this study, the diamond disc successfully polished the entire area outside the corrosion pit, leaving only the corrosion products in the corrosion pit for laser irradiation and analysis.

Figure 0-7 shows the 3D contour of the surface of the specimen exposed to salt deposit amounts of 1000 mg/m^2 after the surface was scanned by a digital microscope before and after pre-treatment. The sectional contour of the center of the corrosion pits was selected at the same position as that in Figure 0-6. After different pre-treatments, the surface contour changes of the three different corrosion degree specimens are shown in Figure 0-8. It can be seen that, in the case of 1000 mg/m^2 salt deposition, different pre-treatment can significantly change the thickness of the remaining rust layer in the corrosion pit, and the residual rust layer after pre-treatment still reaches hundreds of microns. It should be noted that in the case of such high salt deposition, the large corrosion pits are usually accompanied by secondary corrosion pits; therefore, the actual thickness of the rust layer is greater than the estimated thickness. For the slightly corroded specimens, the effect of the pre-treatment was limited. The effect of pre-treatment is only to remove surface particles that are easily shed. The thickness of the rust layer to be cleaned in the corrosion pit was 100 μm when the salt deposits were 10 mg/m^2 and no more than 200 μm when the salt deposits were 100 mg/m^2. The rust is attached to a steel substrate and is usually dense and protective for weathering steels.

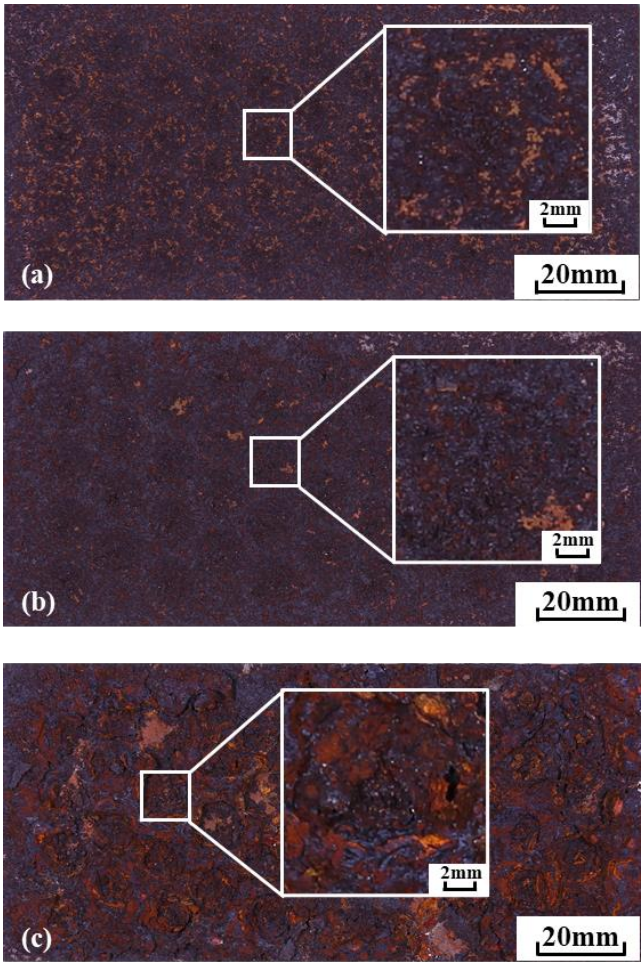

Figure 0-5 Macroscopic characteristics of the surface of three specimens whose pits were exposed to salt deposits conditions of (a)10 mg/m^2, (b)100 mg/m^2, and (c)1000 mg/m^2

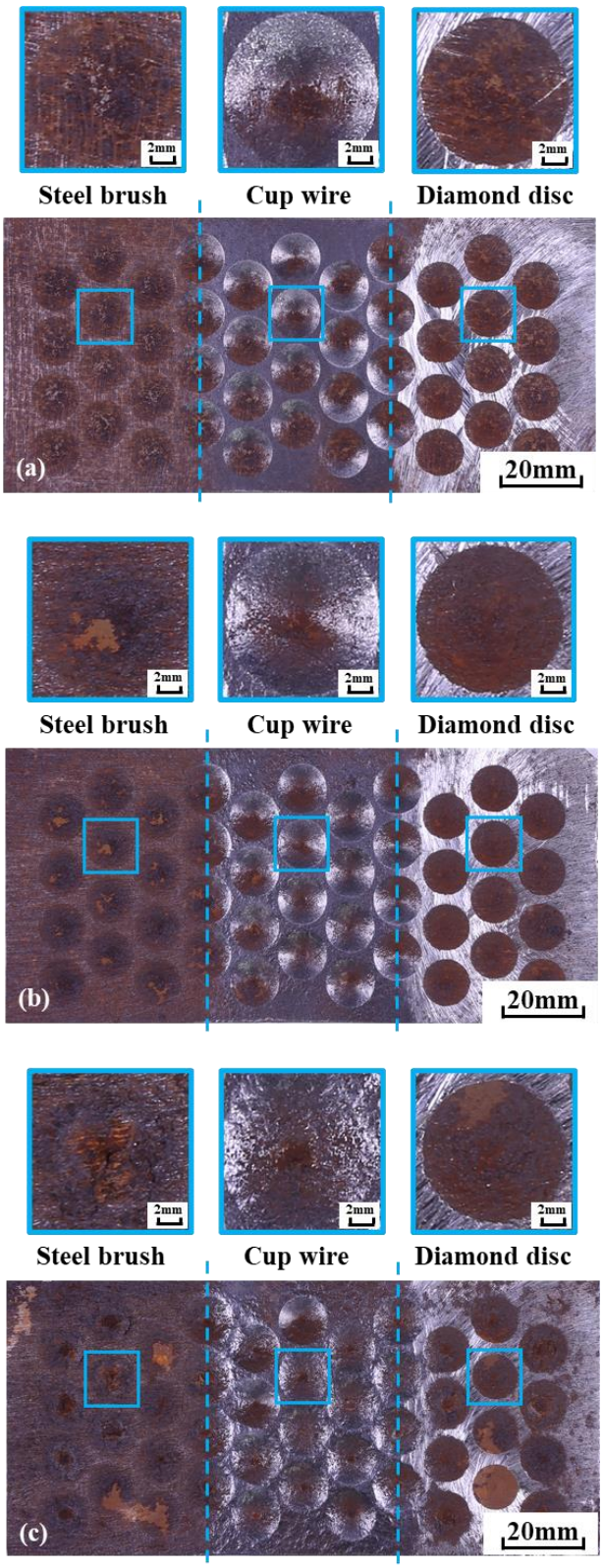

Figure 0-6 Macroscopic characteristics of the surface of three different corrosion grades specimens after pre-treatment with salt deposit amounts of (a)10 mg/m^2, (b)100 mg/m^2, and (c)1000 mg/m^2

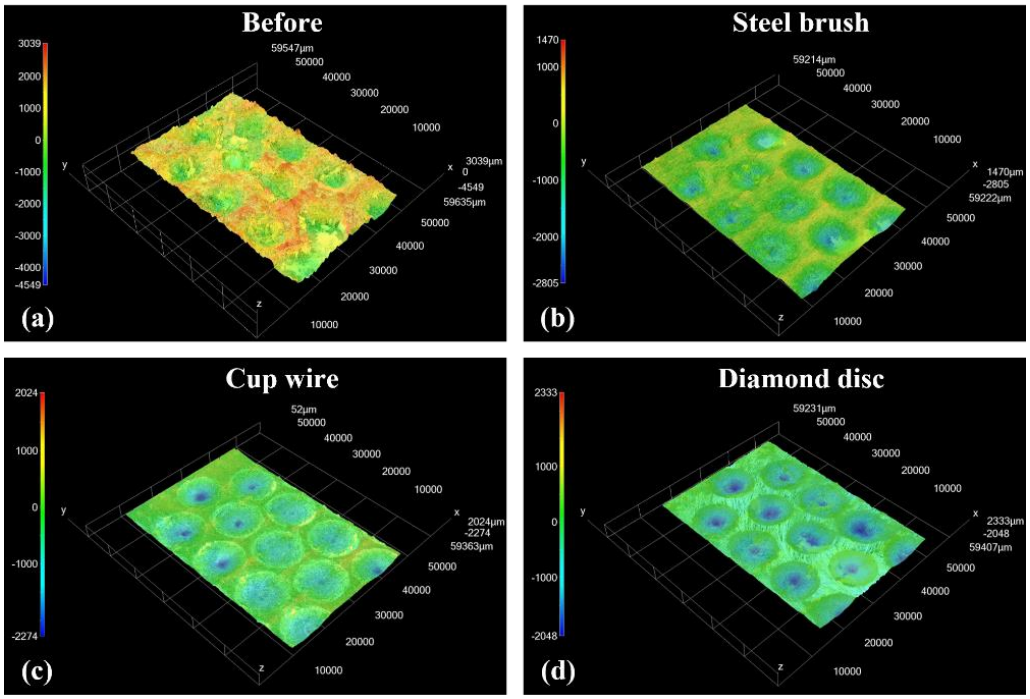

Figure 0-7 3D contour of severely corroded specimen (a) before pre-treatment and after pre-treatment with a (b) steel brush, (c) cup wire, and (D) diamond disc

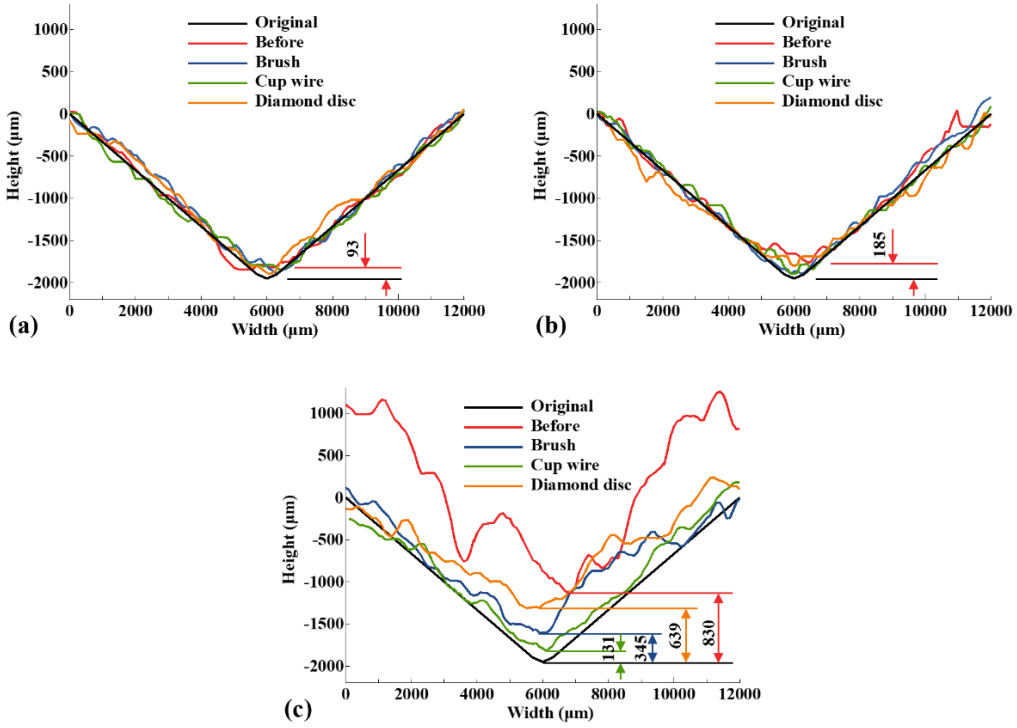

Figure 0-8 Comparison of the rust layer profile before and after pre-treatment of three different corrosion degree with salt deposit amounts of (a)10 mg/m^2, (b)100 mg/m^2, and (c)1000 mg/m^2

The corrosion products from these three types of specimens are collected using a steel brush,

and the rust layer's main composition is analyzed by XRD. The spectra of the rust composition calculated by the Reference Intensity Ratio (RIR) method are drawn in Figure 0-9 and listed in Table 0-4. The protective ability index of the composition of the rust layer calculated through equations (1)–(3) can be used to evaluate the anti-corrosion effect of the rust layer on the weathering steel surface [61–63]. The calculation results are listed in Table 0-5. The corrosion surface of the 100 mg/m^2 salt deposit amount is in the critical corrosion layer protection state. When the weathering steel loses the protection of the dense rust layer, the corrosion rate increases rapidly.

$$\alpha/\gamma = mass\%\ \alpha - FeOOH / mass\%\ \gamma - FeOOH \quad (1)$$

$$\alpha/\gamma^* = wt\%\ \alpha - FeOOH / (wt\%\ \gamma - FeOOH + wt\%\ \beta - FeOOH + wt\%\ Fe_3O_4) \quad (2)$$

$$\alpha^*/\gamma^* = (wt\%\ \alpha - FeOOH + wt\%\ Fe_3O_4) / (wt\%\ \gamma - FeOOH + wt\%\ \beta - FeOOH) \quad (3)$$

Table 0-4 Composition ratio of corrosion products

Composition	Weight ratio (%)		
	10 mg/m^2	100 mg/m^2	1000 mg/m^2
α-FeOOH	19.0	41.0	43.0
Fe3O4	34.0	10.0	2.70
γ-FeOOH	24.0	22.0	38.0
β-FeOOH	2.00	13.0	7.30
Fe2O3	16.0	13.0	8.80
others	5.00	1.00	0.20

Table 0-5 Calculated protective ability index

Index	Salt deposits amount (mg/m^2)		
	10	100	1000
α/γ	0.79	1.86	1.13
α/γ*	0.32	0.91	0.90
α*/γ*	2.04	1.46	1.01

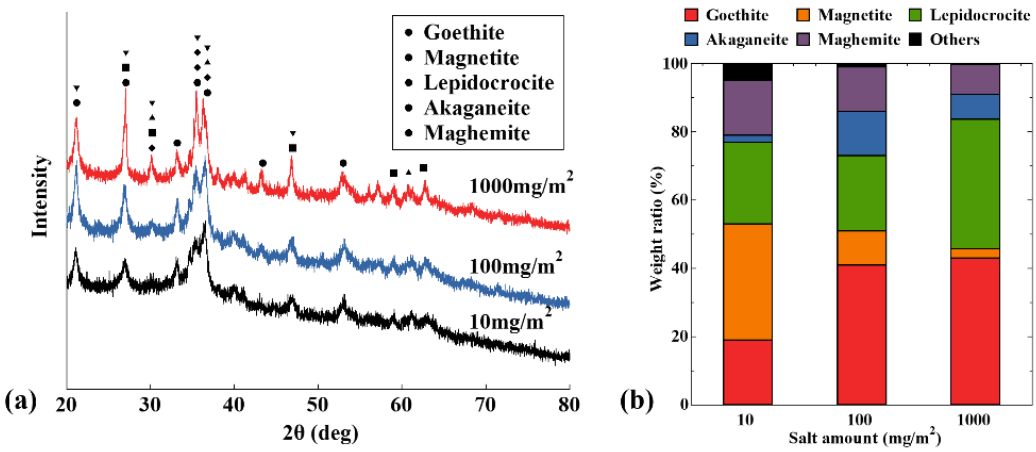

Figure 0-9 Corrosion product powders' (a) XRD spectrum and (b) the ratio of product composition

1.11.2 Surface characteristics after abrasive blasting surface treatment

Abrasive blasting was carried out after pre-treatment. In the first round of blasting, garnet, which with lower hardness was used as abrasive. After garnet blasting for 20 s, the surface of the general corrosion specimens can reach the level of Sa 3, as shown in Figure 0-10(a). However, severely corroded specimens can only reach the level of Sa 2.5, as shown in Figure 0-10(b). Due to the appearance of secondary corrosion pits and the limitation of blasting angle, some shadow parts in corrosion pits cannot be cleaned directly, and there are rust residues. The second round of blasting was completed a week later after the specimens re-rusted. The higher hardness fused alumina abrasive was used in this round, and the treatment duration was controlled in 10 s. As shown in Figure 0-10(c), the surface of generally corroded steel is still cleaned to the level of Sa 3. In the corrosion pits of severely corroded samples, the shadow and residual rust also decreased significantly, as shown in Figure 0-10 (d). The harder fused alumina is more effective at removing stubborn rust. The third round of blasting was also carried out a week later by alumina. As can be seen from Figure 0-10 (e) and (f), after three rounds of blasting, the severe corrosion can reach the same Sa 3 level as the general corrosion, and the rust in the corrosion pit and secondary corrosion pit is also completely removed.

It should be noted that the cleanliness of the blasted surface does not seem to be significantly related to the pre-treatment. After 20 s of garnet blast (GB) treatment there is almost no visible rust

residue on the surface. Only in severely corrosion pits' cleaning, the effect of diamond grinding disc as pre-treatment tool is worse than other pre-treatment tools, especially cup wire. The residual rust in the secondary corrosion pit appeared in the pre-treatment area of diamond grinding disc, while the rust in the secondary corrosion pit pre-treated by cup wire was completely removed, as shown in Figure 0-10(f). Therefore, it is recommended that when abrasive blasting is used for the final cleaning, the residual rust layer in the corrosion pit should be avoided as much as possible. It is recommended to use cup wire type pre-treatment tools.

1.11.3 Surface characteristics after laser surface treatment

Laser surface treatment is carried out after pre-treatment. The laser transmitter is fixed during the process. The specimens were placed on an X-Y direction stage to move at a fixed speed along a preset re-entry route to ensure that the irradiation at each position of the specimens was the same. The surface's macroscopic image after laser irradiation is shown in Figure 0-11. It can be seen that several transverse stripes appeared on the surface of the steel plate, and the high irradiation energy density caused edge tracing at the top of the laser ring during its movement [66]. All parts of the target surface are scanned by the laser spot under the overlapping irradiation of the laser ring. Except the laser ring coverage of the bottom strip is 0%, the overlap rate of other parts is 50%. Only corrosion pits with 50% overlap rate were examined to analyze the cleanliness of the artificial pits. For each pre-treatment condition, ten corrosion pits are included for discussion.

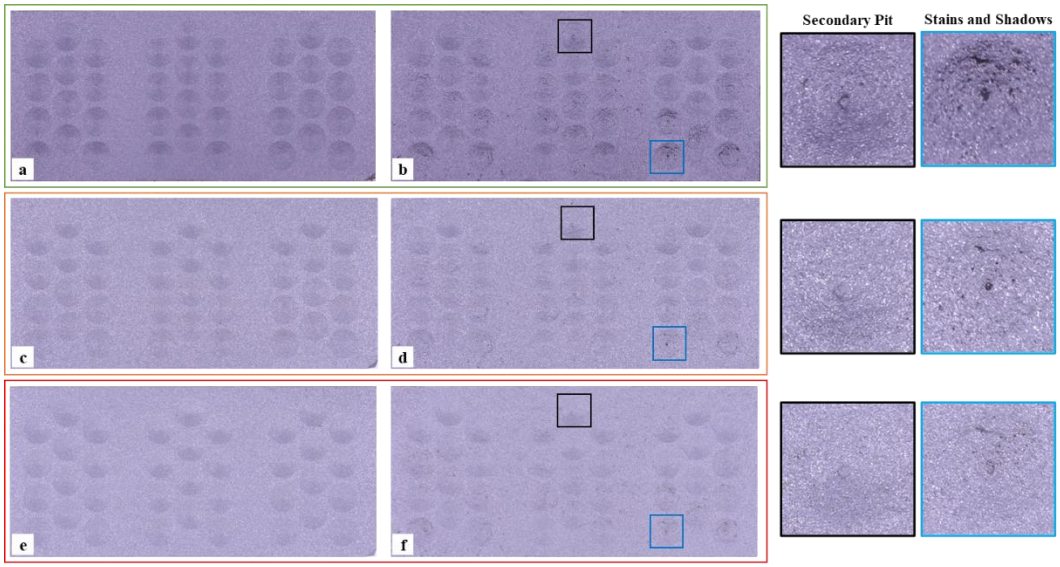

Figure 0-10 Macroscopic characteristics of the surface after abrasive blast treatment of (a, b) 1st round with garnet blasting, (c, d) 2nd round with alumina blasting, and (e–h) 3rd round with alumina blasting

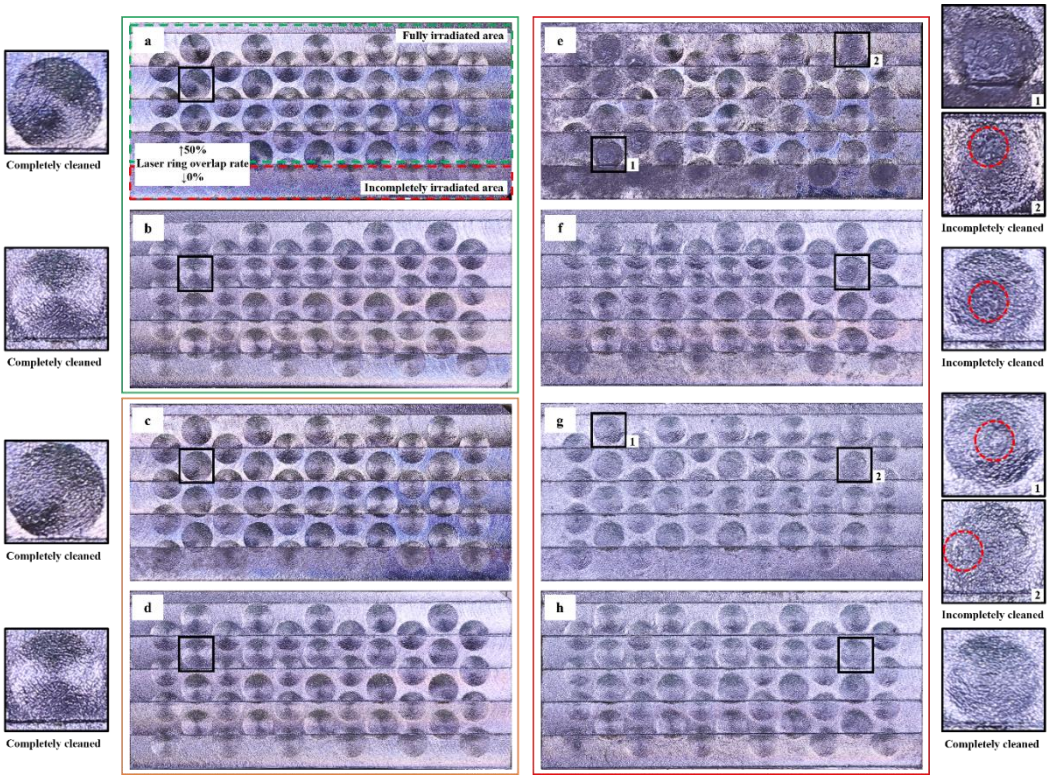

Figure 0-11 Macroscopic characteristics of the surface after laser treatment, with salt deposited amount of (a, b)10 mg/m^2, (c, d)100 mg/m^2, and (e–h)1000 mg/m^2

By visual observation, a single round of laser irradiation can completely remove the rust layer under general corrosion conditions, regardless of pre-treatment conditions. The inside and outside of the artificial corrosion pit are blue, and there is no visible corrosion product residue inside the corrosion pit. However, in the case of severe corrosion, the rust in the corrosion pit cannot be cleaned at one time. As shown in Figure 0-11(e), there is an apparent color difference inside and outside the artificial pit after one laser irradiation. In the areas pre-treated by steel brushes and diamond grinding discs, dark gray rust buds appear inside the corrosion pits, which have not been completely ablated and evaporated. The area pre-treated with the cup wire has better cleaning, but some pits remain as rust buds. In the first round of laser cleaning, the laser directly irradiated the rust and most of the laser energy was absorbed by the rust layer. However, for thick rust layers, the ability of the laser to remove rust remained limited, and it was difficult to ablate a rust layer of hundreds of microns in a single round. Under the premise that the laser parameters cannot be changed, multiple repeated laser irradiations are required to obtain ideal cleanliness of the surface. As shown in Figure 0-11(f)–(h), the severely corroded steel plate requires two to four rounds of irradiation. As the number of laser irradiation increases, the color inside and outside the corrosion pit gradually becomes the same. The apparent corrosion product residue was gradually removed with multiple irradiations. After four rounds of laser irradiations, the presence of the residue was almost not visually detectable.

1.12 Turning time test

Visual observation can be used to subjectively assess the degree of rust removal; however, the effectiveness of salt removal is not known. Insufficient salt removal is one of the main causes of flash rust, re-corrosion, and damage to coatings. There are many methods for surface analysis, including SEM/EDX, Raman spectroscopy, FT-IR spectroscopy, XRD, etc. These scientific analysis methods can be used to distinguish composition combinations, element combinations and functional groups, and can accurately identify rust and salt and other substances that cause re-corrosion. However, these methods have many limitations in surface cleanliness analysis, especially in salinity removal analysis. When the surface is visually clean, it is difficult to find and observe residual salt on the surface using the methods described above, which is largely limited by the observed area. Therefore, the results obtained are not sufficient to describe the overall condition of the surface.

Some engineering salt detection methods are usually more practical. Such as gauze wiping method, water breaking method, conductivity method and Bresle method. Due to the random nature of salt distribution and the dissolution rate of attached salts, these methods are usually only used as a reference and do not provide very accurate values. Among them, Bresle method is the most commonly used method, which is often used for the determination of surface residual soluble salts. However, this method does not help to know where the salt remains, nor can it obtain information about the insoluble salt and the inherent salt.

Because corrosion is a time-dependent change, this study proposes an objective cleanliness inspection method called the turning time method. The time interval between the completion of the surface cleaning work and the occurrence of re-corrosion is defined as the turning time. Cleaned surfaces have higher surface activity, and when exposed to the atmosphere and residual rust and salt on the surface, re-corrosion can occur in a short time. Therefore, the effects of rust and salt removal can be evaluated based on the length of the turning time.

In this study, to investigate the cleanliness of the cleaned surface, the turning time test was carried out under a fixed temperature and humidity environment. The set temperature and humidity are 30°C and 90% RH, respectively, which is the average temperature and humidity in Okinawa Island in summer and is maintained at a dew point of about 27°C, the same as in the accelerated cycle of constant dew point corrosion. The environmental conditions were simulated within hours after surface treatment. For weathering steel, under that fixed high temperature and humidity environment, it is difficult for corrosion products to form a dense corrosion layer to inhibit corrosion[104]. Moreover, in the constant temperature and humidity oven, the salt from the external environment is avoided. This is close to the semi-enclosed environment during cleaning engineering. The occurrence of re-corrosion can accurately show the residual rust and salt position of weathering steel after CWL cleaning, whereas the rate and area of re-corrosion show the amount of salt residue. The turning time test with a fixed temperature and humidity lasted for 15 days to provide sufficient time for residual salts to cause corrosion. The specimens were observed at intervals of one hour, two hours, four hours, 24 hours, seven days, and 15 days. Digital photos were taken to record the surface state at each time interval under different pre-treatment conditions.

1.12.1 Turning time test of blasted specimens

Abrasive blasting cleaned surfaces have high surface activity. Surfaces that come into contact with or have residual salts will quickly corrode in the atmosphere environment. As shown in the Figure 0-12, the surface changes of generally corroded and severely corroded specimens within one week after GB. It can be seen that although the blasted surface was able to achieve Sa 2.5 or 3 levels, the entire surface was rusted after an hour. For general corrosion specimens, the area of rust is small and show color of orange. The corrosion area is negligible even after acceleration corrosion for one day. Even after 24 h, the whole surface can still maintain Sa 2.5 equivalent level. Under the condition of accelerated corrosion for a week, rust will continue to grow and brown rust will appear on the surface. The surface level at this point is a lower level of Sa 2. However, for severely corroded specimen, the rust removal effect of GB is not good. After 20 s of blast by garnet, there are still rust stains in the secondary corrosion pit that cannot be removed, and the surface can only reach the level of Sa 2.5. After one hour of accelerated corrosion, a large number of rust stains can be seen on the surface. These rust stains turn brown and the surface level has been reduced to Sa 2 level, which is not suitable for painting. After 4 h, the rust on the surface was clearly visible, and almost the whole surface was covered by rust layer. After seven days of corrosion, the entire surface is covered with reddish brown granular rust. Even if the surface cleaned by GB can reach the level of Sa 2.5, the coating on this surface has the tendency of re-corrosion under the coating.

In engineering, higher hardness fused alumina is often used for subsequent blasting to remove as much stubborn rust as possible. In cases of severe corrosion, this is usually accompanied by a high-pressure water gun washing for salt removal. As shown in Figure 0-13, after multiple rounds of blasting, the rust in the corrosion pit is removed, and the cleaned surface can reach the level of Sa 3. In the accelerated corrosion process, it was found that the area of re-rust was significantly reduced after the second round of alumina blasting (GAB), and only part of the secondary corrosion pits were not completely cleaned, as shown in Figure 0-13, and brown rust still residue in tiny corrosion pits. The treated surface was able to maintain the level of Sa 2.5 within 4 hours. The corrosion condition after one day and one week is obviously improved compared with that after a round of blasting, and the surface brown rust area is obviously reduced. The second round of

alumina blasting greatly reduces the possibility of re-corrosion under coating. After the third round of alumina blasting (GAAB), the rust in the secondary corrosion pit is almost completely removed, and the surface rust after turning time is mostly orange flash rust. The whole surface can reach the level suitable for painting.

The blast cleaned surface shows metallic gray, with a distinct color difference from the rusty orange and brown. Therefore, the area of re-rusting by color picking and calculating can be used as a method to evaluate salt residual degree. In painting engineering, hope that the surface salt content is less than 50 mg/m^2 before painting[105]. In this study, ultrasonic salt spray device[106] was used to prepare a control group with 50 mg/m^2 surface salt content for comparison. The particle size of the attached salt was not more than 10 μm on the surface, as shown in Figure 0-14. The reference group and the cleaned specimens were subjected to turning time test together. ImageJ software was used to pick up the rust layer on the specimens and calculate the proportion of re-rust, as shown in Figure 0-15. By drawing the relation curve of re-rusting area-time and comparing the reference group, the information of residual salt can be obtained.

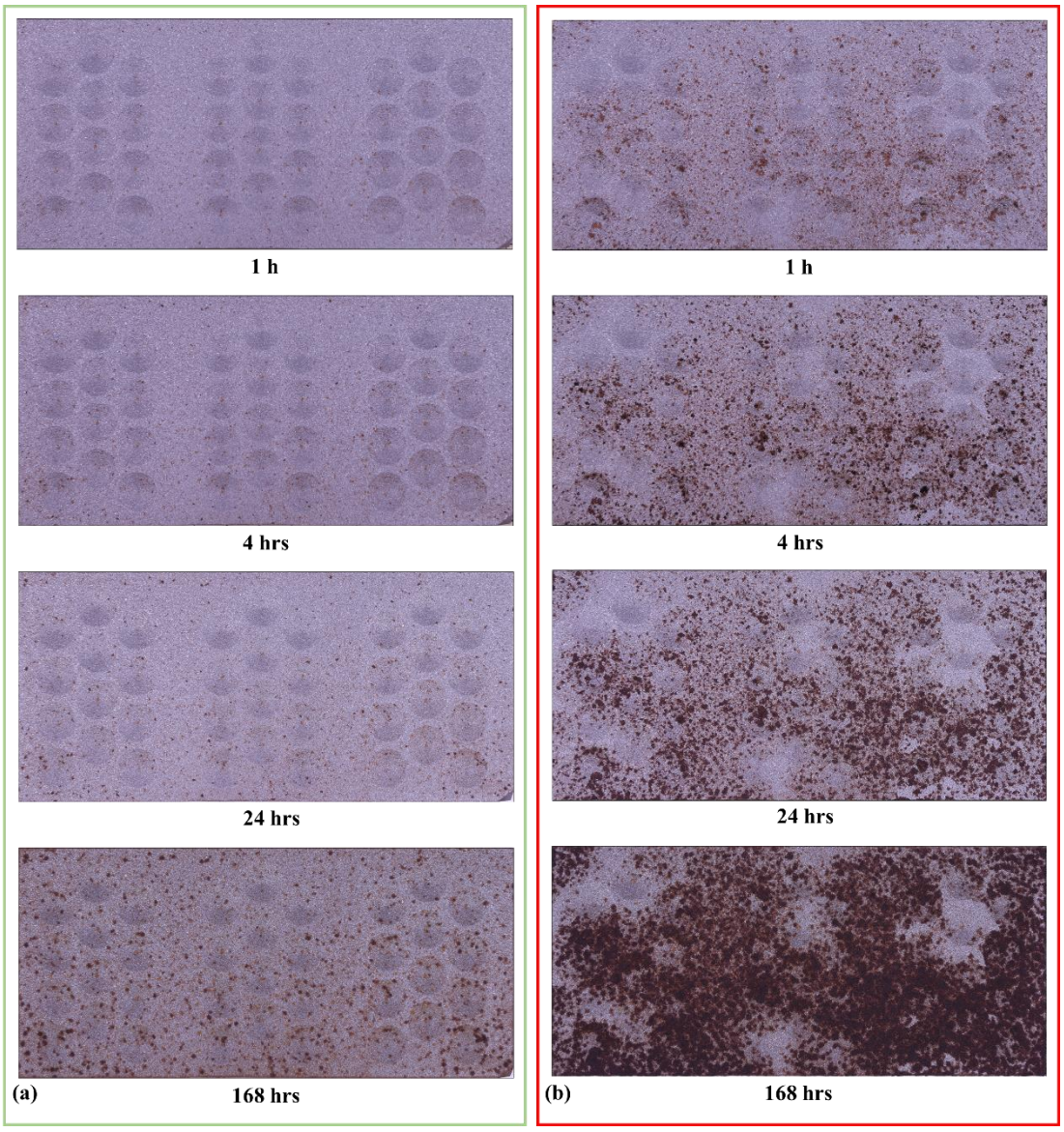

Figure 0-12 Turning time test specimens of (a) general corrosion and (b) severe corrosion

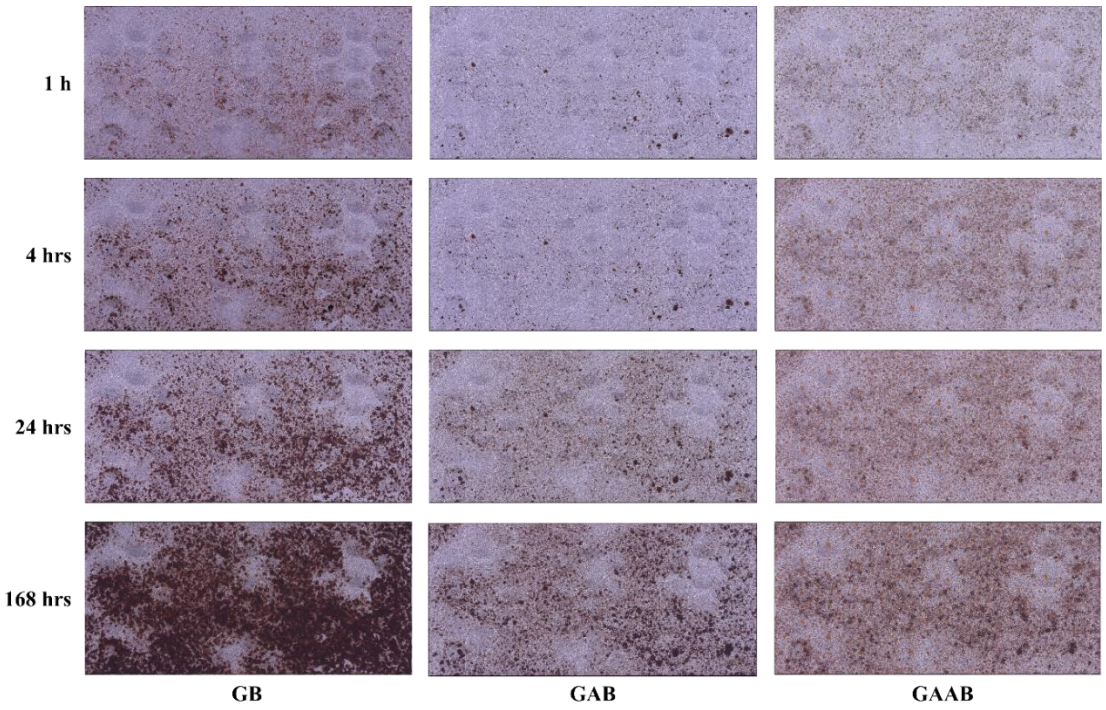

Figure 0-13 Turning time test of severely corroded specimens after different abrasive blast treatment

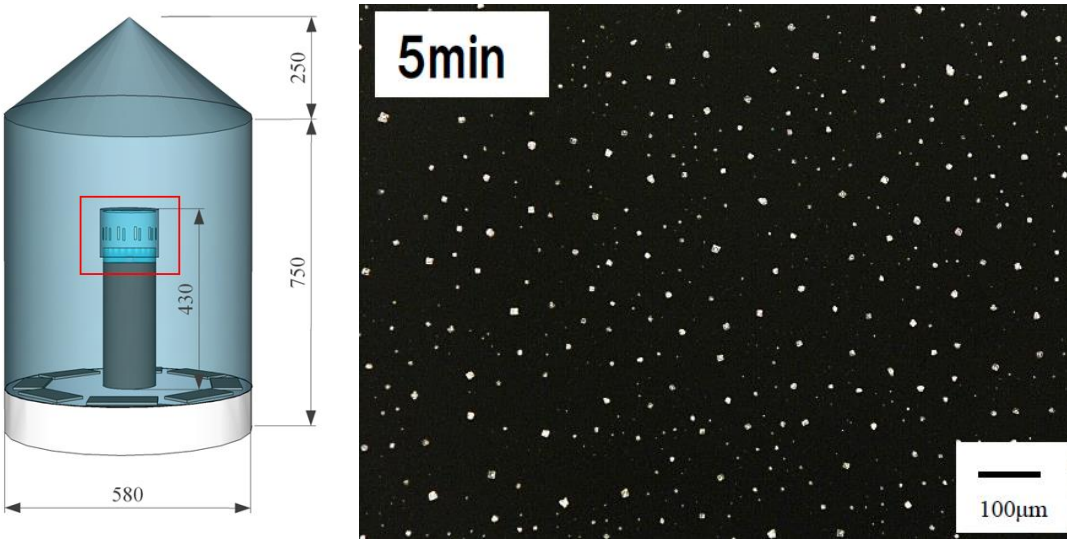

Figure 0-14 Ultrasonic salt spray device and the characteristic of surface adhesion salt

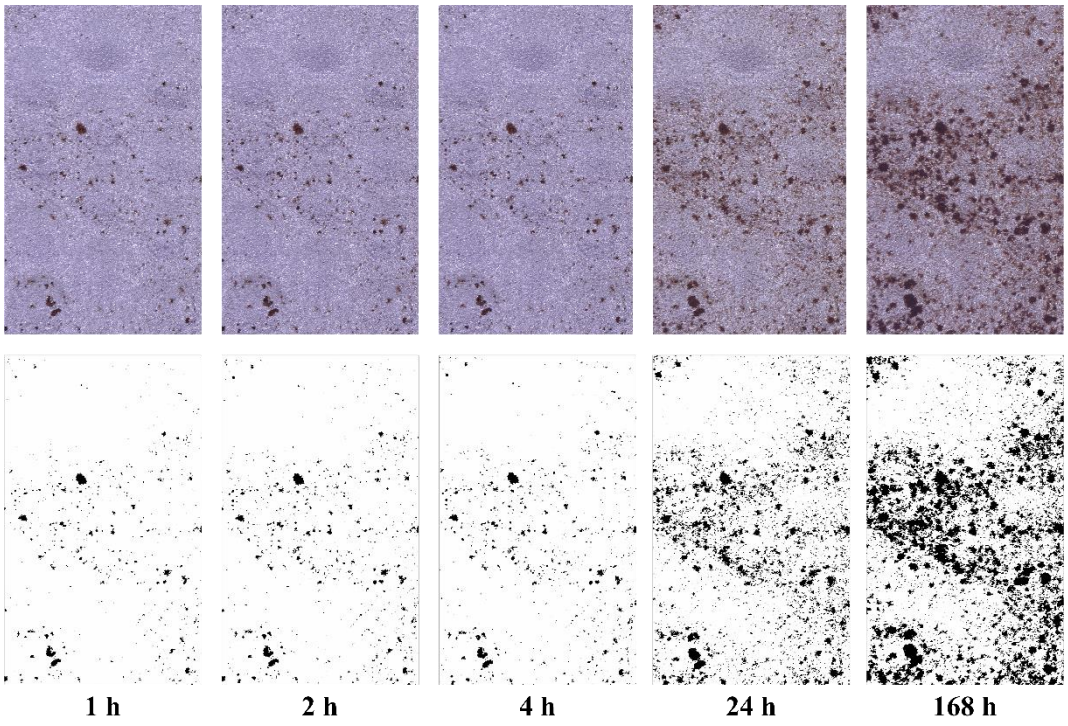

Figure 0-15 Schematic representation of the re-rusted area extracted using ImageJ

As shown in Figure 0-16, the time variation curve of the area of re-rust on the blasted surface of three rounds is drawn. It is found that under the condition of general corrosion, only GB can clean the surface to the level suitable for painting. In the case of severe corrosion, multiple rounds of blasting are necessary. After the blasting of alumina, the re-rust area decreased significantly and fell below the reference group. However, after a long conversion time test, the rust still continued to grow and exceeded the re-rusting area of the reference group, which indicated that the rust and salt components remaining in the corrosion pit could not be ignored, and corrosion under painting was likely to occur. The situation still cannot be resolved after three rounds of blasting. As mentioned above, the duration of abrasive blasting in this study may be longer than that in the actual project, so more times may be required in the actual project, resulting in cumbersome process and increased cost. Therefore, it is recommended to use other surface treatment methods to clean the severely corroded parts.

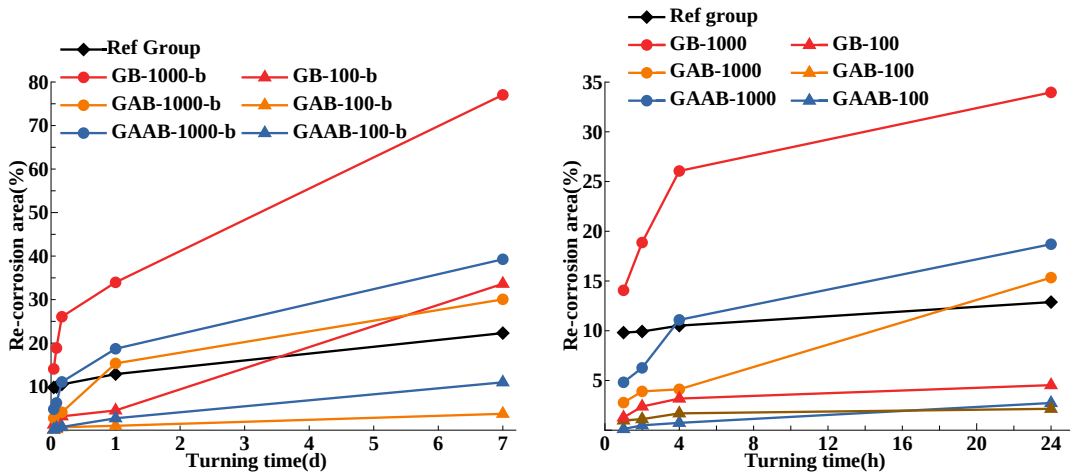

Figure 0-16 The ratio of the re-rusted area to the total area in the turning time test

1.12.2 Turning time test of laser ablated specimens

For the laser treated surface, due to the presence of oxide film and the influence of laser trajectory, the surface color has a certain difference. The color of the laser treated surfaces undoubtedly affects the calculation of the area ratio of the re-rusted layer. Therefore, during the turning test of laser cleaning, the proportion of re-rusting of pits are counted to discuss cleanliness effect.

All general corroded specimens were cleaned entirely after a single round of laser irradiation. There is no rust on the cleaned surface even after 15 days in the high temperature and humidity environment, as shown in Figure 0-17. It can be inferred that one round of irradiation with a 3 kW CWL is sufficient for full ablation and cleaning of a thin rust layer with a thickness of less than 200 μm. Therefore, surface pre-treatment is not even necessary before laser cleaning in the case of general corrosion.

However, for the case of severely corroded condition, the phenomenon of re-corrosion after laser treatment is remarkable in the absence of sufficient laser irradiation, as shown in Figure 0-18. The calculated conclusions are drawn in Figure 0-19. Under the condition of only single-time irradiation, 70%~80% of the artificial pits in the pre-treatment area of steel brushes and diamond grinding discs were re-corroded within 1 h, and all pits were re-corroded in 24 h. For the cup wire pre-treated area, the rate of re-corrosion is 50% in an hour. Remarkably, after two weeks, 1/3 of the

artificial pits remained clean. More sufficient pre-treatment will help laser cleaning and reduce the necessary irradiation rounds. After two rounds of irradiation, almost all surfaces were thoroughly cleaned, especially the area cleaned by cup wire, and the turning time reached 24 h. Even though the specimens were kept in a high temperature and high humidity environment for a week, no more than 30% of the pits re-corroded. However, corrosion is random, even under similar conditions, and the level of corrosion may also differ. The thick and hard rust layer at the bottom of the corrosion pit, the influence of the secondary corrosion pit, and the thickness of the rust layer that needs to be cleaned will be different. In fact, there is no guarantee that only one or two rounds of laser irradiation can completely clean severely corroded surfaces. As shown in Figure 0-11 (g), the specimens irradiated three times still had some rust buds. In the turning time test, it was also found that specimens with more than 30% of the artificial pits' re-corrosion happened within one hour. However, this phenomenon was completely improved after four rounds of irradiation. The turning time of the surface was stabilized at approximately 4 h after four rounds of irradiation. Although rust can still be observed in the artificial pit, these rust areas are very small, even less than 1% of the pit. After 15 days, the probability of re-corroded pits does not exceed 20%. In this case, the entire surface can be considered to be sufficiently cleaned.

From the above tests, we can estimate that the rust removal range of each round of 3 kW CWL irradiation is approximately 200 μm. For samples subjected to severe corrosion conditions, pre-treatment can significantly reduce the thickness of the rust layer and reduce the required rounds of laser irradiation; however, the limitations of pre-treatment and economic efficiency must be considered during structural maintenance because the effect of pre-treatment on rust removal is not linear. To reduce the number of laser irradiation rounds, more time and labor costs would have to be invested, which would be uneconomical in some cases. The laser spot of the 3 kW CWL used in this study has a very fast moving speed, up to 680 cm/s, and the heat-affected zone on the target surface is only tens of microns[71]. Multiple rounds of laser irradiation have a negligible effect on the structure itself. Therefore, multiple rounds of CWL irradiation are recommended for cleaning severely corroded surfaces.

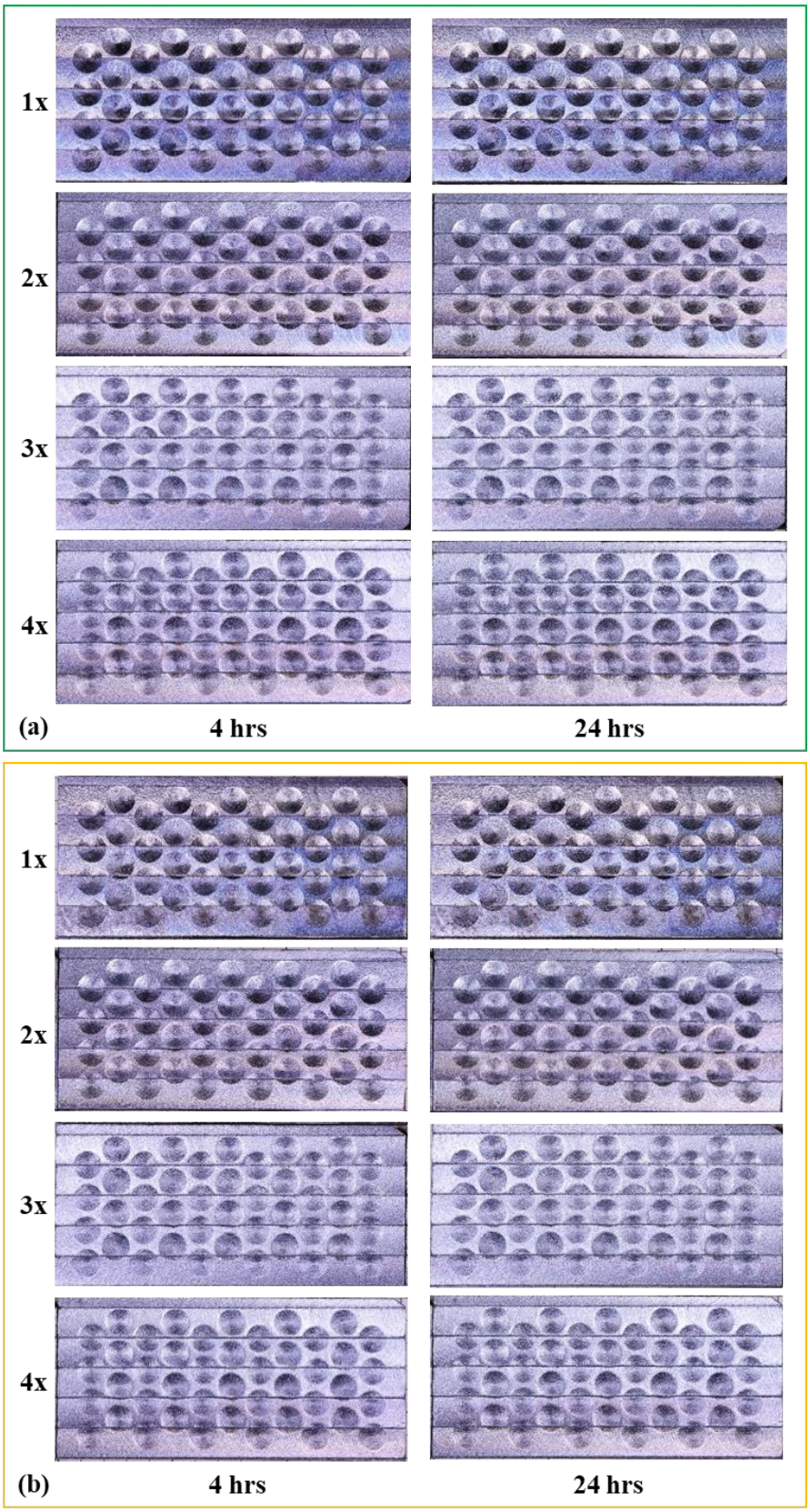

Figure 0-17 Macroscopic characteristics of the laser-cleaned surface of a specimen subjected to salt deposit amounts of (a) 10 mg/m^2 and (b) 100 mg/m^2 after the turning time test

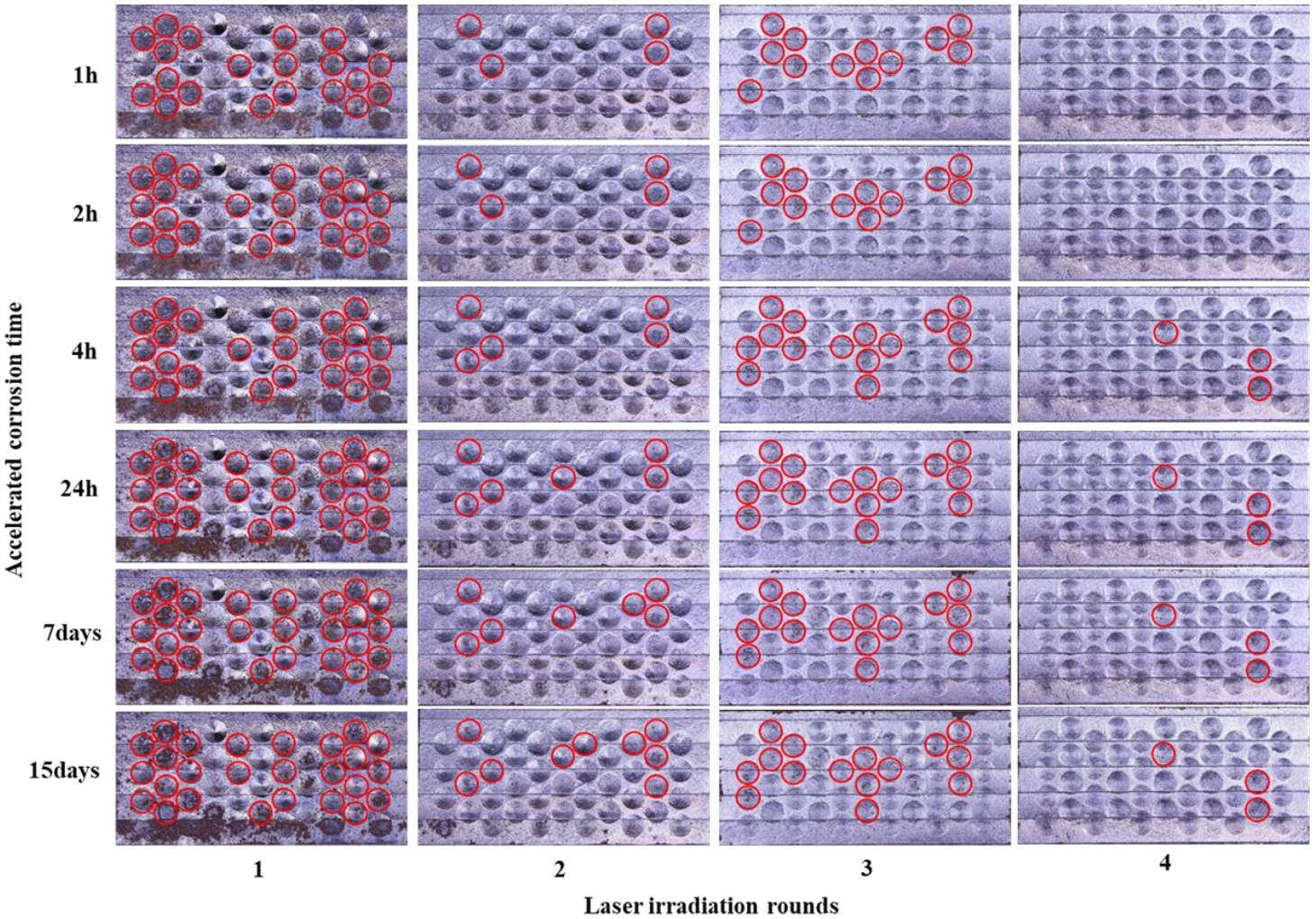

Figure 0-18 Macroscopic characteristics of the laser-cleaned surface of severely corroded specimen after the turning time test

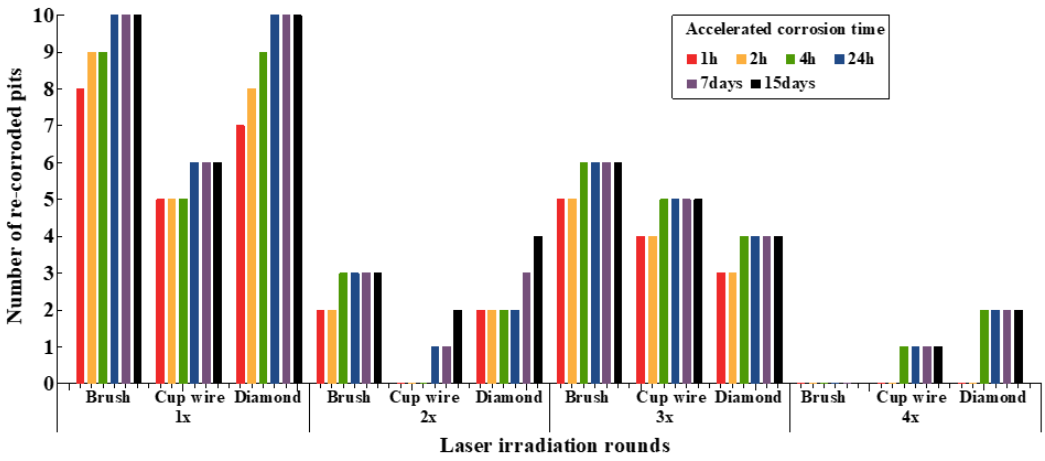

Figure 0-19 Occurrence rate of artificial pits re-corrosion on the surface of different treatment conditions

1.13 Summary

This chapter introduces the preparation method of artificial corrosion pit specimens. Introduced the common used pre-treatment tools, including steel brush, cup wire, and diamond disc, and its rust removal effect. Subsequently, the specimens were post-treated by using abrasive blasting and CWL with different rounds. The turning test, a new method based on image statistics, is proposed to discuss the cleaning effect of the mentioned combination methods. The conclusions are as follows:

1. The efficiency and rust removal ability of pretreatment tools are significantly different. For generally corroded steel components, the rust removal difference of pretreatment tools is negligible. For severe corroded steel components, diamond disc has the worst rust removal ability but the highest efficiency. Cup wire has the strongest rust removal ability, but the remaining rust layer is usually more than 100 μm.

2. The oxide formed on the surface of weathering steel is usually protective when the salt deposit is not more than 100 mg/m^2. For salt deposition of 1000 mg/m^2, severe corrosion occurs in weathering steel and secondary corrosion pits will occur within one year.

3. Using garnet abrasive blasting to remove rust to the level of Sa 2.5 or 3, the re-corrosion will still appear within one hour. After alumina blasting for more rounds, it can achieve ideal clean

condition and suitable for painting operation. Cleanliness has little relation to pre-treatment.

4. It is difficult to use abrasive blasting to clean severely corroded steel members to reduce the residual salt content to less than 50mg/m^2, and there will be a tendency to re-corrosion under the coating.

5. The 3 kW rotating CWL can clean approximately 200 μm of the rust layer per round of irradiation. Pre-treatments are helpful for the laser cleaning of corrosion pits in severely corroded components and for reducing the necessary irradiation rounds of the laser.

6. For severely corroded steel components, four laser irradiations can almost completely remove rust and salt.

QUANTITATIVE EVALUATION OF SURFACE CLEANLINESS OF WEATHERING STEEL TREATED BY CONTINUOUS WAVE LASER

1.14 Introduction

CWL has a good ability to remove rust. Multiple rounds of laser irradiation can remove thick and stubborn rust layer and achieve good salt removal effect. However, due to the continuous input of laser heat energy, the more rounds of laser cleaning is not always the better. At present, the quantitative evaluation of laser cleaning is still not available. As mentioned in Chapter 2, laser-cleaned surfaces cannot be evaluated in the same way as abrasive-blast-cleaned surfaces, due to the effect of oxide film color. Therefore, it is necessary to put forward the quantitative evaluation method in the application of laser cleaning technology in engineering practice.

With the advancement of imaging sensor technology, computer vision algorithm, and artificial intelligence technology, image-based recognition and analysis technology can be considered as potential methods to evaluate the cleaning quality of the laser[107–109]. Digital photography can be utilized to assess corrosion status and cleaning quality owing to its non-contact, reproducible, and inexpensive nature[110–112]. The color of digital photos can be output as the CIE LAB color space coordinates through various graphics software such as Adobe Photoshop, and the calculation and analysis of color change through mathematical formulas can overcome subjectivity[113–116]. Standards and guidelines have already been developed for this image analysis method in many industries, such as medical, mining, agriculture, and manufacturing [117–124], and can be used as a reference for laser cleaning.

In this chapter, a quantitative evaluation method is proposed based on digital photography. The analysis of cleanliness refers to the turning time test of laser cleaning of severely corroded steel components in Chapter 2. Finally, the suggestions of laser cleaning process are put forward, which can be used for reference for the future development of laser cleaning technology and laser cleaning robot.

1.15 Photometric Analysis method

The specimens were photographed in an indoor environment with low natural light, as shown in Figure 0-1(a), similar to a semi-enclosed environment during surface cleaning engineering. Two LED light panel groups (Web LED Photo Light WP-960, L.P.L. Trading) with an illumination of 2180 Lx/50 cm and a color temperature of 5000 K were used to illuminate the surface. Digital photos were taken by Canon EOS 60D digital camera with 18 million pixels equipped with a Canon EF17-40 mm F4L USM wide-angle lens; the device was set as in Figure 0-1(b). The specifications were as follows: shutter speed of 1/8, aperture: F11, ISO:100, and white balance. The images were processed in Adobe Photoshop 2022. The color information from the central part of the corrosion pit in the range 60 × 60 mm (101 × 101 pixels) is extracted to obtain the $L^*a^*b^*$ value, as shown in Figure 0-1(c).

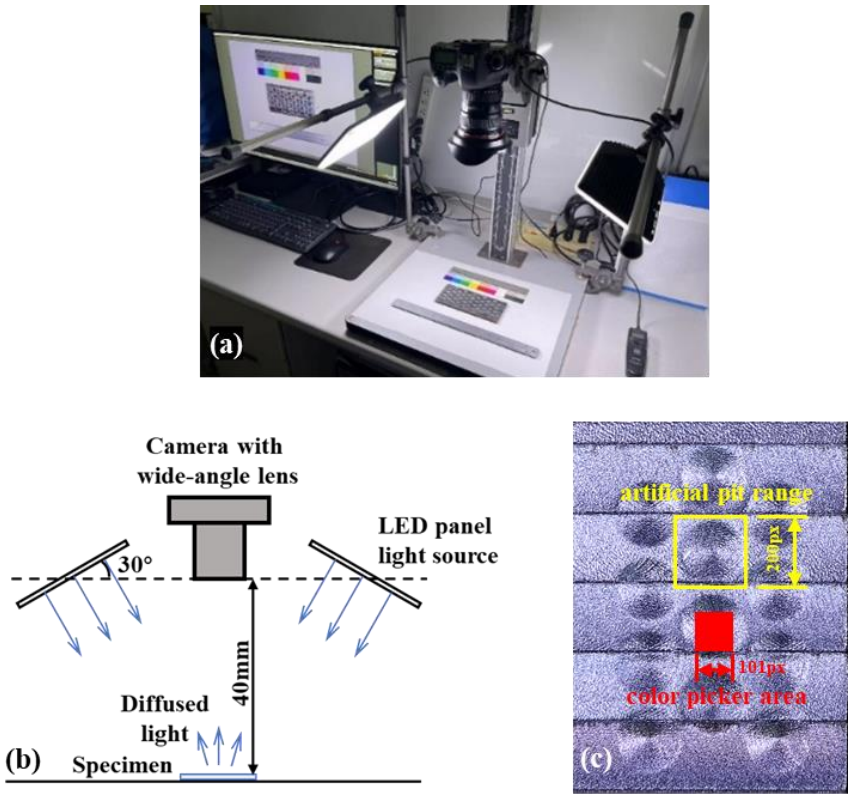

Figure 0-1 Photograph conditions of an (a) indoor environment with low natural light, (b) device settings (c), and the pickup position of the color information

1.16 Photographic analysis with CIE L*A*B* color space

High-temperature limits the contact inspection after laser irradiation, and visual inspection is limited by optical deviation and subjective awareness, which are not suitable for evaluating the surface after laser treatment. Hence, this study proposes using a digital camera to capture the color information of the target surface for a quantitative and objective assessment of laser cleanliness.

The captured color is based on the chromaticity information of the CIE $L^*a^*b^*$ color space under the D50 light source, including the luminance information L^* and the color information a^* and b^*. The color information a^* and b^* can also be equivalently converted into chromaticity C^* and hue $h_{ab}{}^*$, which is more in line with visual observation. The color information of each capture area can be drawn in the form of spatial point coordinates on the CIE $L^*a^*b^*$ or L^*C^*h plane. The distance between the points is the color difference ΔE. Chromaticity C^*, hue $h_{ab}{}^*$, and color difference ΔE can be calculated by equations (1)– (3).

$$C^* = \sqrt{(a^*)^2 + (b^*)^2} \tag{1}$$

$$h_{ab} = arctan\left(\frac{b^*}{a^*}\right) \tag{2}$$

$$\Delta E^* = \sqrt{(L_1^* - L_2^*)^2 + (a_1^* - a_2^*)^2 + (b_1^* - b_2^*)^2} \tag{3}$$

1.16.1 Luminance and color

Figure 0-2 is a graph of the color information change on the surface of each working step during the treatment process. It can be clearly seen that with the continuation of the surface treatment, the brightness L^* of the treated surface gradually increases, and the chromaticity a^* and b^* moves toward the negative axis direction. The three-color indicators have the same change trend as the cleaning process, and the color information change has a corresponding relationship with cleanliness.

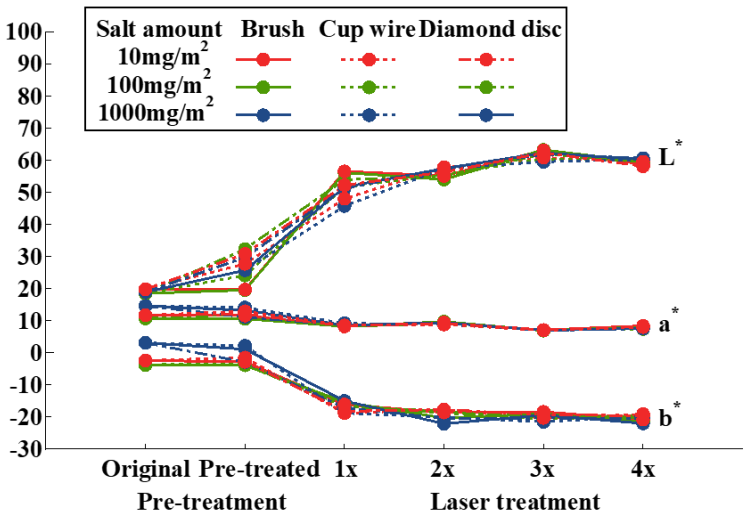

Figure 0-2 Variation diagram of color information at different surface treatment stages

In the pre-treatment process, the difference in the lightness value of the surface is very small. Hence, the color information of the surface at this stage can be compared on the same a^*b^* plane, as shown in Figure 0-3. The dense protective layer of the weathering steel is usually dark red, and the appearance of orange rust delamination is a typical feature of weathering steel that is severely corroded. In Figure 0-3(a), the color point coordinates of the severely corroded and general corroded steel surfaces are located on both sides of the X-axis, clearly distinguishing the corrosion degrees. Therefore, the hue value h_{ab}^* can be used as an index to evaluate the general and severe corrosions. This indicator can directly correspond to the necessary or non-pre-treatment processes for laser surface cleaning engineering. Comparing Figure 0-3(b) and (c), the relationship between surface chromaticity C^* and lightness L^* before and after pre-treatment shows that the surface lightness after pre-treatment is slightly improved, caused by the removal of rust and granules. After surface treatment, the color chroma of the pit area has no specific change rule caused by the randomness of rust formation. However, it can be noticed that the surface chromaticity of the cup wire pre-treatment is much lower than other surface treatments, which is caused by removing the rust layer and leaving a black FeO surface during the cup wire pre-treatment. Although there is a certain trend of color change after cup wire pre-treatment, it is still not recommended to use chromaticity C^* and lightness L^* to evaluate the cleaning effect in the pre-treatment stage. Especially in the case of severe corrosion, pitting corrosion, and surface irregularities, the diffuse reflection interferes with the collection of color information[125].

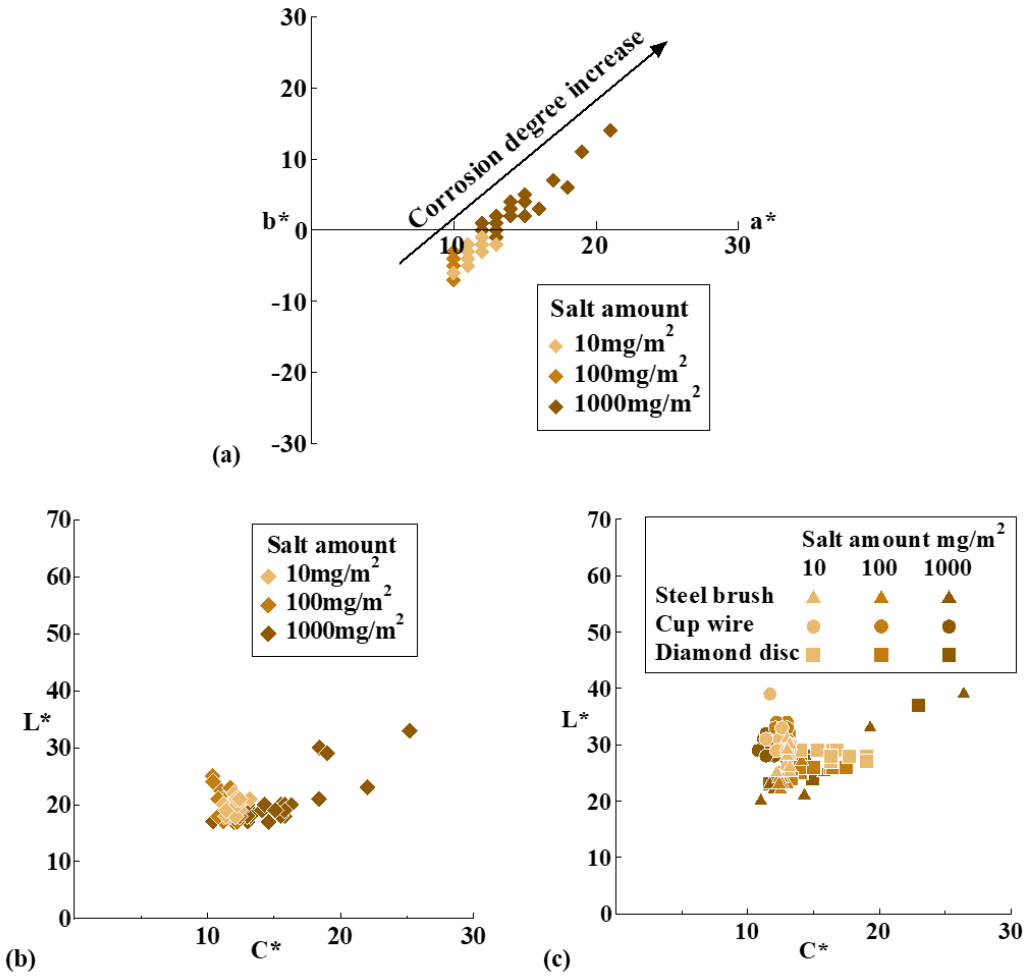

Figure 0-3 Color information of the surface in the pre-treatment stage: (a) a*b* plane, (b) and (c) L*C* plane

The surface rust layer was quickly removed after CWL irradiation. The most apparent manifestation was that the surface redness and yellowness decreased rapidly, and the treated surface appeared light blue. As the rounds of laser irradiations increase, the surface chromaticity and lightness are improved to a certain extent. Since the lightness conditions of each surface during the laser treatment are close, a unified a^*b^* plane can also be used to describe the color information of this cleaning stage. As shown in Figure 0-4, all surface colors are concentrated in a small range; the change of chromaticity C^* is only about 15, and the shift in hue is not more than 20°. Influenced by vision, it is more difficult to identify and distinguish with the naked eye in such a small area of the blue zone. After the rust layer is evaporated by laser ablation, the laser spot is directly irradiated to the surface of the steel substrate, and a molten pool is formed locally. Due to the surface tension of

the molten steel, it flows to the periphery, and the rust that has not been completely removed is covered to form rust buds. This remelting-covering phenomenon directly affects the accuracy of visual assessment of surface cleanliness. Simultaneously, some contaminators that have not been wholly evaporated will also enter the molten metal, remaining in the re-melted layer after cooldown. With the increase of laser irradiation times, the rust buds under the re-melted layer and the impurities in the re-melted layer are ablated completely, and the surface is thoroughly cleaned. In repeated laser irradiation, the molten steel also fills the pitting corrosion pits, making the entire surface look smoother and reducing the diffuse reflection of the surface. Hence, the surface lightness continues to increase with the number of irradiations. A dense Fe_3O_4 film is also formed on the surface during surface cooling[126]. The film tends to thicken with the increase of irradiation times. Due to thin-film interference, the illuminated surface appears bluish and tends to be silvery, increasing the chromaticity of the surface.

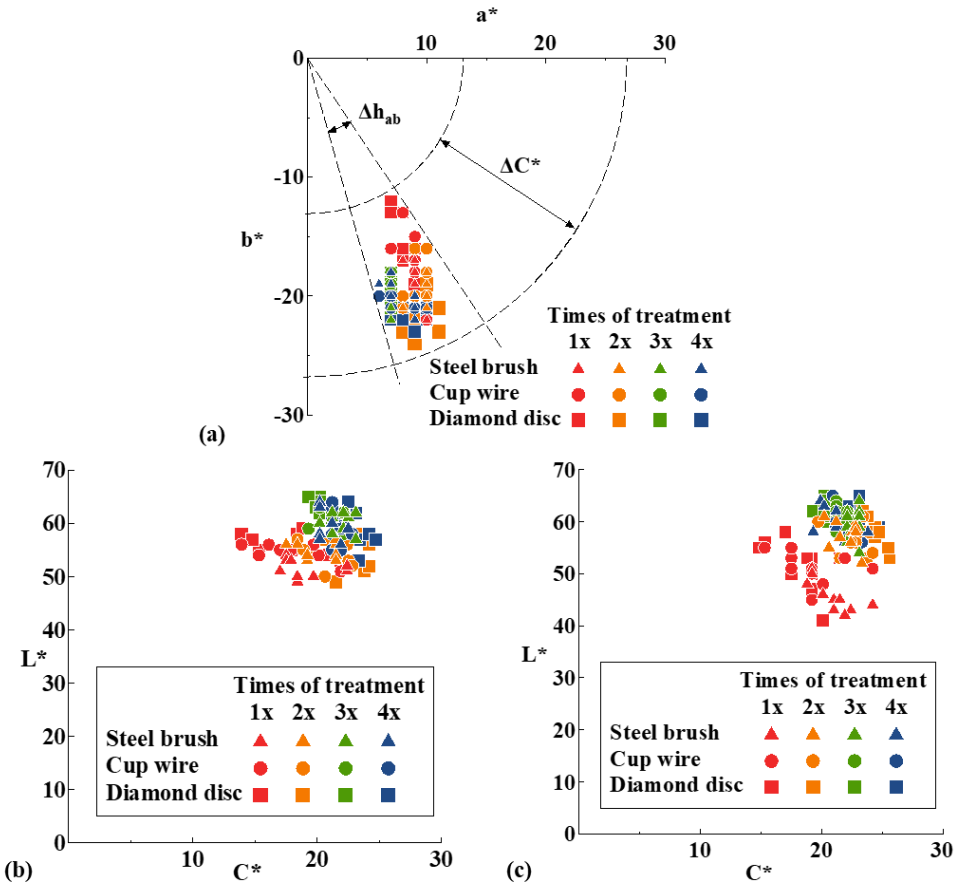

Figure 0-4 Color information of laser treatment surface: (a) a^*b^* plane and L^*C^* plane of (b)100 mg/m^2, and (c) 1000 mg/m^2

1.16.2 Comparison of the color difference

In laser irradiation, we need to consider whether the surface is ideally cleaned and whether it will cause new defects due to laser irradiation. However, more rounds of laser irradiation are not always advisable. Excessive laser irradiation will increase local thermal effects, forming a deeper heat-affected zone and causing surface defects.

The difference in the color information of each surface in the laser processing stage is very small. It is challenging to judge whether the laser irradiation is sufficient or excessive only by color information. However, the lightness and chromaticity increase with the rounds of laser irradiation, and the overall trend is rising. Therefore, there is also a certain chromatic aberration on the surface between different irradiation rounds, which can be used to distinguish the stage reached by laser irradiation.

Determining the benchmark of color is the most crucial factor in discussing the color difference. Li has used the color difference method to realize the cleaning evaluation of PL on general corroded surfaces using a cleaned surface as a benchmark and achieved a very good cleaning effect[74]. However, this benchmark does not apply to this study. As shown in Figure 0-5(a), each surface's color difference is calculated with the benchmark of 10 mg/m^2 salt deposit surface twice irradiated by the laser. The conclusion shows that the color difference under different conditions has no obvious relationship with the laser irradiation rounds. This is because the rust removal ability of the CWL is very strong; in the case of general corrosion or surface with pre-treatment, a single irradiation round is sufficient to expose the steel substrate. As mentioned above, each round of irradiation ablated approximately 200 μm of the rust layer. Compared with that of PL cleaning, the removal thickness of the rust layer may only be tens of microns in one round of cleaning; therefore, more irradiation rounds (pulse times) are required to completely remove the rust layer. In this study, most parts of the corrosion pit were fully cleaned by just one round of CWL irradiation, which has reached the range of excessive irradiation of the PL defined in the study by Li[74]. The most striking feature was the formation of a blue oxide film. Although the obtained results reveal that the color difference between the clean surface and benchmark is approximately 5, this cannot be used to determine whether the corrosion pit is completely cleaned.

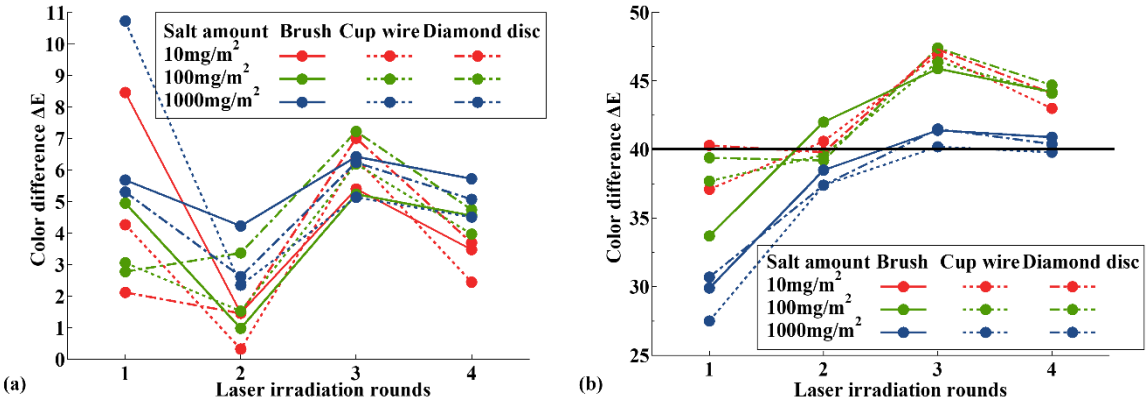

Figure 0-5 Surface color difference change of laser treatment with different benchmarks: (a) standard surface and (b) surface after pre-treatment

This study proposes to use the surface color information before laser treatment as the benchmark to compare the color difference between the same groups. Figure 0-5(b) plots the color difference of each round of laser surface treatment. With the increase of laser irradiation rounds, the color difference also showed a trend of continuous increase. In the case of general corrosion, the color difference changes little between the first and second laser irradiation, while there is a significant increase after the third round of laser irradiation. The first two rounds of laser irradiations were considered to be the cleaning stage. Laser energy is mainly used for ablation and evaporation of the rust layer and contaminants. At this stage, the surface melting effect on the steel substrate and the formation of the oxide film do not change significantly; thus, only a small color difference change is observed. The total laser power was input to the surface during the third and fourth irradiations. For the target surface, the remelting process involves excessive cleaning. This process increases the thickness of the oxide film, and the surface tends to be silver white. The target surface was smoother, and the surface roughness Ra in the corrosion pit decreased from approximately 50 μm to approximately 30 μm. The sudden change in color difference is a sign of overtreatment. In the case of severe corrosion, with the increase in the irradiation rounds, the color difference increases and tends to be the same in the third and fourth irradiation. As mentioned in the turning time analysis, three or four rounds of laser irradiation are necessary for completely cleaning the severely corroded surface, which is consistent with the color difference change. In addition, it was found that the color difference value of the general corroded surface irradiated by laser one for two

rounds and the severely corroded surface irradiated for three to four rounds was in a similar range about 40 ± 2. At this point, the target surface is in the state of being completely cleaned. Therefore, when the 3 kW CWL is used to clean the surface, it can be assumed that when the color difference reaches this range, the surface has just achieved the cleaning condition, and there is no excessive treatment.

1.17 CWL surface treatment procedure

As a new type of surface treatment technology, CWL have the advantages of high efficiency, environmental friendliness, and industrialization. Combined with robotic technology, it can become a fully automatic surface cleaning method in the future. This study recommends three steps to achieve ideal laser cleaning of weathering steel structures, as shown in Figure 0-6. The first stage is the evaluation of the corrosion degree, which is used to determine whether pre-treatment is needed. The degree of corrosion can be judged subjectively by visually checking whether the rust layer is stratified or objectively by image analysis of the hue of the surface color. The second stage is surface pre-treatment, which is necessary for components exposed to severe corrosion conditions. Considering labor costs and maintenance time constraints, as well as the temperature sensitivity of the components, the choice of pre-treatment will be adjusted accordingly. Generally, simple pre-treatment with a high-efficiency diamond grinding disc followed by multiple rounds of CWL irradiation is the recommended approach. However, for some temperature-sensitive components, such as thin plates, which can easily bend when exposed to heat, sufficient pre-treatment should be performed using wire-type power tools, such as a wire cup brush, to thin the rust layer as much as possible. The third stage is laser cleaning. Single laser irradiation can complete laser cleaning for general corroded areas and fully pre-treated corrosion pit areas. For the case of thick rust layer, multiple rounds of laser irradiation are needed. After each round of irradiation, the color difference between the pre-treated and post-treated surfaces can be used for cleanliness evaluation. When the color difference value reaches the 40 ± 2 range, the surface is considered completely clean, and no further irradiation is required. This method ensures that the severely corroded area cleaned by laser has more than 80% cleanliness in this research, which will provide a reference for the cleaning and maintenance of weathering steel structures. Considering the construction period and labor cost, the

construction method based on image recognition and automatic laser surface treatment will become mainstream in the future.

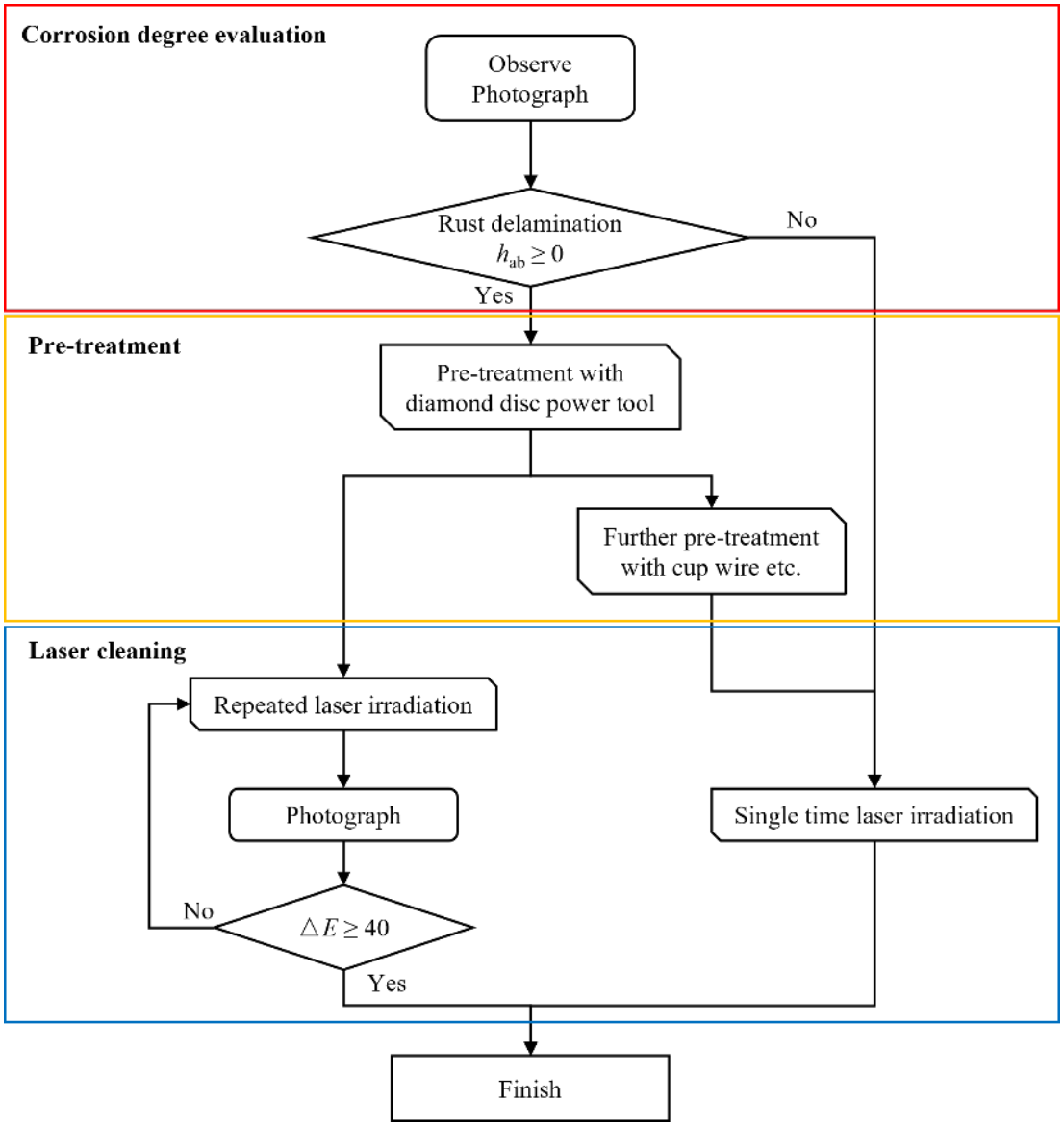

Figure 0-6 Flow chart of CWL surface treatment procedure

1.18 Summary

This chapter discusses the possibility and feasibility of taking photos based on digital cameras, picking up color information by image analysis software, and analyzing the surface cleanliness of laser processing based on CIE LAB color space. The results show a good match with turning time test. The conclusions are as follows:

1. As the cleaning process progresses, the color information of the treated surface changes in the same trend. It is possible and feasible to evaluate the cleanliness by color analysis.

2. Photometric analysis can be used to obtain surface color information for the quantitative evaluation of cleanliness. The hue value can be used to distinguish the degree of corrosion of weathering steel, and the color difference before and after laser irradiation can be used to evaluate cleanliness.

3. The laser surface cleaning method is recommended, and the results of this study can inform the future research and development of CWL automatic cleaning systems.

SURFACE TREATMENT AND CLEANLINESS EVALUATION OF SEVERELY CORRODED STEEL COMPONENTS IN ENGINEERING

1.19 Introduction

Laser cleaning, as an environmentally friendly method for severe corrosion cleaning, will have a wide range of use scenarios in the future. At present, there are still few engineering applications of laser cleaning, how to use the effect of laser cleaning in engineering needs to be verified. In addition, heavily corroded steel structures are usually located in areas of high salt, high temperature, and high humidity, so the surface to be cleaned is usually wet. For abrasive blasting cleaning, the wet surface condition will limit abrasive recycling. Previous studies have shown that underwater laser cleaning can obtain better microscopic cleaning effect, which benefits from the evaporation effect of water vapor and the cleaning effect of underwater cavitation bubbles. Therefore, laser cleaning under wet conditions and even underwater will be a big advantage in engineering application.

To verify the possibility of using high-power CWL for cleaning corroded steel structures, in this chapter, the 3 kW CWL was used to irradiate severely corroded steel members under dry and wet conditions. After the laser treatment, the surface morphologies and microstructures were evaluated and compared with the results of abrasive blasting to determine the cleaning effect of CWL processing on corroded steel members in actual engineering. To accurately evaluate the effect of CWL salt removal in practical engineering, SEM/EDX technology was used to analyze the surface and cross section of the core specimens after turning time test. Discussed the quality of salt removal effect in engineering and the possible influence caused by external pollution. The conclusion obtained will provide reference for the engineering application of laser surface cleaning.

1.20 Experimental

1.20.1 Samples

A severely corroded steel member removed from a rock shed was selected for surface treatment, and the structure was exposed in a coastal region less than 10 m away from the seaside of Kagoshima (Lat. 31°53”51’N, Long. 130°13”20’E) for 41 years, as shown in Figure 0-1 (a) and (b). The amount of airborne salt in this area was high, and the steel members of the rock shed were unaffected by rain. Although the structure was painted, severe corrosion occurred in the thin coating. As shown in Figure 0-1(c), the foot of the rock shed exhibited the most severe corrosion. Before performing surface cleaning via abrasive blasting and CWL, the corroded surface was pretreated with a diamond disc power tool to remove the outermost and compact rust layer, as shown in Figure 0-1(d) and (e).

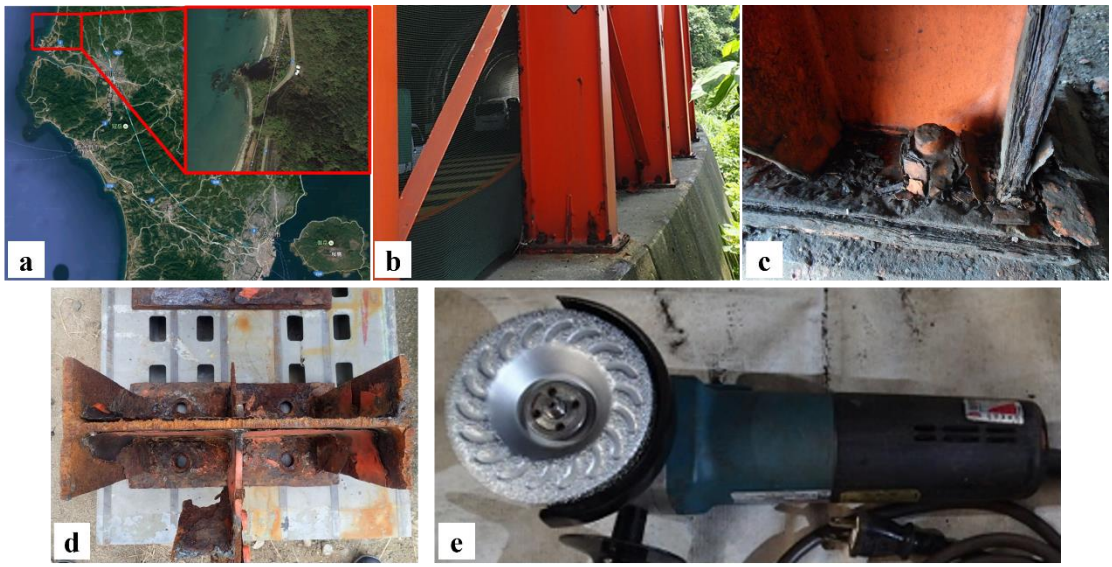

Figure 0-1 Location and surface conditions of severely corroded steel member: (a) Location of rock shed, (b) corroded columns of rock shed, (c) foot of corroded columns, (d) surface treatment target, and (e) used power tools with diamond grinding disc.

1.20.2 Abrasive blast cleaning

Abrasive blasting was regarded as the control group to compare the rust and salt removal effects of the laser cleaning. Garnet was used as the abrasive; it has the same Mohs hardness as steel, and its average particle size was 430 μm. The composition of the abrasive is shown in Table 0-1 and the appearance and particle size distribution of the garnet are shown in Figure 0-2. The pretreated surface was blasted at a spraying angle, stand-off distance, and pressure of 60°, 300 mm, and 0.7 MPa (100 psi), respectively, during cleaning. To achieve an ideal cleaning effect, the garnet abrasives were not recycled during cleaning to avoid rust and salt from being sprayed directly onto the target surface. Before analysis, the blasted surface is cleaned with a high-pressure air gun to remove the abrasive sticking to the steel surface.

Table 0-1 Composition of garnet abrasive

Components	SiO_2	Al_2O_3	Fe_2O_3	CaO	MgO	TiO_2
Composition (%)	35–40	20–25	30–35	1–2	5–7	0.1–1

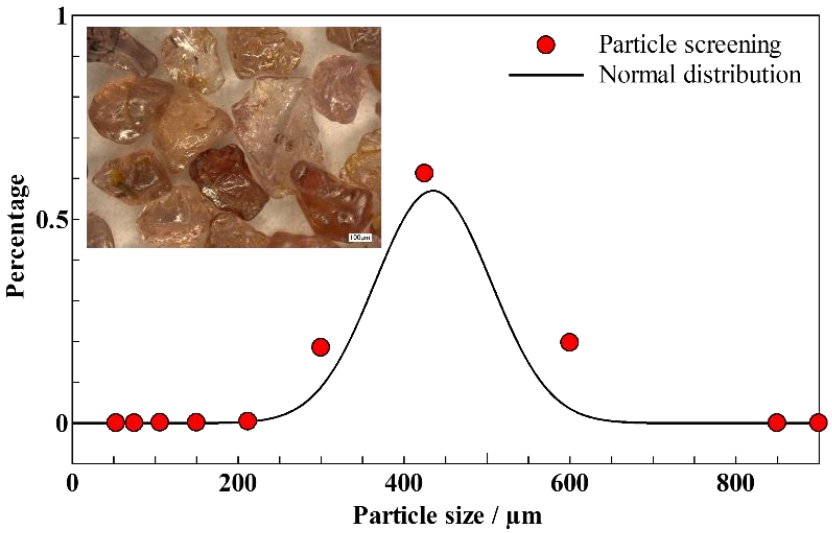

Figure 0-2 Garnet particle size distribution.

1.20.3 Laser cleaning

Laser processing was performed at a factory in Shizuoka, Japan. Laser surface treatment was performed using the CWL rotated by a prism as a spinning 3 kW laser ring, which irradiated the steel surface with the moving ring to remove corrosion products and contaminants[30,71]. The laser processing parameters are listed in Table 0-2. In this study, laser surface treatment was categorized into dry laser cleaning (DLC) and wet laser cleaning (WLC), the schematics of which are shown in Figure 0-3. In WLC, the methods for supplying water are classified into three categories: 1) WLC-1: the drench method - laser cleaning is performed after splashing water on the steel surface following pretreatment, and the thickness of the water film on the surface does not exceed 1 mm; 2) WLC-2: the soak method - laser cleaning is performed by soaking the treatment surface in a 30-mm-deep water layer; 3) WLC-3: the rinse method - laser cleaning is performed while continuously supplying tap water to the steel surface through a shower head at the supply speed of 16 L/min, and the thickness of the water flow on the surface does not exceed 10 mm. The laser continuously sweeps the cleaning surface thrice to ensure that the entire surface is fully cleaned during cleaning. The treatment conditions and cleaned surfaces are shown in Figure 0-3.

After the sample was thoroughly cooled, a hole saw was used to cut specimens with the diameter of 20 mm in each target area (Figure 0-4 (a)), and the cutting area was selected at the location of a corrosion pit of similar size to ensure consistency of the analysis surface morphology as much as possible[95]. The surfaces of the cut specimens were clean without residual rust, as Figure 0-4 (b) shows.

Table 0-2 Laser processing parameters

Parameter	Value	Units
Output	3	kW
Spot diameter	430	μm
Motor speed	5000	rpm
Irradiation ring diameter	26	mm
Spot irradiation speed	680	cm/s
Power density	2066	kW/cm2
Interaction time	31.6	μs

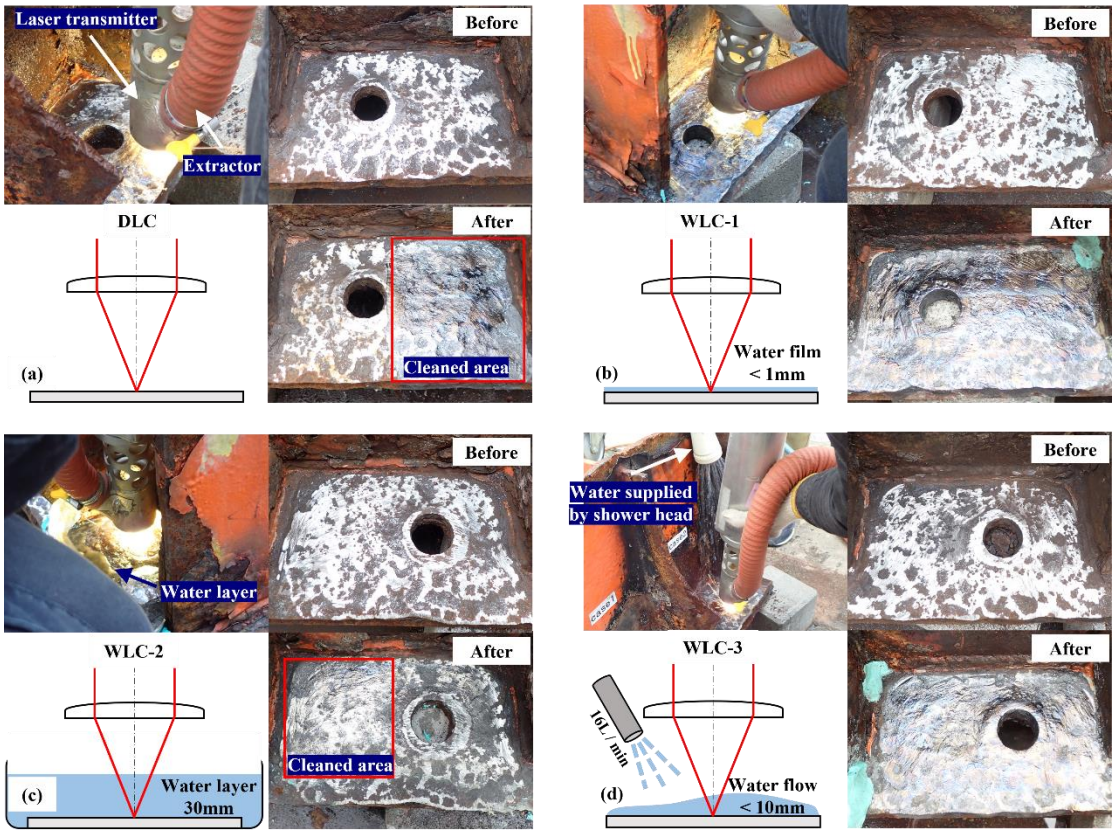

Figure 0-3 Surface conditions of severely corroded steel member treated via laser cleaning: (a) DLC, (b) WLC-1 of drench method, (c) WLC-2 of soak method, and (d) WLC-3 of rinse method.

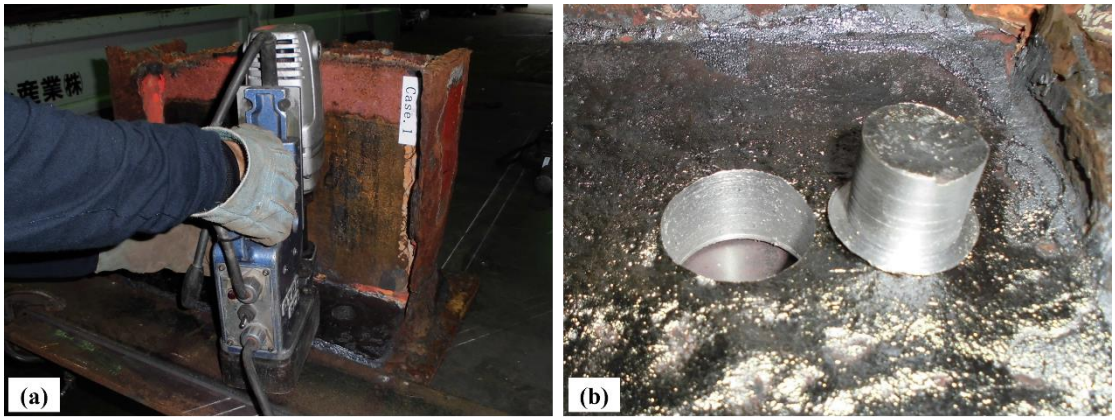

Figure 0-4 Specimens of laser-treated surfaces (a) cut by hole saw and (d) surface condition before transportation.

1.20.4 Observation and characterization

The surface morphologies of all specimens were observed and analyzed using a three-dimensional digital optical microscopy (OM, HRX-01, HIROX, Tokyo, Japan). Information regarding the surface roughness was acquired by analyzing a 0.6 mm × 10 mm area for each sample surface under a laser confocal microscope (OLS-4500, Olympus, Tokyo, Japan).

The elemental chemical composition of the cleaned surface was determined using scanning electron microscope–energy dispersive X-ray spectrometry (SEM–EDX, Model SU3500-Hitachi; Hitachi Corp., Japan) under an accelerating voltage of 15 kV and a vacuum pressure of 30 kPa.

To determine the thicknesses of the melt layer and heat-affected zone of the laser-treated steel surface, the cross sections of the laser-treated specimens were polished and etched with 3% nital, and then the microstructure of the specimens was observed using OM.

1.21 Macroscopic and microscopic characteristics of surface after cleaning

1.21.1 Processing efficiency

For surface treatment in actual engineering, the efficiency of processing, which is associated with the construction period and treatment cost, as well as noise and dust emission during the treatment process, is critical and affects the re-corrosion turning time of the treated surface[127]. In this study, the treated surface was a rectangular area of the foot of rock-shed pillars. The treatment time for each step was recorded. The construction efficiency was calculated based on the processed area per hour.

A diamond grinding disc power tool was used for polishing the surface during pretreatment; however, it cannot remove the corrosion products inside the corrosion pit, which contains more salt than the other corroded areas[1,128,129]. Therefore, the rust and salt removal effect in this area is the key in this study. The surface must be cleaned before painting to avoid premature coating failure. Pictorial standards are often used to evaluate cleanliness in engineering. According to ISO 8501, painting is performed the most economically and efficiently when the surface is cleaned at Sa 2.5 or higher, where the amount of shadows, streaks, and stains remaining on the surface is less than

5%. Therefore, both abrasive blasting and laser cleaning satisfy the visual cleanliness standards of this study.

Regarding engineering experience and research, the efficiency of garnet blasting, which is affected by the type and size of garnet, as well as the shooting pressure, is 15–30 m^2/h. However, for the severely corroded area, it was difficult to achieve the desired surface cleanliness after a single blasting of Sa2.5 or 3 specified by ISO 8501, and flash rust occurred within tens of minutes. To achieve an ideal cleaning effect, repeated water spraying and blasting are typically required. In this case, the amount of blasting required by garnet is 150–200 kg/m^2, which is 8–10 times that required by general blasting. Therefore, the actual garnet-blasting efficiency is only 1.5–3 m^2/h. In this study, garnet blasting was performed on a pretreated surface measuring 50 mm × 80 mm. After 20 s of blasting, the surface exhibited a visual cleanliness level of Sa3, and the converted actual treatment efficiency was 0.72 m^2/h.

In CWL cleaning, laser beam irradiating the entire processing surface is the ideal state. Because the energy distribution of the laser beam conforms to a Gaussian-function-like distribution[130–133], the ideal irradiation conditions in the laboratory were set to the overlap ratio of the laser ring and laser spot of 50% to satisfy the uniform and effective laser irradiation, as shown in Figure 0-5. In this case, the laser-cleaning efficiency was 0.84 m^2/h. During laser cleaning, the target surface was cleaned using a handheld transmitter, with the overlap rate of the laser deviating significantly from the ideal condition. To fully irradiate the target surface, the laser transmitter was manually controlled to irradiate the surface three times with as uniform a movement speed as possible. In this case, the target surface can be fully and effectively irradiated at the same ideal cleanliness level. The treated surface was visually cleaned to the Sa3 level as a blasted surface, without residual corrosion products. The laser irradiation time on each surface was as consistent as possible; the average cleaning time on the 0.03 m^2 target area was approximately 90 s, and the average efficiency of the handheld laser cleaning tool was 1.20 m^2/h .

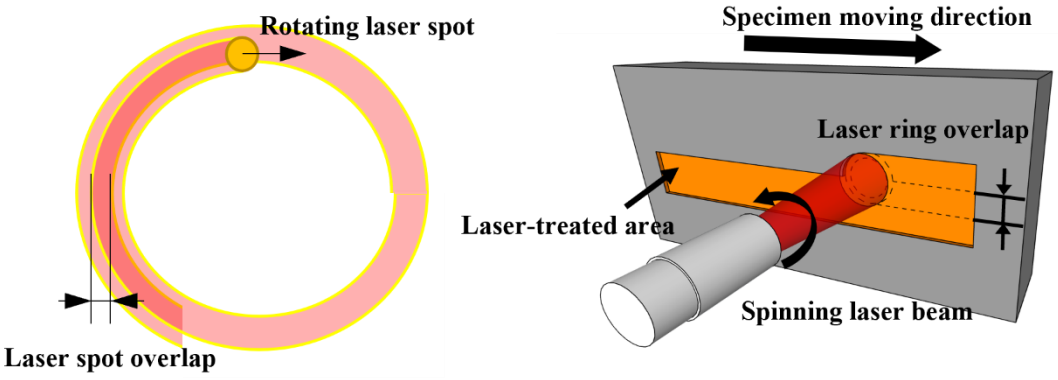

Figure 0-5 Schematic illustration of rotating CWL treatment.

1.21.2 Macroscopic observation

5.3.2.1 Pretreated surface

Figure 0-6 shows macroscopic images of the surface before and after pretreatment. The thickness of the rust layer on the target cleaning surface can reach 20mm; the layer was loose and can be peeled off easily. After removing the loose rust layer using handheld tools, the corrosion products on the surface appeared brown and black. This rust layer was difficult to remove, even when steel brushes and chisels were used, particularly in areas containing corrosion pits. After diamond grinding disc treatment was performed, a portion of the area was polished to expose the silver luster steel substrate, and the polished area exceeded 50%, as shown in Figure 0-6(b). The areas outside the pit were ground using diamond grinding discs, as depicted in Figure 0-6(c), resulting in clear-cutting tracks. This is because of the grinding disc shape and corrosion pit depth. The rust appeared as a stubborn brownish–red cone in the corrosion pits[95], which often contained a large amount of salt. Surface soluble salt content was measured four times via a bresle patch test, and the obtained salt contents were 27.8, 66.1, 122, and 666 mg/m^2. Figure 0-6(d) shows the site where the maximum salt amount was measured. The purpose of this study was to remove rust from these corrosion pits and avoid salt residue on the cleaned surface as much as possible.

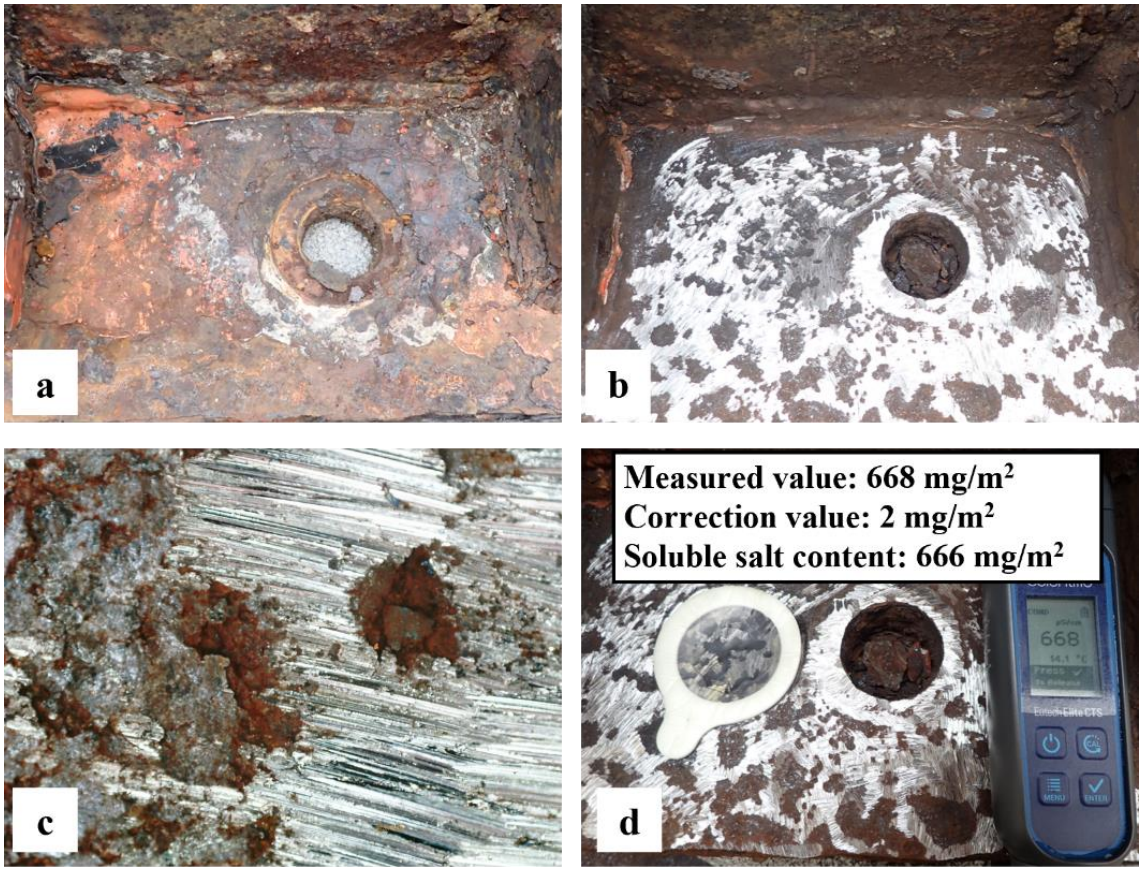

Figure 0-6 Morphologies of target surface: (a) Before cleaning and (b) after pretreatment; (c) local morphology after pretreatment; (d) soluble salt content after pretreatment.

5.3.2.2 Blasted surface

The garnet-blasted surface shows a matte-textured gray metallic luster with no visible rust or contamination, which can reach the cleanliness level of Sa3. Even at the Sa3 level of blasting, flash rust began to appear on the blasted surface within an hour, as shown in Figure 0-7(a), and rust was visible at 100 X optical magnification, as shown in Figure 0-7(b). Additionally, fine white translucent particles, which were residue from the garnet abrasive, were observed on the area near flash rust.

Table 0-3 Surface roughness values of blasted surface of garnet

Laser conditions	Ra (μm)	Rz (μm)	Rsm (μm)	Sa (μm)
Blast	13.6	87.7	411	15.3

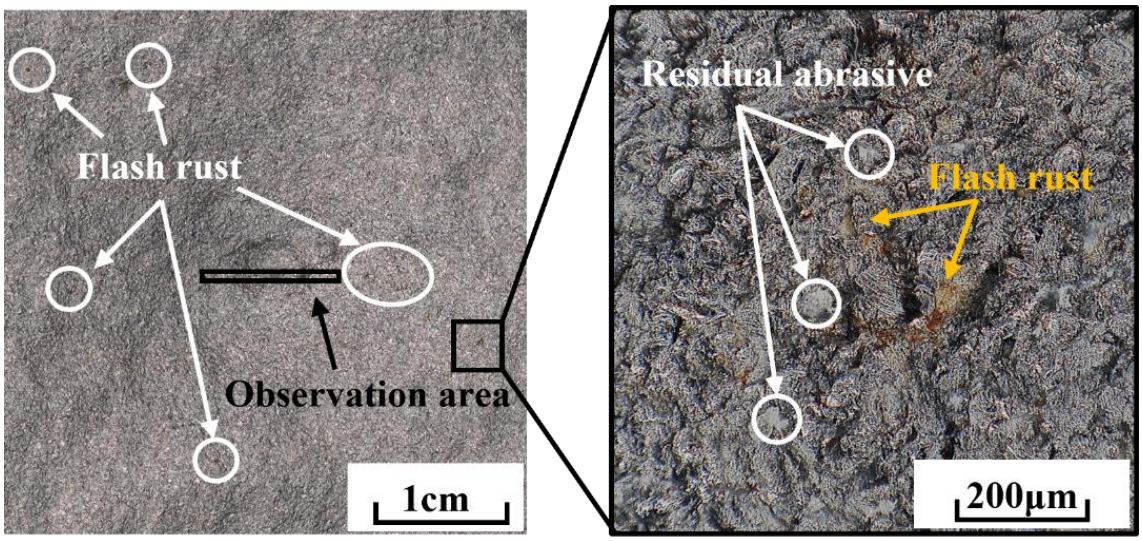

Figure 0-7 OM images showing blasted surface of garnet.

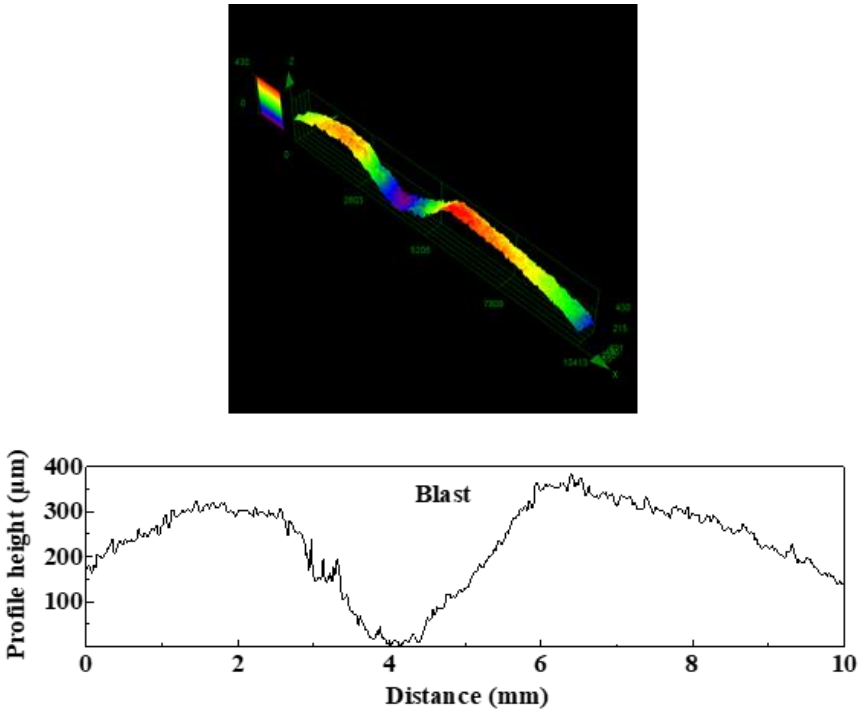

Figure 0-8 Surface and cross-section profile of blasted surface of garnet.

The line area around the corrosion pit (black wireframe in Figure 0-7(a)) was scanned using a laser confocal microscope, and the local surface and cross-section profiles were obtained, as shown in Figure 0-8. The blasted surface was impacted by the abrasive, which resulted in dense craters and a rough matte surface. The line roughness and surface roughness values of the garnet-blasted surfaces are listed in Table 0-3.

5.3.2.3 Laser-cleaned surface

After laser cleaning, the surfaces exhibited a pearlescent texture with a luster of amber, blue, and black. The factor that contributed to this luster is the same as that to the tempering of carbon steel, the difference in thickness of the oxide film formed on the surface after laser irradiation. The laser irradiation track was clearly observed on the laser-cleaned surfaces, as can be seen in Figure 0-9. In this case, the rust layer on the trace was determined as completely ablated and evaporated because the steel substrate was directly swept by the laser beam to form a molten pool trace, which achieved the ideal laser cleaning effect. The formation of laser traces on the entire surface is a major characteristic of a completely cleaned steel surface. It should also be noted that no corrosion residues or flash rust were observed on the laser-cleaned surfaces within hours of cooling, as shown in Figure 0-4. It can be considered that the surface after laser cleaning can also reach the same Sa3 level as the blasted surface. To determine exactly where the salt residue might be, scientific analysis of the cleaned surface was performed one week after the laser cleaning, at which time the laser cleaning surface appeared rusty. All scientific analyses were performed using orange bars, as shown in Figure 0-9. Photoshop 2022 software was employed to select and calculate areas where rust occurs[134], and the re-corroded areas of DLC, WLC-1, and WLC-2 constituted approximately 5% of the entire surface. Nevertheless, the cleanliness of these areas can reach a similar Sa2.5 level to that of a blasted surface. However, the surface re-corroded area of WLC-3 reached approximately 30% of the full surface, which is unacceptable. The cause of re-corrosion must not be excluded from the introduction of contaminants during the cutting process, as most corrosion occurs at the anchor points and edge locations.

By observing the clean region of the specimens, it was observed that the surface that underwent DLC showed a dark blue and gray luster, the surface of WLC-1 appeared blue primarily, and the surfaces of WLC-2 and WLC-3 appeared amber. Laser traces and small pits were observed in the optically magnified 100X images—these pits were formed via pitting corrosion and were similar to the laser beam in terms of size. Even in the magnified state, corrosion products were not observed inside these pits, demonstrating the ability of laser irradiation in cleaning the pitting areas.

Figure 0-10 and 11 show the profiles of four laser-treated surfaces and cross sections. The

contour data are from the orange area in Figure 0-9. Because all surfaces were tested under the same operating conditions, these strip areas were used to indicate the profile characteristics of the specimens. The main factor affecting the surface roughness of laser cleaning was the distribution of the laser trace. As shown in the cross-sectional profile of the DLC case in Figure 0-11, the laser profile in the left region was dense, whereas that in the right half was relatively sparse. In the four laser cleaning cases, the surface of WLC-1 and WLC-2 demonstrated the highest and lowest surface roughness values, respectively. Based on the surface profile maps shown in Figure 0-10, the laser-cleaned surface was smoother than the blasted surface. Except for the case of WLC-1, the roughness values of the laser-cleaned surfaces were slightly lower than those of the blasted surface, as listed in Table 0-4.

Table 0-4 Surface roughness of laser-irradiated surface

Laser conditions	Ra (μm)	Rz (μm)	Rsm (μm)	Sa (μm)
DLC	11.8	76.2	666	12.3
WLC-1	17.3	101	786	19.5
WLC-2	8.03	49.6	519	8.11
WLC-3	14.3	84.3	966	15.3

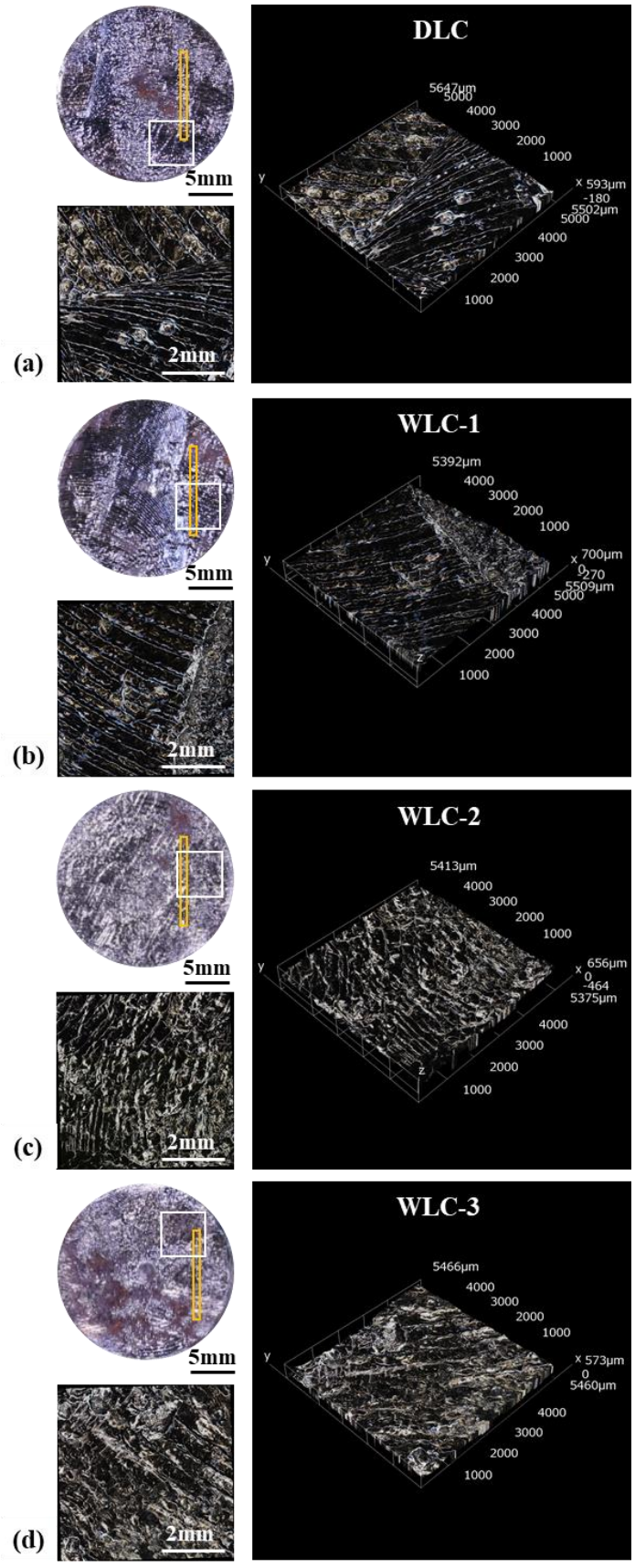

Figure 0-9 Surface morphologies of (a) DLC, (b) WLC-1, (c) WLC-2, and (d) WLC-3 specimens.

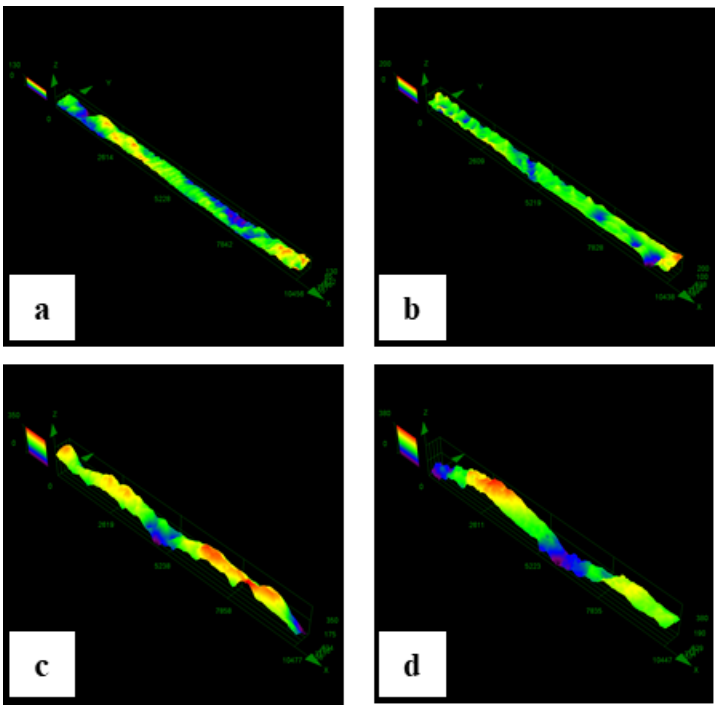

Figure 0-10 Surface profile of laser-treated surfaces.

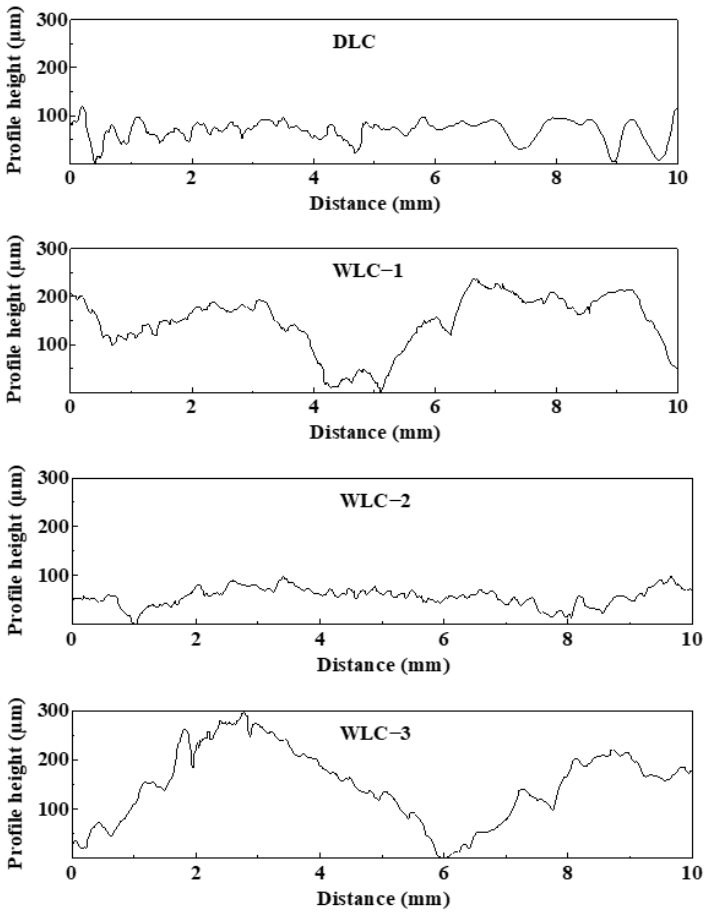

Figure 0-11 Cross-section profile of laser-treated specimens.

1.21.3 Microscopic observation

It can be observed visually that flash rust occurred in a short period on the cleaned surfaces[134], which adversely affected the coating effect. The flash rust occurred because impurities particles and salts remained on or embedded in the cleaned surface[16]. Salt content is difficult to measure using the Bresle patch test. Therefore, studies were conducted to observe the cleaned surface using SEM, as well as to distinguish the location and content of specific elements via EDX.

5.3.3.1 Pretreated surface

The pretreated surface re-corroded rapidly. By observing a corrosion pit area, it was revealed that a significant amount of salt remained on the steel surface, as shown in Figure 0-12, which contributed primarily to the re-corrosion. Figure 0-13 shows the cross section of a pitting corrosion, the maximum depth of which was 100 μm. Furthermore, it was discovered that the salt accumulated under the corrosion products at the bottom of the corrosion pit. Therefore, the primary goal to be achieved in severely corroded steel members is the removal of corrosion products and salts to avoid the occurrence of rapid re-corrosion.

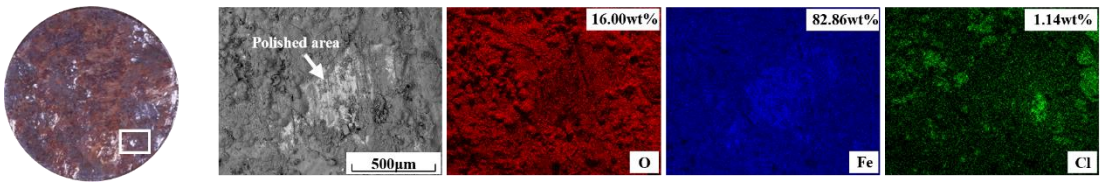

Figure 0-12 SEM–EDX micrographs showing pretreated surface of diamond disc power tool.

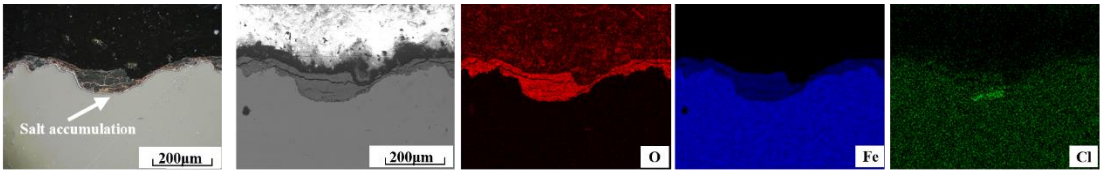

Figure 0-13 OM and SEM–EDX images showing cross-section of pretreated sample.

5.3.3.2 Surface cleaned via blasting

An SEM–EDX image of the corrosion pit on the cleaned surface of the garnet blast is shown in Figure 0-14. Observations were performed immediately after the blasting operation. It was observed that the cleaned steel substrate exhibited a bowl-like shape (light-colored area) after being struck by the abrasive at a high speed, and abrasive residues (black area) were observed in some areas. The residual abrasive appeared in the form of powder or flakes and measured 50–100 μm, which is 1/5–1/10 the size of the abrasive particles. Based on the EDX analysis results, the corrosion pit did not contain any corrosion products or salt residues. However, the residual abrasive on the surface indicated a weight ratio that exceeded 20 wt% and was primarily CaO with lower hardness, followed by SiO_2 and Al_2O_3 with higher hardness. Figure 0-15 shows a cross section at the corrosion pit. As shown, the abrasive was buried in the steel substrate, and the embedded abrasives were primarily Al_2O_3 and SiO_2. This specimen reaches the clean level of Sa3 when the blasting time is much longer than the general treatment time; therefore, no salt residue can be observed at the bottom of the corrosion pit. However, embedding of abrasives could not be precluded as the main reason for re-corrosion within a short time[16].

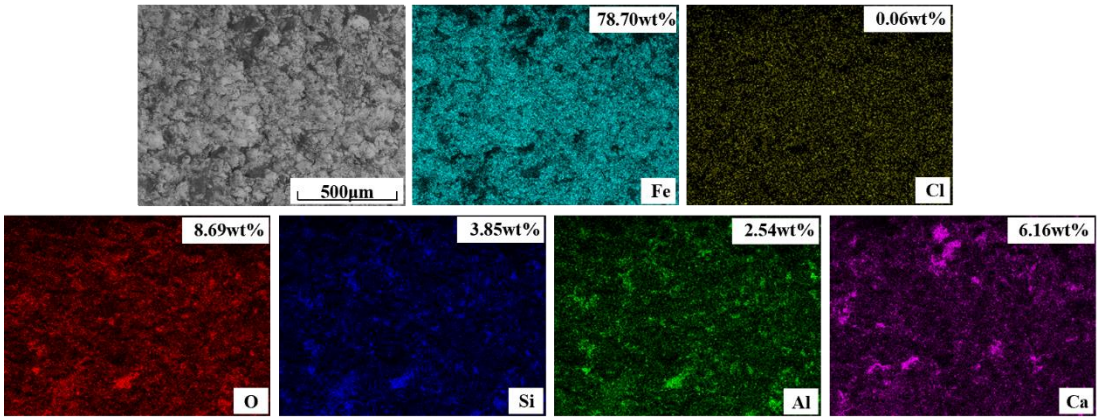

Figure 0-14 SEM–EDX micrographs showing blasted surface of garnet.

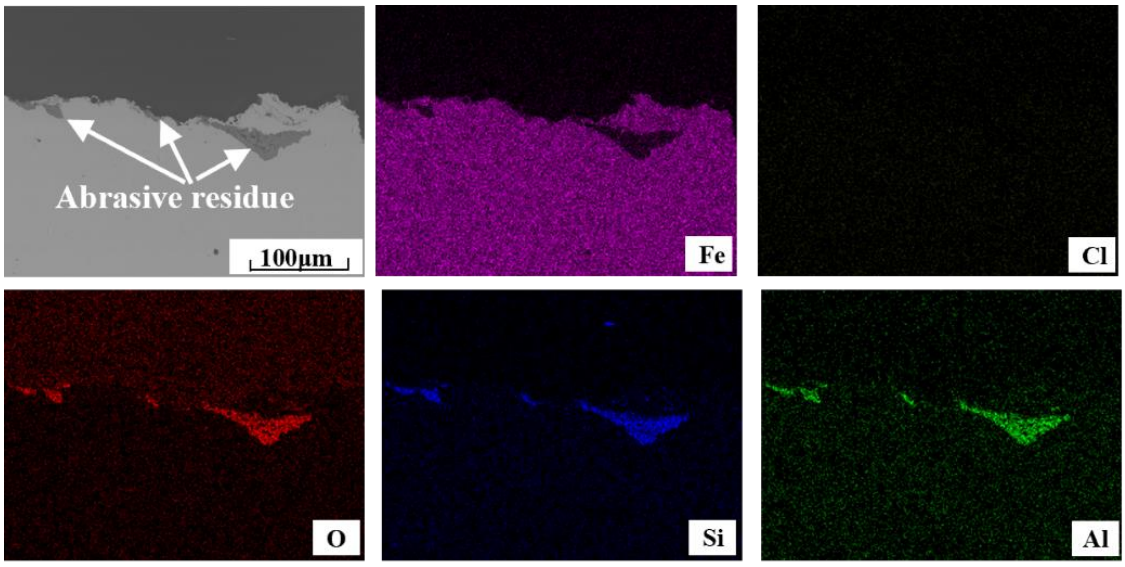

Figure 0-15 SEM–EDX images showing blasted surface of garnet.

5.3.3.3 Surface cleaned via CWL

Figure 0-16–19 show the SEM–EDX images of the surface after laser cleaning. Figure 0-16 shows the DLC measurements, where Point 1 indicates the re-corrosion area. Based on the EDX diagram, the observation area contained a significant amount of Cl, and its weight ratio was approximately 20 times that of the clean area, with a maximum value of 0.92 wt%. The corrosion in this area may have been caused by incomplete laser irradiation or foreign contaminants because this area was near the cut anchor point. At Points 2 and 3, the light and dark areas represent the remelted and oxidized layers in the cleaned area, respectively. The oxidized area contained cracks, and particles measuring 10–20 μm were observed on the surface. Comparing Points 2 and 3 (corresponding to the blue and black areas of the macroscopic observation, respectively), the weight ratios of O were 10.9 wt% and 3.74 wt%, respectively, which confirms that the difference in color of the clean surface was caused by the difference in the surface oxide layer. The SEM image at Point 3 shows the typical melt-pool traces of the laser, and the width of the traces was consistent with the diameter of the laser spot (approximately 500 μm). The sides of the laser path protruded slightly and appeared as dark oxide layers.

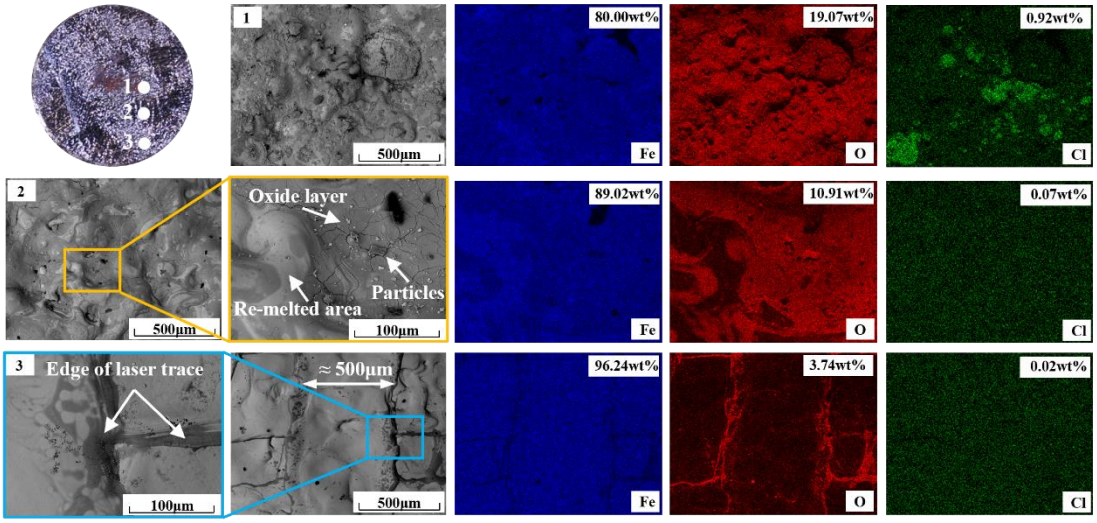

Figure 0-16 SEM–EDX micrographs of DLC.

Figure 0-17 the observation result of WLC-1. At Point 1, corrosion products were observed above the laser trace, which is characteristic of re-corrosion after laser cleaning. A Cl band (the region encircled by a dotted white circle) was observed in the EDX image; in the SEM image, this band appeared as black particles. It was conceivable that external contamination was one of the causes of corrosion since the corrosion area was near the cutting edge. Points 2 and 3 were cleaned areas. The laser tracks at Point 2 overlapped and the arrangement was proportioned well, which reflected the ideal laser cleaning state. Compared with Point 2, the coverage of the laser track at Point 3 reduced significantly, and the oxide layer on both sides of the molten pool track was thinner, which broke and peeled off easily. The broken oxide layer was accompanied by particles that measured only a few microns, i.e., they were significantly smaller than the residual particles from DLC. For both the WLC-2 and WLC-3 cases, shown in Figure 0-18 and 19, respectively, the number and size of particles in the cleaned area decreased significantly, and no incompletely cleaned particles were observed, similar to the WLC-1 case. Furthermore, the area of the oxide layer reduced compared with the DLC and WLC-1 cases, which was consistent with the macroscopic color difference observed on the cleaned surface. In the WLC-2 case, a larger salinity area was discovered in the corrosion zone, which might be caused by the soluble salts in the water. In the WLC-3 case, although no elemental chlorine was observed on the surface of the corroded area, corrosion products remained above the cleaned surface. The running water can wash away the soluble salts, but the

flushing water will introduce impurities from other corrosion areas, thereby resulting in re-corrosion to the surface.

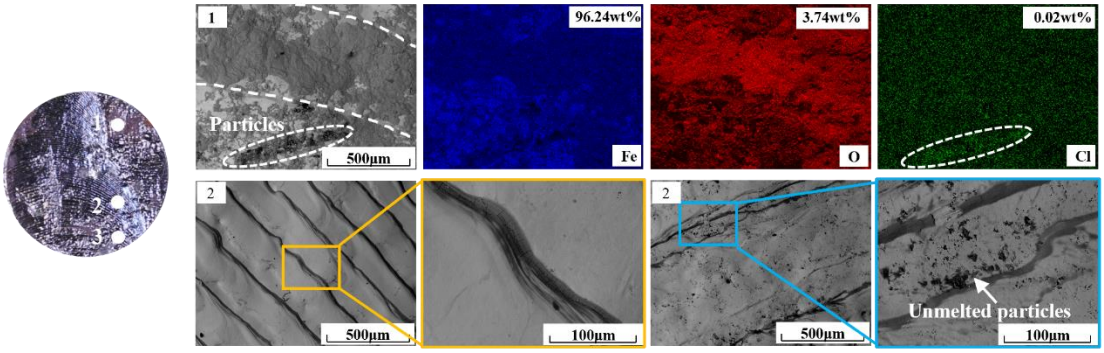

Figure 0-17 SEM–EDX micrographs of WLC-1.

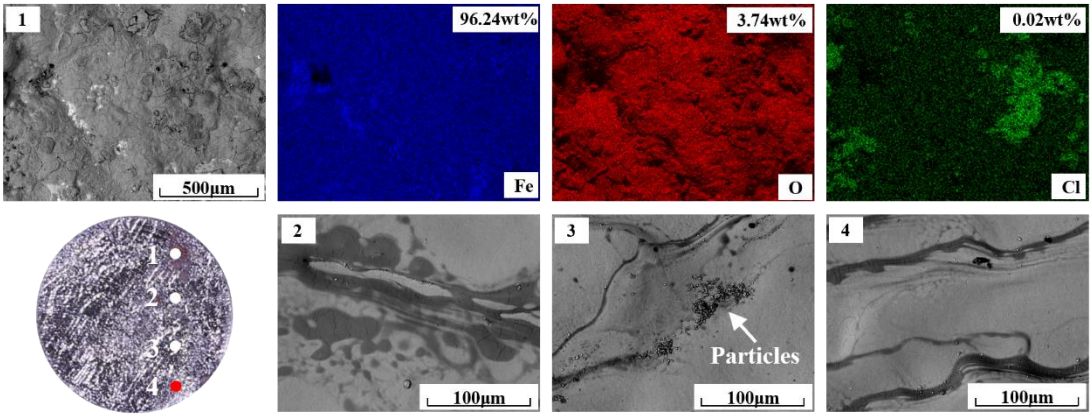

Figure 0-18 SEM–EDX micrographs of WLC-2.

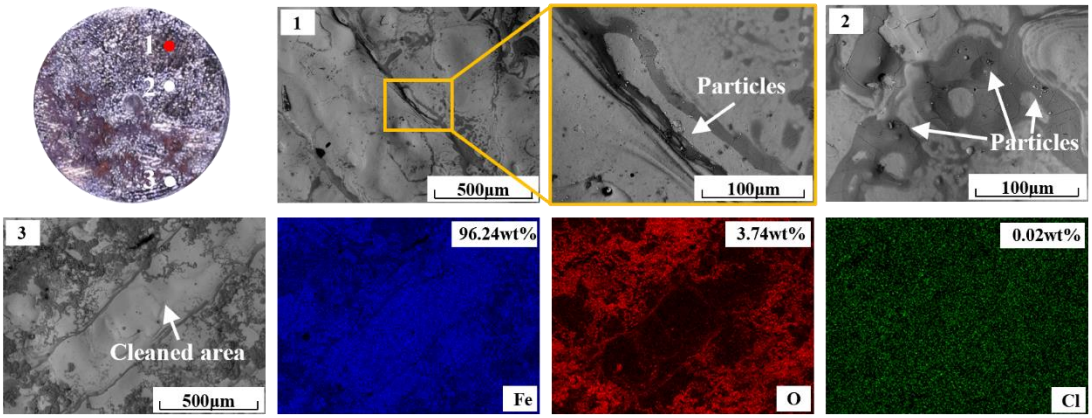

Figure 0-19 SEM–EDX micrographs of WLC-3.

Figure 0-20 shows the cross-sectional views of the DLC and WLC samples. After laser irradiation, an oxide layer of approximately 30 μm thick formed on the metal surface. Figure 0-20(a) and (b) show the uniform oxide layer on the surface of the DLC and WLC-2 samples; no corrosion products or salt residues were observed above and below the oxide layer, and the expected cleanliness level was achieved. To verify the effect of laser cleaning on the corrosion pit area, the conditions at the pitting area of each sample were observed, as shown in Figure 0-20 (c)–(g). Figure 0-20(c)–(f) show that the pitting area was completely cleaned by the laser. An oxide layer was observed in the upper region of the pits, and below the oxide layer, no salt and corrosion residue was observed. However, for the WLC-2 case, as shown in Figure 0-20(e), salt accumulation was observed in the upper region of the oxide layer. This may be because impurities and salts remained in the water film and then adhered to the surface. In the WLC-3 sample, we discovered an area that was not cleaned by the laser, as shown in Figure 0-20(g), which resulted in residual corrosion products in the pitted area. Incomplete cleaning may be caused by flowing water, and engineers cannot assess the completeness of cleaning via visual inspection. No salt agglomeration was observed in the residual corrosion product, which may be due to the dissolution of some soluble salts in the high-temperature flowing water. Although the soak and rinse method in laser cleaning can yield clean surfaces, it presents some drawbacks in engineering applications.

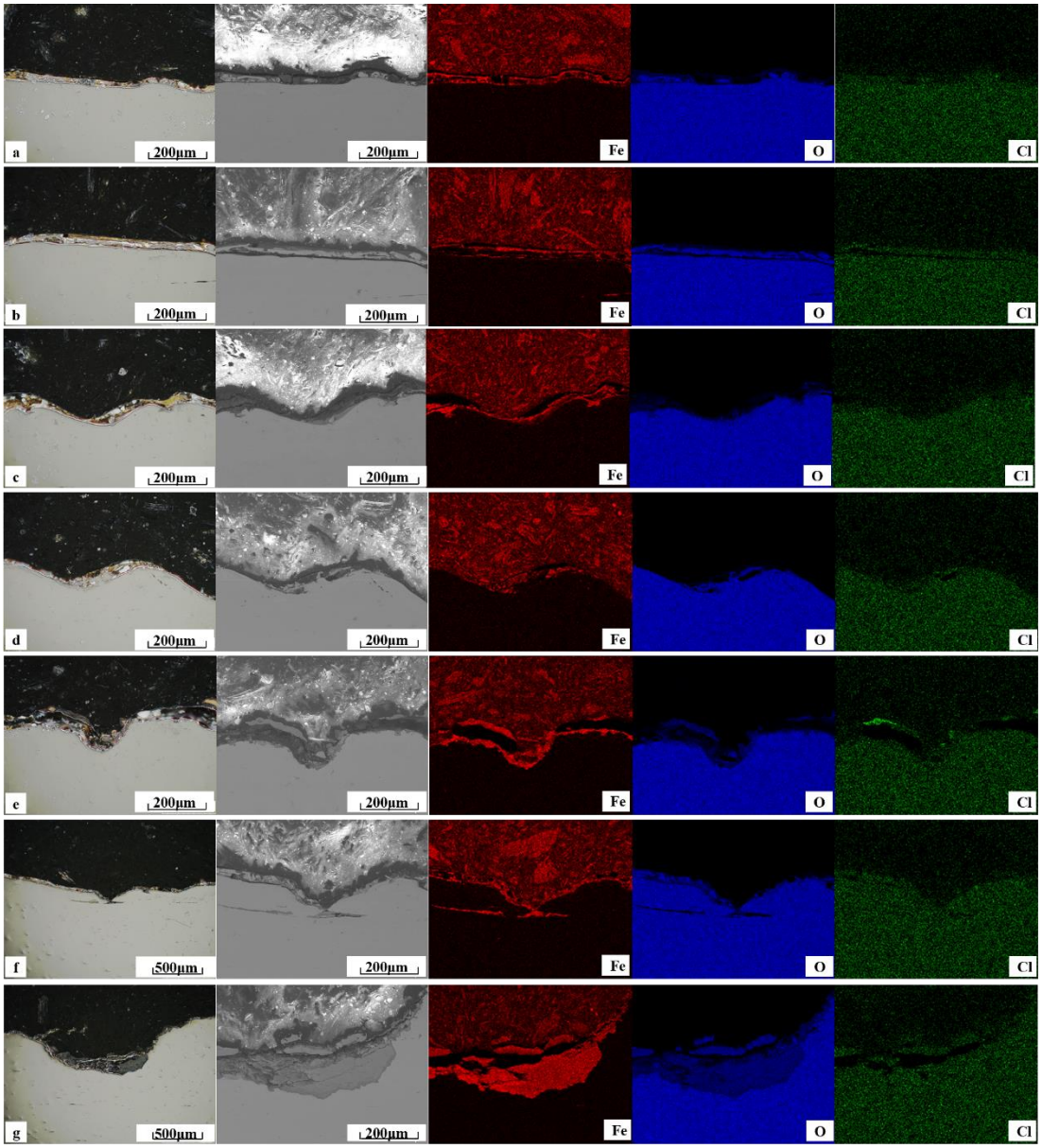

Figure 0-20 OM and SEM–EDX images showing cross section of laser-cleaned sample.

1.21.4 Observation of heat-affected layer after laser cleaning

An etching test was performed to investigate the cross section after etching using 3% nital to reveal the processing range and heat effects during laser cleaning. An optical photograph of the etched section is shown in Figure 0-21. The laser-irradiated surface comprised two layers: an oxide layer and a heat-affected layer. Owing to the high power density of the CWL, a thin melt layer of steel appeared and formed a remelted zone (MZ) after cooling below the oxide layer. Below the MZ, the laser beam affected the substrate and modified a certain depth of the microstructure, which

resulted in the formation of a heat-affected zone (HAZ)[135]. After the etching test, the MZ and HAZ showed different colors and stratifications owing to changes in their microstructures. In Figure 0-21, the surface of the oxide layer is denoted by white contour lines, the boundary of the MZ by yellow contour lines, and the bottom edge of the MZ and HAZ by red contour lines. No HAZ was observed under the MZ, which was due to the higher processing speed. In the case of DLC, owing to the direct thermal effects from the laser beam, the oxide layer was slightly thicker than that achieved via WLC, where the average thickness exceeded 50 μm. In the case of WLC, the oxide layer was thin, uniform, and measured approximately 30 μm thick. In all cases, the average depths of the MZ and HAZ were 40–50 μm and were slightly thicker in the repeated treatment area, reaching a maximum value of approximately 80 μm.

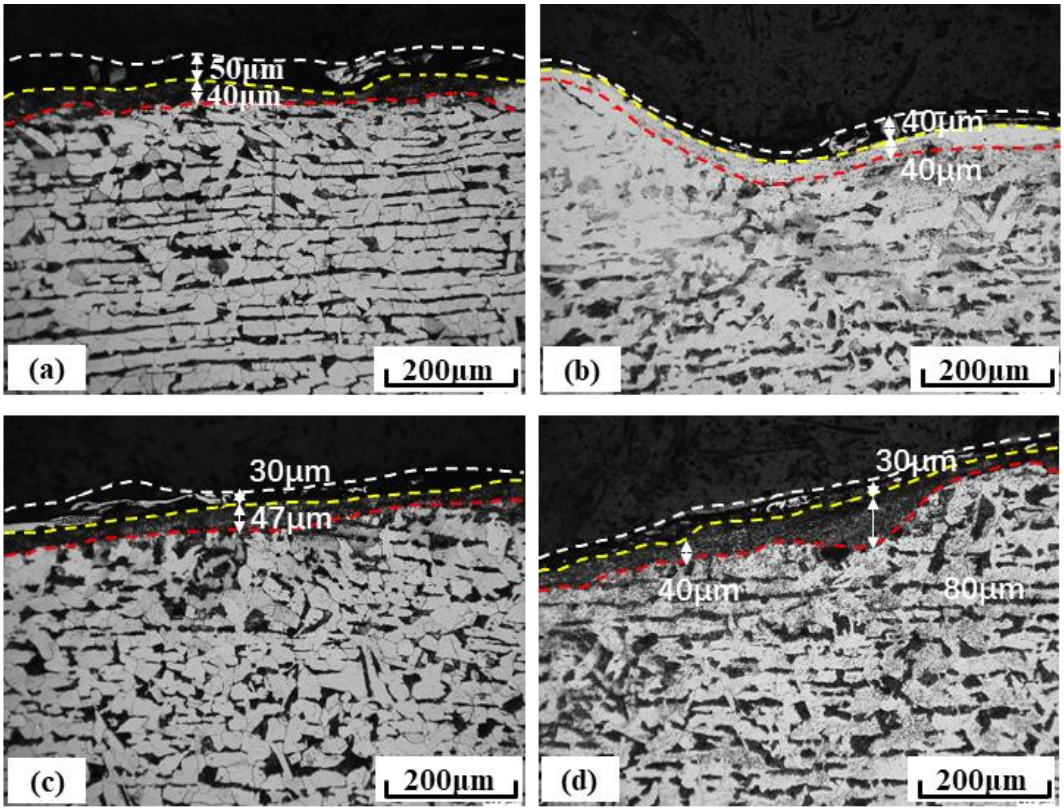

Figure 0-21 Thickness of MZ and HAZ on laser-cleaned specimens: (a) DLC-1, (b) WLC-1, (c) WLC-2, and (d) WLC-3 specimens.

1.22 Mechanism analysis of surface cleaning

Laser surface cleaning is a new and efficient method for cleaning severely corroded members. In this study, laser cleaning achieves same rust removal levels to abrasive blasting (Sa2.5 or Sa3), also achieves a good salt removal effect and avoids the residue of abrasives on the surface. The characteristics of garnet blasting and four types of laser cleaning are summarized in Table 0-5.

Compared with abrasive blasting cleaning, laser cleaning offers a more efficient and stable cleaning efficiency for the same or similar visual cleanliness index. For cleaning severely corroded steel components, the cleaning efficiency of abrasive blasting is only approximately 5% of the theoretical efficiency, which may be much lower in actual engineering. Complete cleaning of severely corroded surfaces often requires more than three rounds of abrasive blasting operations to remove the rust in the corrosion pits[11]. In some cases, warm water washing was necessary between the blasting operation rounds. To achieve ideal cleaning results, relatively expensive abrasives such as fused alumina are sometimes necessary[136]. In contrast, the manual operation of the laser transmitter to clean the severely corroded steel surface can maintain a uniform treatment efficiency, and a clear laser irradiation trace profile can be observed on the cleaned surface, indicating complete removal of corrosion products. The cleaning efficiency was more than 50% higher than that of the abrasive blasting. Therefore, for corrosion cleaning under severe corrosion conditions, the 3 kW CWL transmitter realized in this study has higher efficiency, saving time and cost while achieving the same cleaning results. Even if no corrosion products are observed on the blasted surface, flash rust can be initiated within tens of minutes at room temperature. Studies have shown that after 24 h, regardless of the size of the pit, there will be significant rust on the bottom owing to residual abrasives and salts[14]. CWL-cleaned surfaces take longer to re-corrode compared with blasted surfaces. After the laser-treated samples were cooled, cut, and transported, re-corrosion occurred in only some areas, which cannot rule out external causes. This indicates that laser cleaning offers significant advantages in terms of rust and salt removal. The main difference between laser and abrasive blast cleaning is that the corrosion products are ablated rather than crushed and cut. Without the use of abrasives during laser cleaning, byproduct generation and abrasive residue problems were avoided.

Table 0-5 Characteristics of cleaned surface

Case	Efficiency (m^2/h)		Re-corroded area	Surface roughness (μm)		Color
	theory	actual		Ra	Sa	
Garnet blast	15–30	0.72		13.6	15.3	Gray, matte
DLC		1.20	<5%	11.8	12.3	Black and blue, pearlescent
WLC-1	0.84	1.07		17.3	19.5	Blue, pearlescent
WLC-2		1.23		8.03	8.11	Yellow,
WLC-3		0.95	≈30%	14.3	15.3	pearlescent

The difference between a CWL and a PL is that a high-power CWL has a continuous thermal density input, but the energy density is inferior to that of PL owing to the larger diameter of the laser point. The energy density of the 3 kW CWL used in this study is only 2,066 kW/cm^2, which is not sufficient to excite ionization to form plasma during the cleaning process[69,72,124], and thus avoids the shielding effect of the plasma and thermal energy loss[60]. According to Zhuang[71]. The 3 kW CWL used in this study can instantaneously form a localized high temperature of approximately 1,500–2,000 °C on the surface, which is sufficient to melt and evaporate corrosion products and impurities instantly. Therefore, the main rust removal mechanism of CWL is the melting and evaporation of corrosion products caused by ablation.

Excessive ablation should be avoided during laser cleaning. In PL studies, it is generally considered that excessive ablation of cleaned surfaces is characterized by remelting and the formation of oxide layers[20,62,74]. However, this is difficult to avoid in practical engineering because of the existence of corrosion pits, and the ablation degree at different depths of the surface is not completely consistent. Excessive ablation cannot be avoided to achieve the complete goal of rust removal. In this study, we defined the surface as completely cleaned when the obvious laser trace occurred on all surfaces. These traces were the molten pool traces formed by laser irradiation directly on the surface of the steel substrate after the rust layer was completely removed[137]. In fact, because the CWL used in this research has a high movement speed, the molten pool is shallow and does not cause excessive heat impact on the steel substrate, resulting in a thin MZ and HAZ[28]

of only tens of micrometers. This is acceptable for use in steel structures. Research by Zhuang shows that the microhardness of the surface after the 3 kW CWL irradiation increased no more than 50 HV, which only appeared in the thin MZ and HAZ, which allows the laser-cleaned surface to have a certain wear resistance and corrosion resistance[29]. Because of the surface tension of the melton metal, the laser-cleaned surface profile was relatively smooth. Studies have shown that a flat surface can achieve high corrosion resistance and hydrophobicity[63,64], as was similarly demonstrated via electrochemical experiments by Zhuang[30]. Laser-cleaned surfaces have low surface activity, and hence a low re-corrosion rate. This also explains why the re-corrosion turning time of laser-cleaned surfaces is longer, reaching approximately one week.

In the laser cleaning process, the temperature of the steel component needs to be considered, because the material properties begin to decline when the temperature of the steel reaches 200 ℃[138,139]. Water was supplied to cool the cleaned surfaces and structures. The partial laser cleaning process lasted only a few minutes and then cooled in air or water. This process is similar to the tempering of steel, so the laser-cleaned surfaces appear in different colors owing to the dense oxide layer formed during the cooling process. The thickness and composition of the oxide layer and the luster colors were different. For low carbon steel, tempering color and temperature can be one-to-one matched by tempering steel color chart, oxide film gloss from yellow, light blue to gray corresponding to 200, 300, and 400 °C, respectively. The laser-cleaning water supply can absorb and remove part of the heat energy faster to reduce the temperature of the component. The surface colors of DLC, WLC-1, WLC-2, and WLC-3 are blue, black, light blue, and yellow, respectively, indicating that the water supply can reduce the component temperature to a certain extent and provide a safer range for laser cleaning.

In the case of the WLC, the laser passed through the water film or layer before irradiating the metal surface, causing a slight loss in energy[22]. Most of the energy is absorbed by the target surface, and the local high temperature causes the water film to heat significantly, resulting in the eruption of water vapor, which removes the impurity particles on the surface and improves the micro-cleanliness. The drench method (WLC-1) can be considered as a semi-dry method. The thin water film and water in the corrosion products evaporate instantly and completely during cleaning, and the surface is dry after cleaning. Explosive vaporization of water occurred at the interface

between the water film and corrosion products, which facilitated the removal of contaminant particles and provided an excellent cleaning effect. Contaminants on the surface of the WLC-1 sample were significantly reduced, as confirmed by Kim and Tian[63,66]. Unlike the drench method, the surface cleaned by the soak (WLC-2) and rinse (WLC-3) methods remained wet after laser irradiation. In the cases of WLC-2 and WLC-3, the laser energy was not completely input to the target surface, but part of the energy was dissipated in the water film. In this study, because the water film measured as only tens of millimeters thick, a loss of laser energy of no more than 10% will not change the cleaning effect. The CWL mechanisms of WLC-2 and WLC-3 are completely different from those of WLC in PL. It is difficult for a CWL to form underwater cavitation bubbles[69], as shown in Figure 0-22(a). Owing to the rapid sweep of the CWL, water vapor ejects from the irradiated area and blows around the water film. The WLC of the CWL is not even under the water film, as can be observed in Figure 0-3(c). Therefore, in the WLC of the CWL, the eruption of water vapor plays a major role in microscopic cleaning. In addition, the rapidly blown water film can also provide water washing, cooling, and dissolution of soluble salts on the surrounding surface, as depicted in Figure 0-22(b). In both WLC-2 and WLC-3, the water layer was able to repeatedly wet and cool the irradiated area; therefore, the surface was theoretically cleaner than WLC-1 during repeated cleaning. However, in the actual operation, we found that the dissolved impurities in the water film of WLC-2 and foreign pollutants in the water flow of WLC-3 would cause secondary pollution to the surface, which is also the reason why the discovered salts accumulated on the top of the oxide film, as shown in Figure 0-20 (e). In addition, water flow and the large amount of water vapor formed during CWL irradiation affected the observation of the operator, particularly WLC-3, resulting in a decrease in irradiation efficiency and the appearance of imperfect irradiation, as shown in Figure 0-20(g).

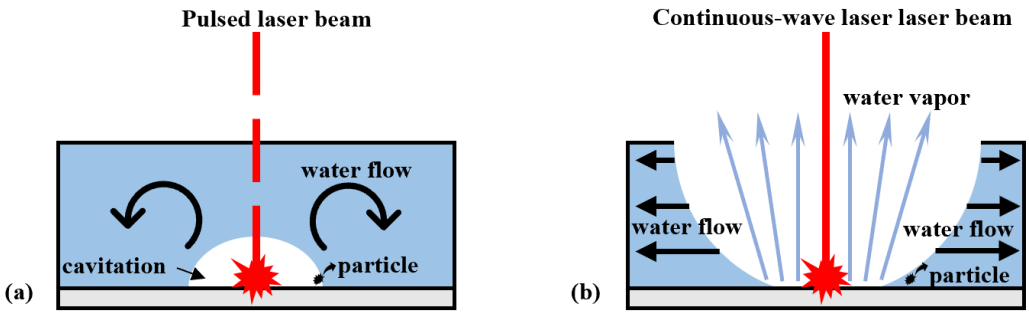

Figure 0-22 Mechanism of laser surface cleaning with water supply.

Although laser cleaning in water is advantageous in terms of its mechanism, it exhibits many limitations in engineering. For example, in the corrosion cleaning of steel bridges, the soak method cannot be used for the most severely corroded lower flange or bottom plate. Although the rinse method can be used for all steel members, it is difficult to drain water and prevent contaminants from entering a clean surface. Hence, the drench method is recommended for cleaning the laser surface. This method can be used in oceanic climates with high relative humidity or cleanliness during the rainy season or in a long-term dew condensation environment. The re-corrosion of the laser-cleaned surface is much longer than that cleaned via abrasive blasting, and the surface state can be maintained at the same level as that of Sa2.5 for more than a few days. The surface after laser cleaning exhibits high corrosion resistance, which facilitates the planning of the corrosion-cleaning cycle.

1.23 Summary

In this study, an environmentally effective 3 kW CWL transmitter was innovatively used to directly remove corrosion products from steel surfaces of real structures. The morphologies and microstructures of laser-cleaned surfaces under different treatment conditions were examined and analyzed. The main results are as follows, which can contribute to steel structure rust removal and anti-corrosion maintenance.

In this study, CWL was used for rust removal and corrosion maintenance. Corrosion products and salt in the pits of severely corroded steel components were successfully removed, and the cleaning effect reached the same Sa2.5 or Sa3 level as abrasive blasting.

In the case of cleaning severely corroded steel components, the efficiency of 3 kW CWL treatment is more than 50% higher than that of garnet blasting, which can reach 1.2 m^2/h through manual operation.

The 3 kW CWL laser transmitter can effectively ablate, melt, and evaporate corrosion products and impurities, form a molten pool track on the steel substrate, and achieve rust and salt removal.

The water supply can reduce the laser thermal effect on the steel surface, and the generation of steam and water flow can help clean the surface impurity particles.

The WLC drench method has the best cleaning effect and can be promoted and applied in actual cleaning engineering. The soak-and-rinse method may not be suitable for use because of restrictions on the construction site.

CWL SURFACE CLEANING OF HIGH STRENGTH BOLTS: ANALYSIS OF BOLT AXIAL FORCE LOSS

1.24 Introduction

Owing to the hexagonal shape of bolt heads and nuts, the coating on the corner parts is frequently thinner than that on the other parts[75]. Coating failure and corrosion problems are evident in these parts. In addition, the structure of bolt joints is frequently complicated, where deposited rainwater and pollutants also aggravate the deterioration [105]. Studies have shown that corrosion damage to the bolt head and nut directly affects the axial force of the bolt [76–79], which is unacceptable, particularly for friction-type high-strength bolted components.

The reduction in the bolt axial force is the main cause of bolt looseness and joint failure; therefore, research based on bolt looseness detection has become an important topic in related research. Measurement methods based on impedance, vibration, and ultrasonic, among others, have been widely proposed[84,140–142], which can quickly and accurately detect the bolt axial force. Cleaning and maintenance will be an economical option for high-strength bolts that have coating failure and corrosion but still have sufficient axial force. The friction surface of the clamped bolt will not be corroded[143]; therefore, cleaning and coating the outer surface of the bolt will effectively prevent the failure of the bolt due to corrosion and extend the service life.

Currently, the primary methods for bolt coating and maintenance include power tools, paint strippers, and thermal stripping[80]. Often, they cannot achieve very good cleaning results, particularly because the rust removal effect cannot fully satisfy the standard of repainting[43]. Commonly used surface treatment technologies for large areas, such as abrasive blasting, are limited by the narrow space; therefore, it is difficult to use them for bolts in maintenance. Laser treatment as an alternative method can be applied to corrosion cleaning of local and narrow spaces, which provides new options for bolt maintenance. In addition, the laser excitation vibration measurement of the bolt axial force has been a hot topic in recent years[83,85,144]. The use of a laser to confirm the bolt axial force will help determine if a bolt is loose and needs to be cleaned. Applying laser

technology to bolt detection, cleaning, and maintenance is a major direction for future development.

The purpose of this study was to discuss the possibility of using a 3-kW rotary-type continuous-wave laser (CWL) to clean and maintain an M22 high-strength bolt. The 3-kW CWL can continuously and stably output the energy density of 2070 kW/cm^2[145], which is sufficient to realize the high temperature of approximately 2000℃ instantly of the irradiated spot area[71], and ablative heavy anticorrosive coating and thick rust layer to achieve the optimal cleaning effect[146]. Considering the possible influence of temperature and vibration on the strength and stiffness of the bolt joints [147–149] caused by CWL irradiation, the corresponding relationship between the bolt axial force, different irradiation durations, and multiple rounds of irradiation was discussed. Through axial strain and temperature monitoring and FE model temperature field analysis, the appropriate 3-kW CWL irradiation maximum duration was determined, and the bolt axial force loss could be guaranteed within an acceptable range. The results of this study can provide a reference for 3-kW CWL cleaning and the maintenance of M22 high-strength bolts.

1.25 Preparation of high force bolt specimens

1.25.1 Specimen design

To obtain the change in the axial force of the bolts and examine the relationship between the axial force loss and laser irradiation duration, fabricated bolts with an embedded 1G3W type strain gauge (impedance of 120 Ω, length of 2 mm and heatproof temperature of 200℃) and a T type thermocouple, as Figure 0-1(a) shows. To avoid the influence of the buried thermocouple on the accuracy of the strain gauge, the thermocouple is buried on the side far away from the irradiation, and the distance between the thermocouple and the strain gauge is 30 mm. The bolts used for the test were friction-type high-strength F10T M22 bolts specified in Japanese Industrial Standard (JIS) with a diameter of 22 mm and a tensile strength of 1000 N/mm^2. A friction connection specimen consisting of a three-layer steel plate was selected as Figure 0-1(b) shows. Six friction connection specimens were fabricated, and 12 bolts were used for laser irradiation. For convenience, the details of the specimens and irradiation durations are listed in Table 0-1. Two different irradiation conditions were considered in the test. Continuous irradiation means that each bolt was only

irradiated one round until the cleaning process was complete. The durations of continuous irradiation were 15, 30, 45, and 60 s. Multiple rounds of irradiation consider the tolerance of bolts to high temperatures. The irradiation duration for each round is short. Additional irradiation rounds were performed after the bolts were cooled to the ambient temperature. In this study, multiple rounds of irradiation were divided into two conditions: the first was four rounds of 15 s irradiation; the second was two rounds of irradiation, with the first round of irradiation for 15 s, and the second round of irradiation for 15, 30, and 45 s, respectively. The maximum total irradiation duration under the two conditions was 1 min.

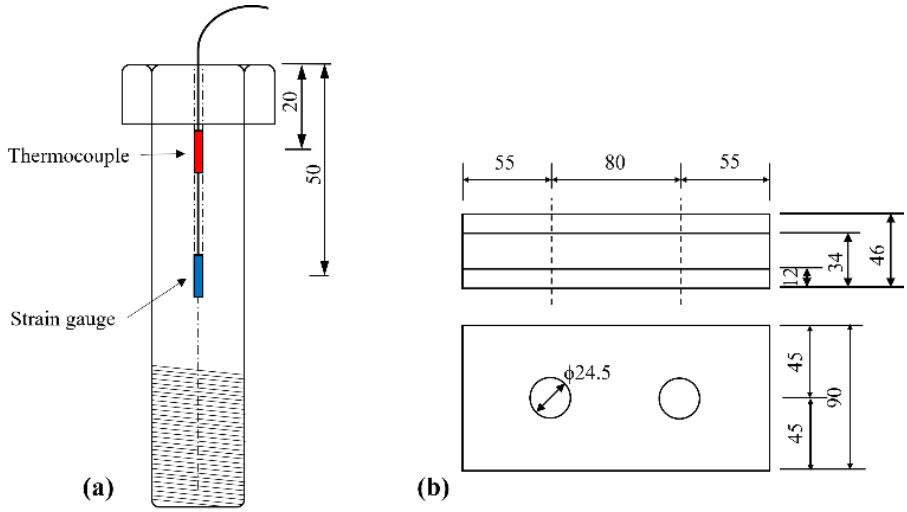

Figure 0-1 (a) High-strength bolt with strain gage and (b) dimensions of the friction connection specimen (unit: mm)

Table 0-1 Laser treatment specimens' irradiation duration

Specimen	No.	Irradiation conditions	Irradiation duration (s)
S1	B1 B7	Multiple irradiation	15+15+15+15
S2	B2 B8	Multiple irradiation	15+30
S3	B3 B9	Multiple irradiation	15+45
S4	B4 B10	Continuous irradiation	30
S5	B5 B11	Continuous irradiation	45
S6	B6 B12	Continuous irradiation	60

1.25.2 Specimen assembly

The steel plates of the specimens were subjected to steel slag blasting before assembly. All bolts were wiped with xylene to clean oil before assembly to avoid the loss of axial force caused by friction [150,151]. The specimens were assembled at a room temperature of 25°C, and all bolts were tightened with an electric torque wrench. Because the bolts with strain gauges were subjected to an axial force–strain test during fabrication, the axial force value of each bolt could be obtained directly through the strain value from the datalogger when tightening. The design axial force of the M22 bolt used in the experiment was 205 kN, and the standard axial force applied during the actual tightening was approximately 110% of the axial design force, reaching 226 kN. The tightening process was divided into two parts: tightening to approximately 70% of the designed axial force and tightening to the standard axial force of 226 kN.

1.25.3 Laser Surface Treatment

Laser treatment was performed three weeks after the specimens were assembled to avoid errors caused by the initial loss of the bolt axial force [152]. The CWL used for cleaning was refracted through a high-speed rotating prism, forming a spinning laser ring[30], as shown in Figure 0-2. The focusing distance between the prism and target surface was controlled at 200 mm, and the diameter of the laser ring was 26 mm. The power density of the laser spot reaches 2,070 kW/cm^2, which is sufficient to melt and evaporate the coating and rust layer instantly and achieve a cleaning effect. The laser processing parameters are listed in Table 0-2.

A rotatable platform was used to implement uniform laser irradiation of the nut. The bolts were rotated at a speed of 12 rpm during irradiation and the laser transmitter was set at a fixed angle of 45° to ensure that the same conditions irradiated on the nut, as shown in Figure 0-3(a). The irradiation speed and angle settings were kept as close to manual or mechanical cleaning engineering as possible [153]. Under this setting, the upper and side surfaces of the nut and washer are completely irradiated, as shown in Figure 0-3(b). The video showing the bolt-cleaning process is included in the supplementary data. During the entire irradiation process, the bolt axial force (strain of the gauge) and the temperature change of the bolt were recorded using a data logger (TDS-530,

Tokyo Measuring Instruments Lab, Japan).

Table 0-2 CWL parameters

Parameter	Value	Unit
Output power	3	kW
Spot diameter	430	μm
Motor speed	5,000	rpm
Irradiation ring diameter	26	mm
Spot moving speed	681	cm/s
Input power density	2,070	kW/cm^2

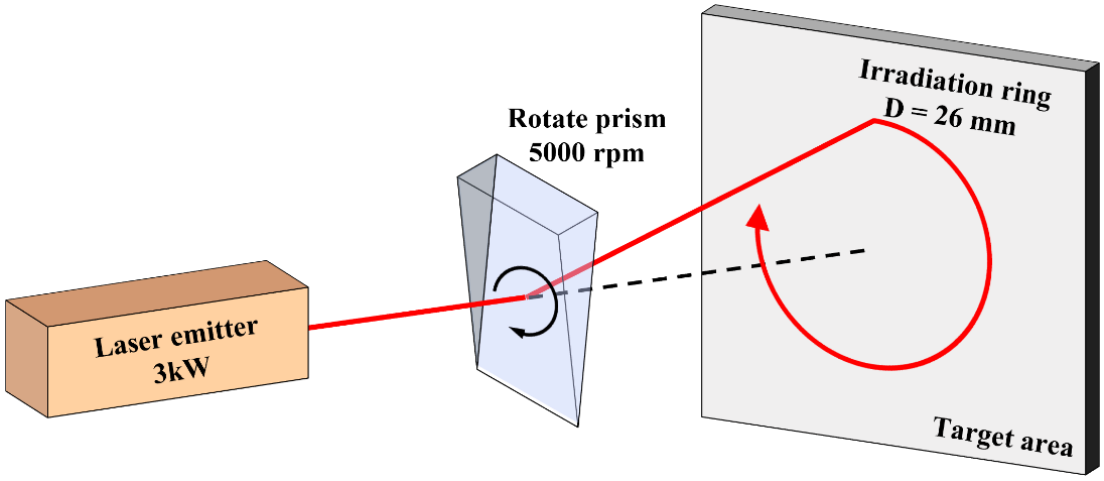

Figure 0-2 Schematic diagram of rotating CWL transmitter

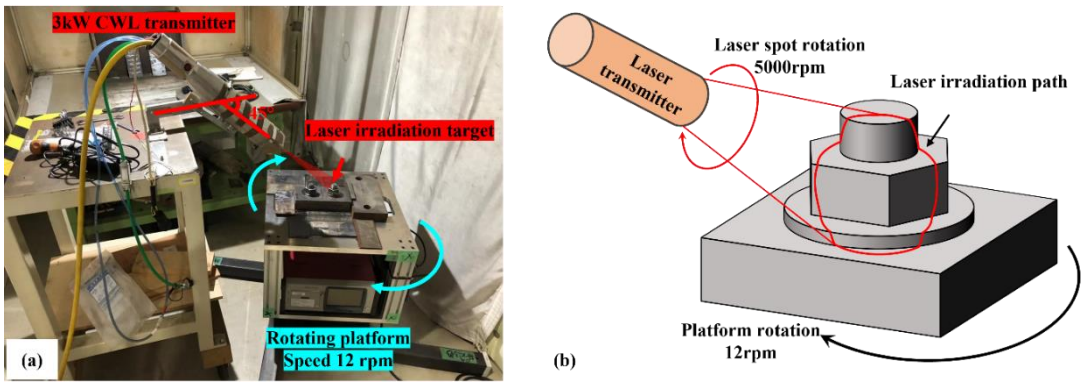

Figure 0-3 Laser transmitter and rotating platform of (a) setting of laser treatment device and (b) diagram of laser cleaning on nut side

1.25.4 Finite-element temperature simulation

A solid model of the friction connection specimen was constructed using the finite element (FE) code MSC Marc/Mentat 2020. The steel plate size was set to 190 mm long, 90 mm wide, and 46 mm thick, similar to the specimens used in the experiment. The specimen was discretized to an 8-node solid element. The steel plate was meshed to a size of 5 mm × 5 mm. Both sides of the steel plate were constrained directly. To improve the efficiency, dense meshes were present around the heated region. To facilitate the loading of the load step, the bolts, nuts, and washers were meshed into 24 pieces around the central axis. The mesh size was approximately 1 mm × 1 mm. The outermost element layer of the bolt is simply defined as threads. Steel plates, washers, bolts, threads, and nut components are shown in different colors in Figure 0-4, and their contact relationships are defined as direct contact. Heat flux was applied to the nut, washer, and steel plate to simulate the laser-beam irradiation process [70]. Owing to the fast movement of the laser spot, the heat energy input was simplified as laser ring loading, as shown in Figure 0-4. The laser thermal energy is vertically input as a stream of heat flux of 6.5×10^{10} W/m^2 to the element surface [154,155]. The action position changes continuously with time. As the load step continued, the heat load moved around the nut, and the duration of each load step was 0.2 s. The specimen cooled in the air after laser irradiation, and the ambient temperature was set at 18℃ consistent with the test site. Because all parts of the specimen were fabricated from carbon steel, the elastic modulus E, thermal expansion coefficient α, specific heat C, thermal conductivity λ, and thermal convection heat transfer coefficient h were set to be the same; their changes with temperature are listed in Table 0-3.

Table 0-3 Materials properties of FE model

Temperature (℃)	E (GPa)	α (10^{-6}/℃)	C (kJ/(kg·℃))	λ (W/(m·℃))	h (W/(m^2·℃))
25	206	14.6	0.462	45	25
300	193	11.3	0.560	41	500
500	170	11.8	0.652	38	3,400
800	86	17.8	1.297	32	11,000
1,000	34	19.6	0.604	30	18,000
1,300	30	19.6	0.604	30	33,000
1,500	30	19.6	0.604	30	45,000

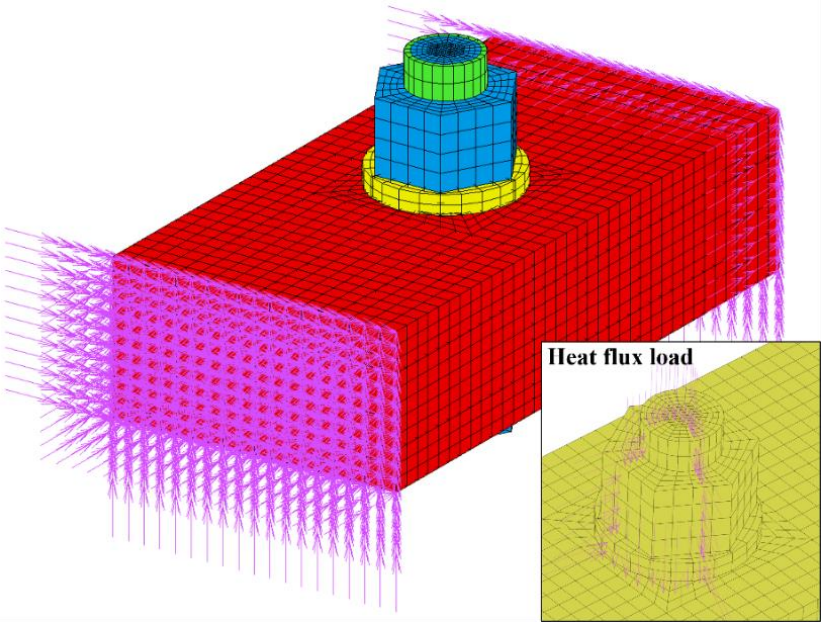

Figure 0-4 FE model of friction-type bolt components

1.26 Analysis and mechanism of axial force change during CWL cleaning

Research has shown that the axial force of high-strength bolts significantly decreases once corrosion occurs [75,77,143,156]. This study simulated the process of cleaning the coating and rust of bolts using a 3-kW CWL . The bolts to be cleaned should at least maintain sufficient axial force and be in working condition, with the remaining axial force value close to the standard value. Therefore, the bolts with an initial loss were selected for this study. It should be noted that bolts that are severely corroded or loose are not considered for cleaning in this study because they are outside the working conditions and need to be replaced. In addition, this study has certain applicability limitations; for narrow and corner bolt joints, the rotary cleaning method is not applicable.

The axial force of the bolt was obtained by measuring the strain value of the gauge embedded in the bolt. Table 0-4 shows the initial strain ε_0 and corresponding axial force F_0 of the 12 bolts before the laser treatment, and the ratio of the axial force to the standard axial force F%. The axial force of each bolt cannot be exactly the same after the initial loss of stress. Here defines the ratio of the real-time axial force F_t to the initial axial force F_0 as the axial force change ratio F_t/F_0 used for the analysis and equation fitting. The difference between F_t and F_0 is defined as the axial force change ΔF, which is used to monitor the actual axial force change and avoid excessive loss.

Table 0-4 Initial strain and axial force of measured bolts

Bolt	ε_0	F_0 (kN)	F%
B1	5,260	210	102
B2	3,970	215	105
B3	4,510	214	104
B4	6,400	226	110
B5	5,880	221	107
B6	4,910	212	103
B7	3,760	223	108
B8	4,360	218	106
B9	5,820	216	105
B10	5,070	228	111
B11	4,820	217	105
B12	5,930	220	107

Table 0-5 Changes in axial force after continuous irradiation

Bolt	Irradiation duration (s)	F_0 (kN)	F_{max} (kN)	F_{max}/F_0	ΔF_{max} (kN)	F_{min} (kN)	F_{min}/F_0	ΔF_{min} (kN)	F_s (kN)	F_s/F_0	ΔF_s (kN)
B1	15	210	220	1.04	10	201	0.96	-9	204	0.97	-6
B2	15	215	223	1.03	8	205	0.95	-10	207	0.96	-8
B3	15	214	222	1.04	8	206	0.96	-8	208	0.97	-6
B4	30	226	235	1.04	9	203	0.90	-23	210	0.93	-16
B5	45	221	228	1.03	7	192	0.87	-29	203	0.92	-18
B6	60	212	220	1.04	8	176	0.83	-36	187	0.88	-25
B7	15	223	232	1.04	9	210	0.94	-13	213	0.96	-10
B8	15	218	226	1.04	8	210	0.96	-8	213	0.98	-5
B9	15	216	225	1.04	9	206	0.95	-10	212	0.98	-4
B10	30	218	227	1.04	9	188	0.86	-30	201	0.92	-17
B11	45	217	226	1.04	9	180	0.83	-37	199	0.92	-18
B12	60	220	229	1.04	9	184	0.83	-36	197	0.89	-23

1.26.1 Axial force loss related to continuous irradiation of laser

To evaluate the loss of the axial force of high-strength bolts using laser irradiation, we compared the bolt stress changes at different irradiation durations. Figure 0-5 shows the time-dependent changes in the bolt axial force before and after the laser surface treatment. The change in the bolt axial force can be divided into three stages for irradiated bolts. The axial force rapidly increased to the maximum value F_{max} in the first 15 s of irradiation, and the axial force increased by

no more than 10 kN, less than 5% of F_0. For irradiation over 15 s, F_{max} did not increase with increasing irradiation time. After the irradiation was stopped, the axial force decreased steeply to the minimum value F_{min} within 60 s, and F_{min} decreased with increasing irradiation time. As the specimen continued to cool, the axial force gradually recovered and stabilized to F_s within minutes after irradiation. As shown in Figure 0-5, the axial force of the bolt exhibited different degrees of loss after laser irradiation, affected by the irradiation time. The axial forces of the adjacent non-irradiated bolts were also recorded simultaneously. Observed that the axial force of the adjacent bolts varied by no more than 1% during irradiation, and almost no loss of axial force occurred after cooling. It can be considered that when an M22 bolt is irradiated by a 3-kW CWL with a 26-mm-diameter laser ring, there is no effect on the adjacent bolts. After the specimens were cooled sufficiently, the adjacent bolts were irradiated in the same manner. The F_{max}, F_{min}, F_s, and ΔF values, and ratios F_t/F_0 of each bolt during irradiation are listed in Table 0-5. In the test, six bolts were irradiated for 15 s was carried out from specimens S1, S2 and S3. Continuous irradiation for 30, 45, and 60 s was carried out in two bolts respectively from specimens S4, S5 and S6. The obtained results were consistent, and the trend of the time-dependent curves was the same, proving that the test had good repeatability.

For frictional-bolted components, an excessive loss of axial force can cause joint failure. Therefore, this study aimed to maintain the loss of axial force within 20 kN, no more than 10% to F_0, to ensure that each bolt maintained normal operating conditions after the laser treatment. The axial force deviation is typically approximately 30% for bolt tightening with a calibrated torque wrench[140]. Therefore, it is reasonable and biased toward engineering safety to control the bolt axial force loss at 10%. The experimental results in Table 0-5 show that when the continuous irradiation duration exceeded 30 s, the decrease in F_{min} reached approximately 30 kN, but this state only lasted for tens of seconds; thus, it can be considered within the allowable range. However, when the irradiation time exceeded 60 s, the axial force loss of the bolt was over 10% of F_0, which cannot guarantee the normal use of the bolt. However, in some scenarios, laser irradiation for more than 60 s is required, such as for cleaning severe localized corrosion or removing thick coatings. Therefore, a method of multiple short-time irradiations is proposed to solve the excessive axial force loss caused by continuous long-term irradiation.

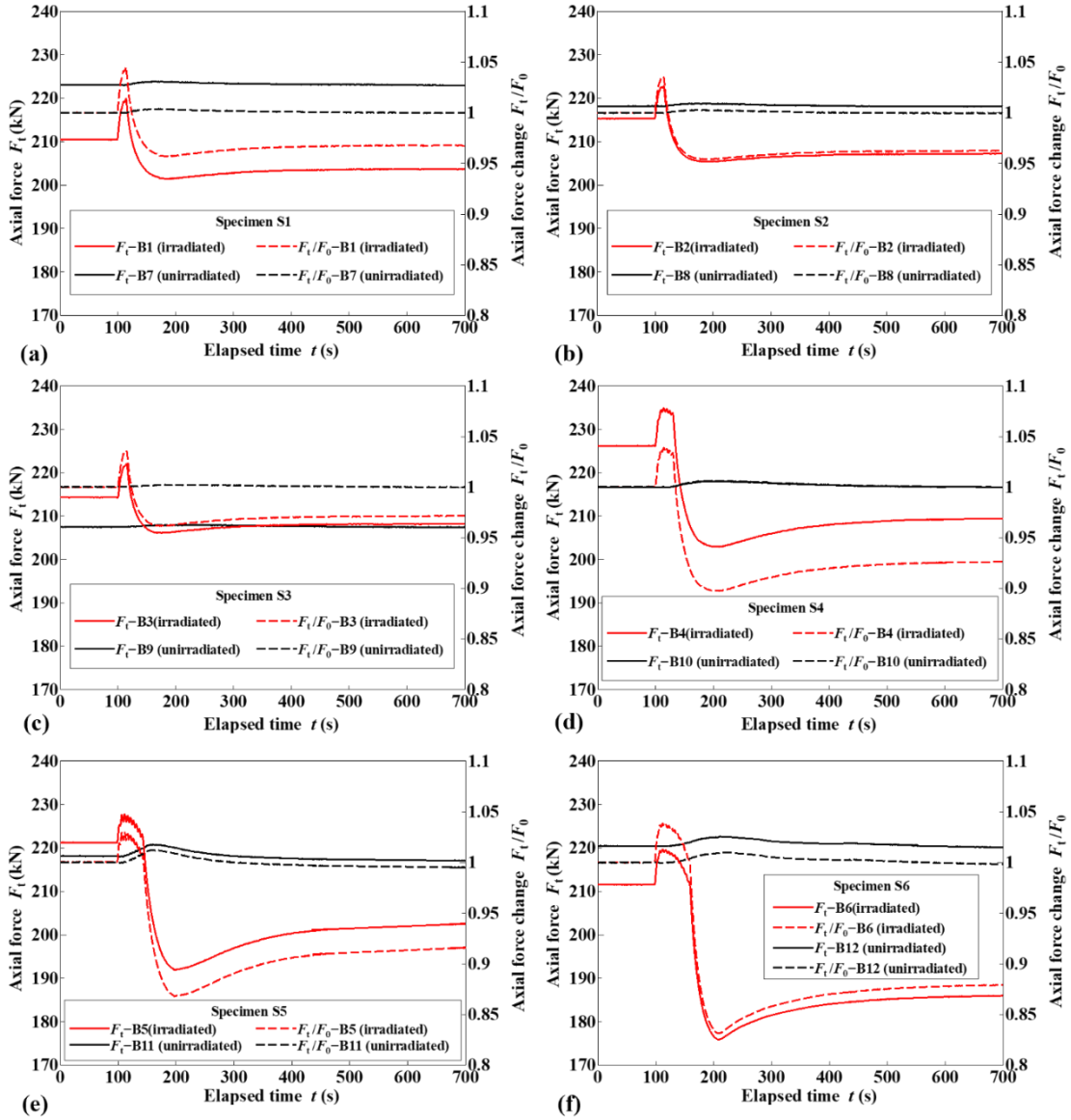

Figure 0-5 Time-dependent change in bolt axial force during laser processing of (a)15 s for specimen S1, (b) 15 s for specimen S2, (c) 15 s for specimen S3, (d) 30 s for specimen S4, (e) 45 s for specimen S5, and (f) 1 min for specimen S6

1.26.2 Axial force loss related to multiple rounds irradiation of laser

Bolt B1 was irradiated four times with laser irradiation for 15 s, and each irradiation was performed after the bolt was cooled for 30 min. Figure 0-6 shows the splicing of the axial force change–time curve for 10 min before and after each round of irradiation. Although the axial force of the bolt decreased, F_{max} still reached approximately 1.04 times the value of F_0 in the subsequent

irradiation. With an increase in irradiation time, the F_s of the bolts decreased, and F_{min} also gradually decreased with the addition of irradiation rounds. The decreasing range gradually reduced, particularly in the third and fourth rounds of irradiation, and F_{min} and F_s remained almost unchanged. As shown in Table 0-6 and Figure 0-6, in the first 15 s of laser irradiation, the axial force of the bolt decreased by 9 kN, which was 3.12% of F_0. However, in the second and third 15 s of irradiation, the axial force decreased by only approximately 3 kN, which was 1.26 and 1.43% of F_0, respectively. In the fourth 15 s of irradiation, the axial force did not change much, and the axial force decreased within 1 kN; the decline was only 0.54%. After four 15-s laser irradiations, the total axial force loss was 6.35% of F_0, and the axial force loss could be controlled within 15 kN, which was far less than the 60-s continuous irradiation. In addition, during irradiation, F_{min} was maintained within 20 kN, which is less than 10% of F_0. It can be considered that the bolts were guaranteed to be in safe operating conditions during the entire process of laser surface treatment.

Table 0-6 Changes in axial force after multiple rounds of irradiation

Irradiation duration (s)		F_0 (kN)	F_{max} (kN)	F_{max}/F_0	ΔF_{max} (kN)	F_{min} (kN)	F_{min}/F_0	ΔF_{min} (kN)	F_s (kN)	F_s/F_0	ΔF_s (kN)
15	15	210	220	1.04	10	201	0.96	-9	204	0.97	-6
15×2	30		219	1.04	9	198	0.94	-12	201	0.96	-9
15×3	45		219	1.04	9	194	0.92	-16	198	0.94	-12
15×4	60		216	1.03	6	193	0.92	-17	197	0.94	-13

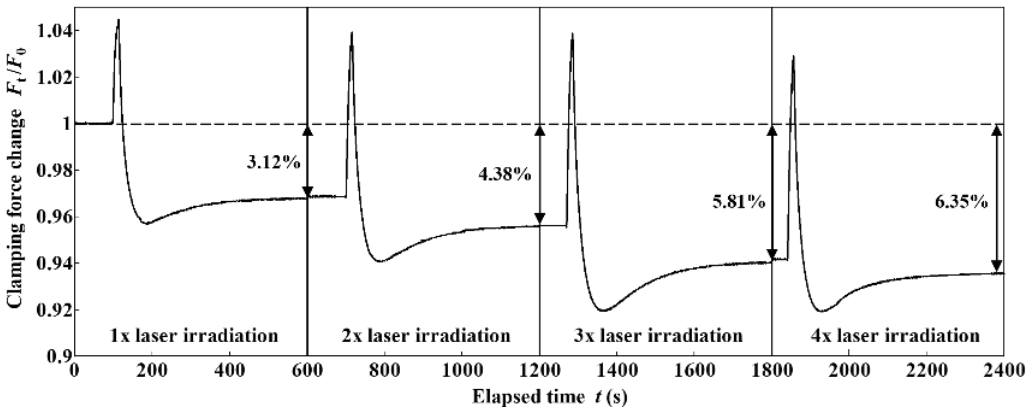

Figure 0-6 Time-dependent change in the axial force during four rounds of 15 s irradiation

During the first irradiation, the axial force of the bolts decreased the most significantly, and the axial force loss for each subsequent irradiation decreased gradually. Therefore, two rounds of irradiation are proposed to reduce the maintenance period. Specimens S1, S2, and S3 were subjected to laser irradiation for 15, 30, and 45 s after cooling. As shown in Figure 0-7 and Table 0-7, axial force change and loss were smaller after the second round of irradiation compared with continuous irradiation of the same total irradiation duration. For two rounds of irradiation, the axial force loss after a total of 60 s of irradiation can be controlled within 20 kN. It can be found in Figure 0-7, in the second round of irradiation, the axial forces of bolts B3 and B9 decreased less than those of bolts B2 and B8, although the total irradiation duration was shorter. The reason for this phenomenon may be that during the first round of irradiation, the molten pool formed on the irradiated surface was poured into the gap between the thread and nut, so that the nut was locked to the screw thread, thus limiting the slip of the nut. In particular, bolt B9 exhibited almost no loss of axial force after the second round of irradiation. The locking of the nut caused by the molten pool is beneficial in preventing loosening of the bolt, and the CWL-treated bolt is less prone to loosening.

1.26.3 Evaluation of the axial force loss ratio as a result of the laser irradiation

For a full cleaning of high-strength bolts, the number of laser irradiation rounds required differs depending on the degree of corrosion and type of coating used for maintenance of the nut. Therefore, in this study, the total time of laser irradiation corresponded to different processing conditions, and the relationship with the axial force loss rate was analyzed. Figure 0-8 shows the axial force change–total irradiation time curves of different irradiation sequences, which confirms that the bolt axial force was affected by the total irradiation time and process: the longer the total irradiation time, the more the axial force was lost. Multiple rounds of processes can reduce the axial force loss.

Table 0-7 Changes in axial force after two rounds of irradiation

Bolt	Irradiation duration (s)	F_0 (kN)	F_{max} (kN)	F_{max}/F_0	ΔF_{max} (kN)	F_{min} (kN)	F_{min}/F_0	ΔF_{min} (kN)	F_s (kN)	F_s/F_0	ΔF_s (kN)
B1	15+15 30	210	219	1.04	9	198	0.94	-12	201	0.96	-9
B7		223	224	1.01	1	209	0.94	-14	212	0.95	-11
B2	15+30 45	215	223	1.04	8	185	0.86	-30	194	0.90	-21
B8		218	227	1.04	9	195	0.89	-23	202	0.93	-16
B3	15+45 60	214	223	1.04	9	187	0.87	-27	195	0.91	-19
B9		216	223	1.03	7	195	0.90	-21	208	0.96	-8

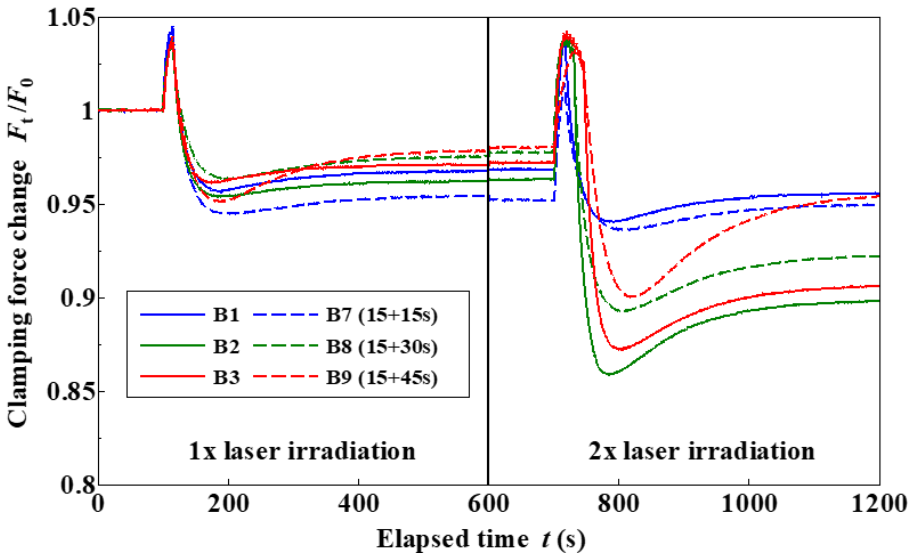

Figure 0-7 Time dependence of axial force during two rounds of irradiation

Figure 0-8(a) shows the relationship between continuous irradiation and the change in axial force. During the laser irradiation, the bolt axial force increased rapidly and reached the maximum value F_{max}. F_{max} was not affected by irradiation duration, and the increase was approximately 4%. This value did not change even under other irradiation conditions. The total irradiation duration affected the axial force's minimum F_{min} and the stable value F_s. The regression curve of F_s and F_{min} ratio change can be fitted to logarithmic formulas (1) and (2) and the coefficients of determination R^2 reached 0.936 and 0.952, respectively, with a good fit.

$$F_s = (-0.056\ln(t) + 1.120) \cdot F_0 \quad (1.)$$

$$F_{min} = (-0.092\ln(t) + 1.202) \cdot F_0 \quad (2.)$$

Figure 0-8(b) shows the changing relationship of the axial force during multiple rounds of irradiation, and the total irradiation duration was completed by increasing the same 15 s irradiation rounds. Similarly, the change in the axial force can also be described by logarithmic formulas (3) and (4), with R^2 values of 0.980 and 0.948, respectively.

$$F_s = (-0.024\ln(t) + 1.034) \cdot F_0 \quad (3.)$$

$$F_{min} = (-0.029\ln(t) + 1.037) \cdot F_0 \quad (4.)$$

Because the loss of axial force is most noticeable in the first round of irradiation, and multiple rounds of irradiation can reduce the loss of axial force, a two-round irradiation method of short-time irradiation followed by long-time irradiation was attempted. Figure 0-8(c) shows the changing relationship of the axial force during the two rounds of irradiation. Logarithmic equations (5) and (6) can still be used to describe the changing relationship of the axial force, with R^2 of 0.820 and 0.858. As mentioned in section 3.2, locking of the nut and thread during multiple rounds of irradiation is a possible cause for the deviation.

$$F_s = (-0.045\ln(t) + 1.093) \cdot F_0 \quad (5.)$$

$$F_{min} = (-0.049\ln(t) + 1.089) \cdot F_0 \quad (6.)$$

Generally, an increase in the total laser irradiation time directly affects the lower limit of the bolt axial force variation range F_{min} and the remaining axial force F_s. The excessive reduction in the axial force can be reduced using multiple rounds of irradiation. The logarithmic axial force variation formula has a very good fit and can be used to plan the laser cleaning process of the bolt surface.

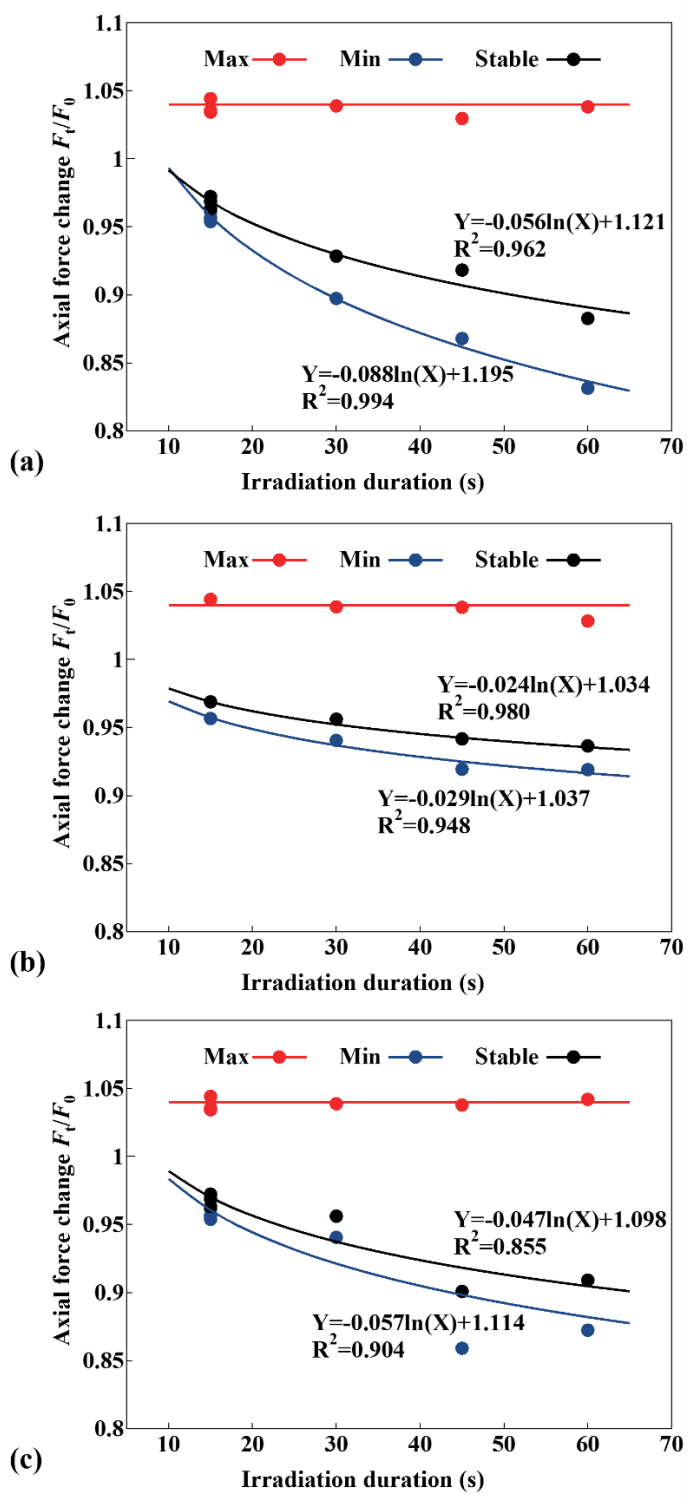

Figure 0-8 Relationship between the axial force and irradiation duration of (a) continuous irradiation, (b) four rounds of 15 s irradiation, and (c) two-round irradiation with 15 s irradiation followed by additional irradiation for 15, 30, and 45 s

1.26.4 Evaluation of the temperature change during laser irradiation

The change in the axial force of the bolt during laser irradiation is affected by the temperature. The cleaning mechanism of CWL relies on a high-energy-density laser spot that continuously burns and evaporates the coating and rust layer, and can leave obvious burning traces on the target surface, as shown in Figure 0-9 [44]. Although the rapid sweep of the laser spot does not cause excessive thermal effects on the target surface, continuous irradiation can still cause the bolt temperature to rise to several hundred degrees Celsius within a short time. High temperatures, particularly at the thread, lead to bolt failure. Therefore, an FE model was used to analyze the bolt temperature field. A thermocouple was used to verify the accuracy of the model, and was embedded 20 mm closer to the bolt head to avoid high-temperature damage. A three-dimensional solid model was established to analyze the temperature change during the bolt laser treatment process. As shown in Figure 0-10(a), after 15, 30, 45, and 60 s of laser irradiation, the temperature data of the embedded thermocouple were compared with the simulation results, indicating a very good match.

Figure 0-10(b) shows the distribution of bolt temperature under different laser irradiation duration. It focuses on the temperature distribution in the nut tightening area, including both column and thread parts. It can be seen that at the location where the strain gauge was buried, the temperature did not exceed the heatproof temperature of 200℃ during the test; therefore, the strain data obtained in the experiment are real and reliable. In the first 15 s of laser irradiation, the temperature of the thread area quickly reached 100-150℃. In this condition, the material properties of the bolt have not been affected by temperature. A 15 s irradiation duration as first or multiple cleaning methods will leave the bolt undamaged. When the continuous irradiation reaches 30 s, the highest temperature at the thread will reach 300℃. When the temperature of the steel material exceeds this value, it is generally believed that the material properties will decline. When the continuous irradiation reaches 45 s, 1/3 of the bolt area away from the washer will reach a high temperature of more than 300℃, and the first few meshing threads on the nut-loaded surface will have the greatest contact pressure in the safe range. Therefore, continuous irradiation of 3 kW CWL cleaning for more than 45 s is not recommended in order to avoid thread damage and even peel off due to high temperature.

The high-temperature effects caused by laser cleaning are local and transient, which is very different from the effects of fire on structures. The temperature field generated by CWL on the target surface has an obvious temperature gradient phenomenon, Zhuang's study reveals that the laser irradiated surface temperature reaches above 2000℃, but at tens of micrometers the temperature quickly decays to hundreds of degrees Celsius [71]. This is because of the high moving speed of the laser spot and short treatment duration of laser cleaning. As a result, only the irradiated surface was affected by high temperature; whereas, the studs and clamped steel plates were almost unaffected. For high-strength bolts commonly used in bridges, the 26-mm laser ring covers the target surface exactly; thus, the temperature effect on adjacent bolts can be avoided. As the CWL treatment was conducted by rotating around the bolt, the temperature distribution on the surface perpendicular to the bolt column was uniform and the bolt axial force loss due to eccentric deformation of the nut did not occur.

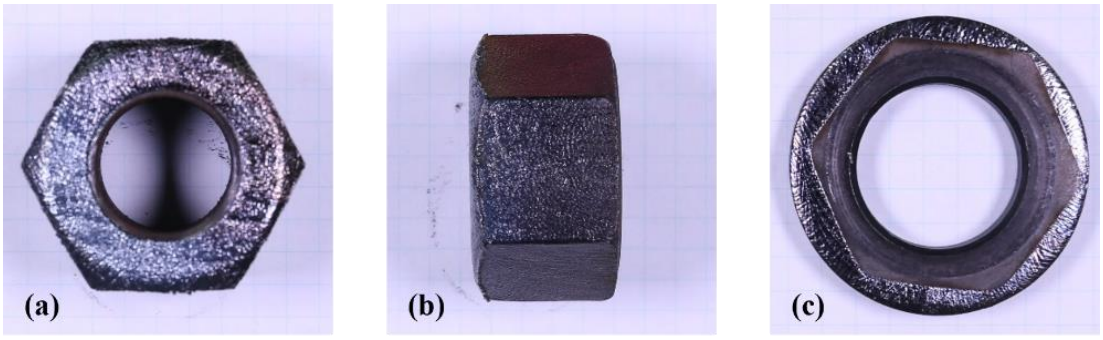

Figure 0-9 Surface after laser irradiation of (a, b) top and side surface of nut and (c)top surface of washer

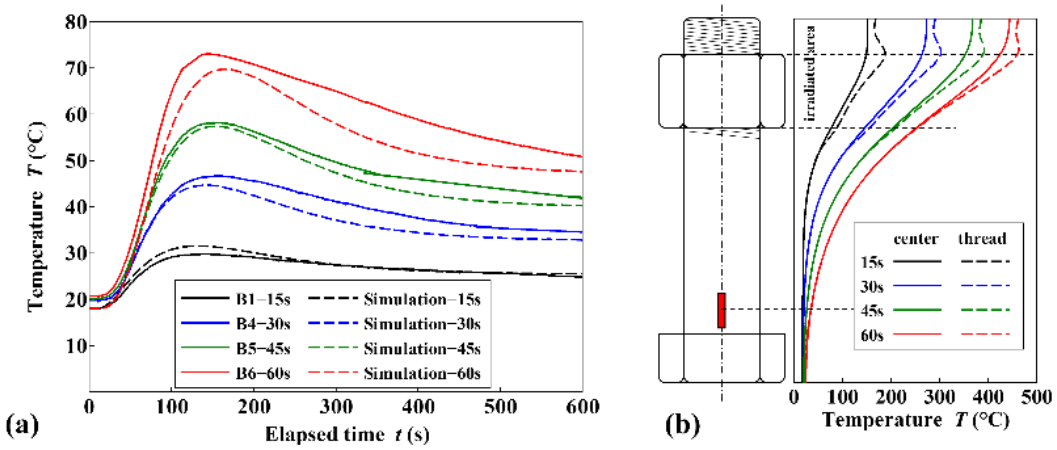

Figure 0-10 Temperature distribution during laser irradiation at (a) the position of the thermocouple and (b) center axial and column surface of the bolt

1.26.5 Mechanism of the axial force change during laser irradiation

During the laser irradiation, the temperature of the nut and washer increased steeply with rapid expansion. The axial force of the bolt reached F_{max} approximately 15 s after the beginning of irradiation, and the bolts were clamped until irradiation was completed. Because of the size of the nut and washer, the expansion range was limited so that F_{max} did not exceed 5% of F_0 regardless of the irradiation conditions. The first few meshing threads on the nut-loaded surface were the areas with the highest contact pressure[157]. With periodic circular irradiation, the washers and nuts repeatedly expand and contract locally, accompanied by vibration and repeated friction of the meshing part. This causes the meshing threads to be subjected to greater contract force circulation, as shown in Figure 0-11 , as the bolt axial force fluctuates during irradiation. Friction damage and local plastic deformation occurred in the threaded part during irradiation. The vibration and high temperature caused by the laser reduce the stiffness of the bolt joints, making it possible for the bolt to lose its axial force[148]. However, it is worth noting that the nut and washer were in a clamped and constrained state, and the vibration effect was significantly limited. In addition, it can be seen from Figure 0-11 that the amplitude and frequency of vibration are small, that is far less than the vibration response of the vehicle load to the bridge. Therefore, the influence of such a short vibration time on axial force loss can be neglected[158]. After laser irradiation, the temperature inside the bolt

was transferred in the direction of the bolt head. Because the laser ring was set to cover only the size of the bolt and washer, and because the clamped steel plate is larger, there will be a significant thermal difference in the local area between the bolt and the clamped steel plate. The expansion and elongation of the bolt causes relaxation of the bolt joint and natural slip of the nut, which will last approximately one minute. The axial force of the bolt was restored by the gradual cooling of the bolt and steel plate. The main causes of axial force loss are the local plastic deformation of the thread during clamping and the slip of the nut during relaxation.

The temperature field distribution of the bolt is the same when the bolts are irradiated for the same duration in different rounds; therefore, the natural slip of the nut during relaxation is no longer significant. Friction damage and plastic deformation between threads were the main causes of axial force loss during multiple rounds of laser irradiation. With an increase in the number of irradiation rounds, the friction damage and plastic deformation overlay, leading to an increase in the contact friction coefficient and a decrease in the loosening rate[159,160]. This explains the gradual decrease in the axial force loss.

After the specimens were cooled, all the bolts were removed using an electric wrench. It was found that the molten pool formed by surface remelting during laser irradiation locked the nut and screw together; therefore, it was very difficult to reverse screw the nut with the same torque as when tightening. This also explains the phenomenon depicted in Figure 0-7 in which the axial force change of bolts B3 and B9 during the second round was smaller than that of bolts B2 and B3 with less irradiation duration. In particular, it can be seen from bolt B9 that there was almost no loss of axial force after the second round of irradiation compared with the first round of irradiation. If the lock between the nut and screw is not remelted during the second round of irradiation, the friction and plastic deformation at the thread and the natural slip of the nut are greatly limited. The locking effect of remelting after laser irradiation helps the cleaned bolt maintain the axial force, even in the case of long-term vibration of the structure. The remelted thread also ensures that the nut will not easily fall off because of axial force drop and vibration.

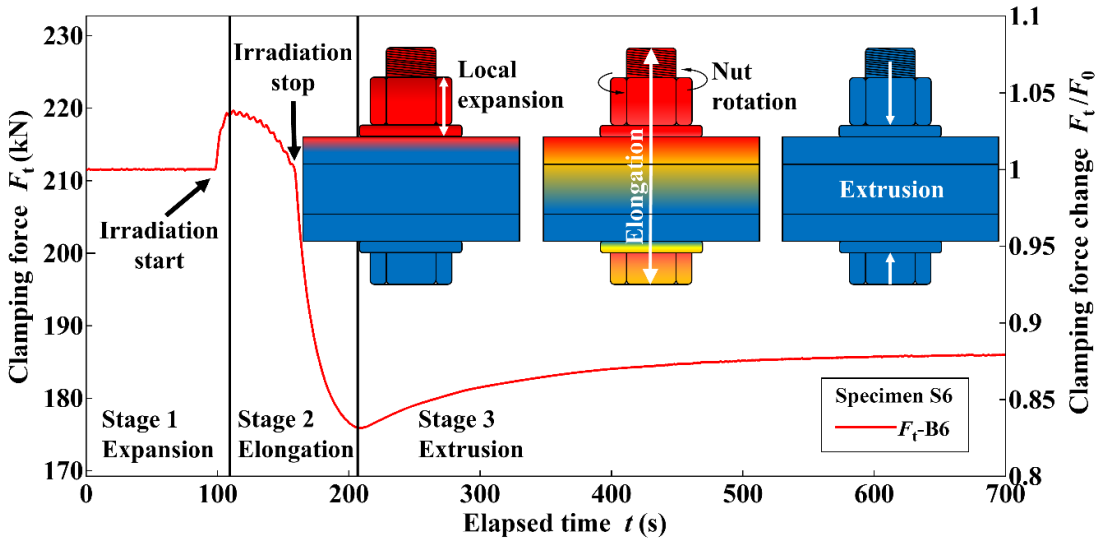

Figure 0-11 Schematic representation of the three stages of a bolt during laser cleaning

1.27 Summary

To clean and maintain the bolted joints in the steel bridges and improve the durability and safety of high-strength bolts, a 3 kW rotating CWL was used to perform laser surface treatment on the nuts of M22 high-strength bolts under different irradiation durations, and the relationship between the change in the bolt axial force and the distribution of the temperature field to the irradiation duration was investigated. The conclusions are as follows.

1. During laser irradiation, the axial force of the high-strength bolt increased by approximately 10 kN, independent of the total irradiation duration.

2. After the laser irradiation, the bolt axial force rapidly decreased to the minimum value F_{min} and recovered to a stable value F_s after cooling. The decreasing amplitudes of F_{min} and F_s were positively correlated with total irradiation time.

3. The 3 kW CWL is recommended to continuously clean the nut for no more than 45 s to avoid an axial force loss of more than 10% and bolt failure caused by high temperature.

4. When irradiation is required for a long time, multiple short-duration irradiations can effectively reduce axial force loss.

5. The logarithmic equations of F_{min} and F_s with the irradiation duration were defined, which

can be used as a reference for making maintenance plans for bolt joints.

The results of the rotary laser cleaning method for high-strength bolts proposed in this study are satisfactory and can provide a reference for the design of laser cleaning robots in the future. However, current research focuses on a single M22 bolt. It should be supplemented with additional sizes and types of bolts and rivets, such as double nut bolts, through further experimental analysis. In addition, it is found that CWL irradiation will cause local vibration of bolts, which may improve the cleaning effect and help detect the change in bolt axial force, which will be the focus of future studies.

CONCLUSIONS AND FUTURE WORKS

1.28 Summary and conclusions

Corrosion is one of the common diseases of steel structure. Influenced by the atmospheric environment such as temperature, humidity and airborne salt content, as well as the differences in steel and anti-corrosion types, steel structures usually form different levels of corrosion, mainly shown in different thickness of rust layer and corrosion depth. Corrosion cleaning is an important step in the maintenance of steel structures. In order to clean corrosion products efficiently, various surface treatment methods have been proposed and widely used. Although there are a large number of engineering experience and specifications of various countries on the surface treatment and painting standards to make provisions, in the actual surface cleaning engineering still appear incomplete rust removal and the occurrence of corrosion under the coating after painting. This phenomenon is particularly obvious in the case of severe corrosion. Fundamentally, it is caused by insufficient salt removal in the process of surface cleaning. Efficient corrosion cleaning method should be carried out according to different corrosion degrees, especially severely corroded condition. In this dissertation, a series of research on field investigation, artificial corrosion pit specimens test and hybrid surface cleaning method are carried out. The effect of pre-treatment tools on corrosion cleaning and the cleaning effect and applicable corrosion grade of post-treatment methods were discussed. Finally, the cleaning effect and scope were verified by engineering application.

In Chapter 2 investigated and summarized the corroded characteries of common steel and weathering steel, the shape of the corrosion pit is clarified, and the difficult of corrosion cleaning are pointed out. **In Chapter 3** verified and evaluated the cleaning effect of different hybrid surface treatment method with artificial corrosion pit specimens of three different corrosion degrees by turning time test. It is suggested to use CWL cleaning technology to clean severely corroded steel components. **In Chapter 4** verified and proposed a quantitative evaluation method and cleaning process for 3 kW CW cleaning based on image analysis. **In Chapter 5** verified the possibility of hand-held 3 kW CWL cleaning severely corroded steel components by engineering case. And also

presented a attempt of laser cleaning in wet and underwater condition. In Chapter 6 proposed CWL cleaning on high strength bolt components and analyzed the possible axial force loss during the cleaning process. In this dissertation, through a series of tests and engineering attempts to verify the help of pretreatment method, abrasive blasting technology in general corrosion cleaning superiority and CWL in severe corrosion cleaning and bolt cleaning applicability. And the following conclusions are obtained:

(a) The thickness of the rust layer has a linear relationship with the mean corrosion depth. Without rain washing effect, the depth-to-thickness ratio is about 0.2, with rain washing the ratio up to 0.3, and in the case of rainwater stagnant, the ratio is 0.5.

(b) Pitting corrosion, especially severely corrosion pits, will show as rust buds over the pit, and the size of the rust buds is the same as the size of the corrosion pits, which can be used for corrosion pit size analysis.

(c) With the increase of corrosion degree, the conical Angle of severe corrosion pit will approach 145°. The conical Angle of corrosion pit of weathering steel is larger than that of ordinary steel.

(d) Secondary corrosion appears at the bottom of the severely corroded pits. The conical angle of the secondary corrosion pit is much smaller than the corrosion pit itself, which will be the difficulty of surface treatment.

(e) Pre-treatment tools are only helpful for cleaning severely corroded steel components, among which the cup wire power tool has the best effect, but the diamond grinder power tool has the highest efficiency.

(f) Severely corroded steel members cannot be guaranteed salt removal effect even with clean level of Sa 2.5 or 3 after abrasive blasting, and there is a risk of corrosion under the coating.

(g) The 3 kW rotating CWL can clean approximately 200 μm of the rust layer per round of irradiation and the salt can be removed efficiently in the laser ablation process, suitable for cleaning severely corroded steel components.

(h) Photometric analysis can be used to obtain surface color information for the quantitative evaluation of cleanliness. The hue value can be used to distinguish the degree of corrosion of weathering steel, and the color difference before and after laser irradiation can be used to evaluate cleanliness.

(i) The hand-held 3 kW CWL can achieve the same level of rust removal as abrasive blasting verified by an engineering case and the cleaning efficiency of CWL can reach to1.2 m^2/h

(j) Wet and underwater laser cleaning method can help improve the cleaning effect. Laser ablated on the wet rust layer will achieve the best cleaning effect in engineering.

(k) 3 kW CWL is suitable for high-strength bolt cleaning engineering and can control the bolt axial force loss within 10 kN.

1.29 Recommendations for future work

(a) This dissertation summarizes and evaluates the application scope and effect of various surface treatment methods, discusses the engineering applicability of the hybrid method, introduces the advantages of 3 kW CWL in severe corrosion cleaning, and through the actual engineering verification, provides a reference for the corrosion of steel components and bolt components cleaning. However, the current research still has the possibility of progress, which needs to be further studied in the future:

(b) Develop CWL with higher power and energy density. In this dissertation, only the 3 kW CWL was used to remove rust and salt, and good results have been obtained. In order to improve the efficiency and effect of laser cleaning, increasing laser power will be the most direct and effective method.

(c) Improve the quantitative evaluation index of laser cleaning. In this dissertation, the quantitative evaluation index of 3 kW CWL cleaning corrosion weathering steel is discussed. In the process of developing new laser parameters, it is necessary to improve the evaluation of surface cleanliness at the same time for engineering application.

(d) Study the applicability of laser cleaning surface coating. The laser clean surface will form oxide layer and remelting layer, or will affect the adhesion and durability of the coating, laser clean surface is suitable for coating needs to be further verified.

(e) Supplement and improve the laser cleaning bolt experiment. This dissertation only discusses the possibility and applicability of 3 kW CWL for cleaning M22 high-strength bolts. Further investigation of bolts of different sizes and classes is needed to determine the effect of different laser conditions on different bolts.

REFERENCES

[1] D. Dwivedi, K. Lepková and T. Becker, *Carbon steel corrosion: a review of key surface properties and characterization methods*, RSC Adv 7 (2017), .

[2] P. Refait, A.-M. Grolleau, M. Jeannin, C. Rémazeilles and R. Sabot, *Corrosion of Carbon Steel in Marine Environments: Role of the Corrosion Product Layer*, Corrosion and Materials Degradation 1 (2020), pp. 198–218.

[3] Z. Wang, J. Liu, L. Wu, R. Han and Y. Sun, *Study of the corrosion behavior of weathering steels in atmospheric environments*, Corros Sci 67 (2013), pp. 1–10.

[4] J. Alcántara, D. de la Fuente, B. Chico, J. Simancas, I. Díaz and M. Morcillo, *Marine Atmospheric Corrosion of Carbon Steel: A Review*, Materials 10 (2017), pp. 406.

[5] *Modelling of pitting corrosion in marine and offshore steel structures - A technical review*. 2015.

[6] D. Wells, T. Hopwood, B. Meade and S. Palle, *Longer Service Life Bridge Coatings*, 2020.

[7] M. Hirohata, T. Nakahara and K. Jármai, *Life cycle cost analysis on anti-corrosion coatings for steel bridges in Japan*, Multidiszciplináris tudományok 11 (2021), pp. 92–103.

[8] P.P. Chung, J. Wang and Y. Durandet, *Deposition processes and properties of coatings on steel fasteners — A review*, Friction 7 (2019), pp. 389–416.

[9] M. Damiano, *Efficient Blast-Cleaning: Back to Basics*, Journal of Protective Coatings & Linings 37 (2020), pp. 6, 8.

[10] J. Brezinová, A. Guzanová and D. Draganovská, *Abrasive Blast Cleaning and Its Application*, Trans Tech Publications Ltd., Zurich, 2015.

[11] T.R. Board, of Sciences Engineering and Medicine, *Guidelines for Detection and Remediation of Soluble Salt Contamination Prior to Coating Steel Highway Structures*, The National Academies Press, Washington, DC, 2019.

[12] F. Bonnin-Pascual and A. Ortiz, *Corrosion Detection for Automated Visual Inspection*, in *Developments in Corrosion Protection*, InTech, 2014, .

[13] P. Dillmann, F. Mazaudier and S. Hœrlé, *Advances in understanding atmospheric corrosion of iron. I. Rust characterisation of ancient ferrous artefacts exposed to indoor atmospheric*

corrosion, Corros Sci 46 (2004), pp. 1401–1429.

[14] S. Kainuma, *Steel Surface Preparation by Abrasive Blast Treatment in Existing Steel Road Bridges*, Journal of the Surface Finishing Society of Japan 72 (2021), pp. 12–16.

[15] Anonymous, *On the time between blasting and priming*, Journal of Protective Coatings & Linings (2012), pp. 1–2.

[16] A. Kim, S. Kainuma and M. Yang, *Surface Characteristics and Corrosion Behavior of Carbon Steel Treated by Abrasive Blasting*, Metals (Basel) 11 (2021), .

[17] S.X. Zhu and T.A.C. Benjamin, Wet Abrasive Blast /Decontamination Chemical for Offshore Maintenance Coatings, in CORROSION 2021, Virtual, 2021.

[18] H. Teimourian, B. Mutabi and A. Soleimanzadeh, TECHNICAL AND ECONOMICAL COMPARISON OF WATERJET AND ABRASIVE BLAST METHODS TO BE USED IN DE-COATING AND CLEANING PROCESSES, 2013.

[19] C. Phipps, M. Birkan, W. Bohn, H.-A. Eckel, H. Horisawa, T. Lippert et al., *Review: Laser-Ablation Propulsion*, J Propuls Power 26 (2010), pp. 609–637.

[20] R. Zhiguo, W. Changzhong and C. Huaining, *Mechanism of laser derusting and surface properties of low carbon steel*, Opto-Electronic Engineering 44 (2017), pp. 1210–1216.

[21] *Laser Cleaning of Grey Cast Iron Automotive Brake Disc: Rust Removal and Improvement in Surface Integrity*. Oldcity Publications USA, 2018.

[22] K.L. Mittal and W.S. Lei, *Laser Technology: Applications in Adhesion and Related Areas*, 2017.

[23] G.X. Chen, *High-Power Fibre Laser Cleaning for Green Shipbuilding*, Journal of Laser Micro/Nanoengineering 7 (2012), pp. 249–253.

[24] J.-E. Kim, M.-S. Han and J.-D. Kim, *Removal characteristics of shop-primer paint by laser energy density in Q-switching fiber laser cleaning*, Modern Physics Letters B 34 (2020), pp. 2040042.

[25] G.X. Chen, T.J. Kwee, K.P. Tan, Y.S. Choo and M.H. Hong, *Laser cleaning of steel for paint removal*, Applied Physics A 101 (2010), pp. 249–253.

[26] B. Mao, A. Siddaiah, Y. Liao and P.L. Menezes, *Laser surface texturing and related techniques for enhancing tribological performance of engineering materials: A review*, J

Manuf Process 53 (2020), pp. 153–173.

[27] J.P. Padilla-Martinez, C. Berrospe-Rodriguez, G. Aguilar, J.C. Ramirez-San-Juan and R. Ramos-Garcia, *Optic cavitation with CW lasers: A review*, Physics of Fluids 26 (2014), pp. 122007.

[28] W.J. Suder and S. Williams, *Power factor model for selection of welding parameters in CW laser welding*, Opt Laser Technol 56 (2014), pp. 223–229.

[29] S. Zhuang, *Surface and mechanical properties of carbon steel affected by rotating continuous wave laser treatment*, PhD thesis, Kyushu University, 2021.

[30] S. Zhuang, S. Kainuma, M. Yang, M. Haraguchi and T. Asano, *Characterizing corrosion properties of carbon steel affected by high-power laser cleaning*, Constr Build Mater 274 (2021), pp. 122085.

[31] Y.S. Koh, J. Powell, A. Kaplan and J. Carlevi, Laser Cleaning of Corroded Steel Surfaces: A Comparison with Mechanical Cleaning Methods, in Lasers in the Conservation of Artworks, 2007, pp. 13–20.

[32] S. LEE, J. OH and B. SHIN, *Dissolution of Iron Oxide Rust Materials using Oxalic Acid.*, Shigen-to-Sozai 115 (1999), pp. 815–819.

[33] J.H. Brannon and J.F. Asmus, *Citric acid augmented flashlamp cleaning of corroded steel surfaces*, Applications of Surface Science 9 (1981), pp. 14–21.

[34] I.A. Chaves, R. Jeffrey and R.E. Melchers, *Rust Removal from Steel Coupons After Short-Term Marine Immersion*, Corrosion 71 (2015), pp. 811–818.

[35] S.A. Jafar, A.A. Aabid and J.I. Humadi, *Corrosion behavior of carbon steel in 1 M, 2 M, and 3 M HCl solutions*, Mater Today Proc 57 (2022), pp. 412–417.

[36] J. Ding, B. Tang, M. Li, X. Feng, F. Fu, L. Bin et al., *Difference in the characteristics of the rust layers on carbon steel and their corrosion behavior in an acidic medium: Limiting factors for cleaner pickling*, J Clean Prod 142 (2017), pp. 2166–2176.

[37] B. Tang, W. Su, J. Wang, F. Fu, G. Yu and J. Zhang, *Minimizing the creation of spent pickling liquors in a pickling process with high-concentration hydrochloric acid solutions: Mechanism and evaluation method*, J Environ Manage 98 (2012), pp. 147–154.

[38] A. Guerra-Contreras, A. Camacho-Ramírez, M. Olvera-Sosa, R. González-García and G.

Palestino, *Evaluation of a rapid and long-effective pickling method for iron rust removal on metallic surfaces using carboxylic acid-based polymers*, Journal of Polymer Research 28 (2021), pp. 104.

[39] *Optimization of Electrolytic Cleaning of Low Carbon Steels*, European Journal of Sustainable Development 5 (2015), .

[40] S. Iio, S. Kainuma, S. Ishihara, Q. Wang and D. Inoue, *Fundamental study on electrochemical preparation of heavily corroded unpainted weathering steel members*, Journal of Constructional Steel 28 (2020), pp. 1–9.

[41] R. Stango and P. Khullar, *Fundamentals of bristle blasting process for removing corrosive layer*, (2009), .

[42] R. Stango, R. Edu and P. Khullar, *Recently Developed Bristle Blasting Process for Corrosion Removal*, (2009), .

[43] S. Guo, R. Si, Q. Dai, Z. You, Y. Ma and J. Wang, *A critical review of corrosion development and rust removal techniques on the structural/environmental performance of corroded steel bridges*, J Clean Prod 233 (2019), pp. 126–146.

[44] S.S. Jamali and D.J. Mills, *Steel surface preparation prior to painting and its impact on protective performance of organic coating*, Prog Org Coat 77 (2014), pp. 2091–2099.

[45] D.J. Varacalle, D.P. Guillen, D.M. Deason, W. Rhodaberger and E. Sampson, *Effect of Grit-Blasting on Substrate Roughness and Coating Adhesion*, Journal of Thermal Spray Technology 15 (2006), pp. 348–355.

[46] J. Flanagan, P. Schütze, C. Dunne, B. Twomey and K.T. Stanton, *Use of a blast coating process to promote adhesion between aluminium surfaces for the automotive industry*, J Adhes 96 (2020), pp. 580–601.

[47] Y. Zhang, F. Lai, S. Qu, V. Ji, H. Liu and X. Li, *Effect of shot peening on residual stress distribution and tribological behaviors of 17Cr2Ni2MoVNb steel*, Surf Coat Technol 386 (2020), pp. 125497.

[48] I.-T. Kim and Y.-S. Jeong, *Fatigue strength improvement of welded joints by blast cleaning for subsequent painting*, International Journal of Steel Structures 13 (2013), pp. 11–20.

[49] A. ben Rhouma, C. Braham, M.E. Fitzpatrick, J. Leidion and H. Sidhom, *Effects of Surface*

Preparation on Pitting Resistance, Residual Stress, and Stress Corrosion Cracking in Austenitic Stainless Steels, J Mater Eng Perform 10 (2001), pp. 507–514.

[50] C. Reed, S. Olthof, K. Coronado and H. Cui, *THE EFFECT OF ABRASIVE BLAST MEDIA ON THE CORROSION OF STEEL*, Journal of Protective Coatings & Linings 37 (2020), pp. 24–30.

[51] D. Stephenson, T. Spear, M. Seymour and L. Cashell, *Airborne Exposure to Heavy Metals and Total Particulate During Abrasive Blasting Using Copper Slag Abrasive*, Appl Occup Environ Hyg 17 (2002), pp. 437–443.

[52] B. Karpuschewski, T. Emmer, K. Schmidt and M. Petzel, *Cryogenic wet-ice blasting—Process conditions and possibilities*, CIRP Annals 62 (2013), pp. 319–322.

[53] V. Máša and P. Kuba, *Efficient use of compressed air for dry ice blasting*, J Clean Prod 111 (2016), pp. 76–84.

[54] T. Marquardt and A.W. Momber, *The determination of fractal dimensions of blast-cleaned steel substrates by means of comparative cross-section image analysis and contact stylus instrument measurements*, J Adhes Sci Technol (2022), pp. 1–20.

[55] L.R. Millman and J.W. Giancaspro, *Environmental Evaluation of Abrasive Blasting with Sand, Water, and Dry Ice*, International Journal of Architecture, Engineering and Construction 1 (2012), pp. 174–182.

[56] G. Andronikos, D. Labrakis and D. Kaliampakos, *Evaluation of Surface Preparation Alternatives for Abrasive Blast Cleaning in Ship Repairing*, Journal of Ship Production 20 (2004), pp. 7–15.

[57] P.M. Randall, P.B. Kranz, M.L. Sonntag and J.E. Stadelmaier, *Evaluation of Needle Gun and Abrasive Blasting Technologies in Bridge Paint Removal Practices*, J Air Waste Manage Assoc 48 (1998), pp. 264–270.

[58] K. Kambham, S. Sangameswaran, S.R. Datar and B. Kura, *Copper slag: optimization of productivity and consumption for cleaner production in dry abrasive blasting*, J Clean Prod 15 (2007), pp. 465–473.

[59] K. Dickmann, C. Fotakis and J.F. Asmus, *Lasers in the Conservation of Artworks*, Vol. 100, Springer Berlin Heidelberg, Berlin, Heidelberg, 2003.

[60] G. Raciukaitis, M. Brikas, P. Gecys and M. Gedvilas, Accumulation effects in laser ablation of metals with high-repetition-rate lasers, 2008, pp. 70052L.

[61] A. Pereira, P. Delaporte, M. Sentis, A. Cros, W. Marine, A. Basillais et al., Laser treatment of a steel surface in ambient air, in Thin Solid Films, 453–454 (2004).

[62] V. Narayanan, R.K. Singh and D. Marla, Laser cleaning for rust removal on mild steel: An experimental study on surface characteristics, in MATEC Web of Conferences, 2018, pp. 01007.

[63] Z. Tian, Z. Lei, X. Chen, Y. Chen, L.C. Zhang, J. Bi et al., *Nanosecond pulsed fiber laser cleaning of natural marine micro-biofoulings from the surface of aluminum alloy*, J Clean Prod 244 (2020), .

[64] P. Gregorčič, M. Conradi, L. Hribar and M. Hočevar, *Long-Term Influence of Laser-Processing Parameters on (Super)hydrophobicity Development and Stability of Stainless-Steel Surfaces*, Materials 11 (2018), .

[65] T.S. McComb, I. Metsios, D. Dai, S.P. Chard and Y.K. Kwon, High pulse energy kW average power nanosecond lasers enable breakthrough in rapid coating removal, in High-Power Laser Materials Processing: Applications, Diagnostics, and Systems VII, 2018, pp. 24.

[66] T. Hoon Kim, A. Busnaina, J.-G. Park and D. Kim, *Nanoscale Particle Removal Using Wet Laser Shockwave Cleaning*, ECS Journal of Solid State Science and Technology 1 (2012), .

[67] L. Sobotová and M. Badida, *NEW POSSIBILITIES OF ENVIRONMENTALY FRIENDLY CLEANING METHOD BY LASER TECHNOLOGY*, Advances in Science and Technology Research Journal 10 (2016), pp. 224–229.

[68] M.K.A.A. Razab, A. Mohamed Noor, M. Suhaimi Jaafar, N.H. Abdullah, F.M. Suhaimi, M. Mohamed et al., *A review of incorporating Nd:YAG laser cleaning principal in automotive industry*, J Radiat Res Appl Sci 11 (2018), pp. 393–402.

[69] X. Jia, Y. Chen, G. Zhu, H. Wang, K. Aleksei and X. Zhu, *Experimental study on the optimum matching of CW-nanosecond combined pulse laser drilling*, Appl Opt 58 (2019), pp. 9105.

[70] M.-A. Lapointe, S. Chatigny, M. Piché, M. Cain-Skaff and J.-N. Maran, Thermal effects in

high-power CW fiber lasers, 2009, pp. 71951U.

[71] S. Zhuang, S. Kainuma, M. Yang, M. Haraguchi and T. Asano, *Investigation on the peak temperature and surface defects on the carbon steel treated by rotating CW laser*, Opt Laser Technol 135 (2021), pp. 106727.

[72] J. Provines, R. Rickard and S. Sharp, *Evaluation of a Continuous Laser Ablation Coating Removal Device for Steel Bridges*, Transportation Research Record: Journal of the Transportation Research Board 2676 (2022), pp. 767–778.

[73] K. Fujita, S. Okihara, H. Inagaki, K. Toyosawa, K. Takahara, T. Utsushikawa et al., *kW-class laser cleaning for steel structure maintenance and decontamination*, Nippon Genshiryoku Gakkai-Shi (Atomos) 62 (2020), pp. 259–262.

[74] J. Li, H. Liu, L. Shi and J. Lan, *Imaging Feature Analysis-Based Intelligent Laser Cleaning Using Metal Color Difference and Dynamic Weight Dispatch Corrosion Texture*, Photonics 7 (2020), pp. 130.

[75] J.-H. Ahn, J.M. Lee, J.-H. Cheung and I.-T. Kim, *Clamping force loss of high-strength bolts as a result of bolt head corrosion damage: Experimental research A*, Eng Fail Anal 59 (2016), pp. 509–525.

[76] J.-H. Ahn, J.M. You, J. Huh, I.-T. Kim and Y.-S. Jeong, *Residual clamping force of bolt connections caused by sectional damage of nuts*, J Constr Steel Res 136 (2017), pp. 204–214.

[77] M. Li, L. Yao, S. Zhang, D. Wang, Z. He and G. Sun, *Study on bolt head corrosion influence on the clamping force loss of high strength bolt*, Eng Fail Anal 129 (2021), pp. 105660.

[78] T. Masayuki, N. Yoshitomo, S. Tetsuhiro and T. Yoshiaki, *Residual Clamping Force for Corroded Tension-Control Bolts*, Journal of Structural Engineering 147 (2021), pp. 04020343.

[79] T. Masayuki, S. Tetsuhiro, N. Yoshitomo, A. Yasunori and Y. Tetsuya, *Dependence of Residual Axial Force on Thickness and Shape in Corroded High-Strength Bolts*, Journal of Structural Engineering 144 (2018), pp. 04018069.

[80] T. Nakahara, M. Hirohata, S. Kondo and T. Furuichi, *Paint Coating Removal by Heating for High-Strength Bolted Joints in Steel Bridge and Its Influence on Bolt Axial Force*,

Applied Mechanics 2 (2021), pp. 728–738.

[81] H. Gong and J. Liu, *Some factors affecting the loosening failure of bolted joints under vibration using finite element analysis*, Proc Inst Mech Eng C J Mech Eng Sci 232 (2018), pp. 3942–3953.

[82] H. Gong, J. Liu and X. Ding, *Study on the mechanism of preload decrease of bolted joints subjected to transversal vibration loading*, Proc Inst Mech Eng B J Eng Manuf 233 (2019), pp. 2320–2329.

[83] R. Miao, R. Shen, S. Zhang and S. Xue, *A Review of Bolt Tightening Force Measurement and Loosening Detection*, Sensors 20 (2020), pp. 3165.

[84] F. Huda, I. Kajiwara, N. Hosoya and S. Kawamura, *Bolt loosening analysis and diagnosis by non-contact laser excitation vibration tests*, Mech Syst Signal Process 40 (2013), pp. 589–604.

[85] K. Mikami, Y. Zhao, M. Morita, T. Sakamoto and H. Nishikawa, *Highly Sensitive Low-Energy Laser Sensing Based on Sweep Pulse Excitation for Bolt Loosening Diagnosis*, J Nondestr Eval 40 (2021), pp. 12.

[86] N. Hosoya, T. Katsumata, I. Kajiwara, T. Onuma and A. Kanda, *Measurements of S0 mode Lamb waves using a high-speed polarization camera to detect damage in transparent materials during non-contact excitation based on a laser-induced plasma shock wave*, Opt Lasers Eng 148 (2022), pp. 106770.

[87] J. Ouyang, P. Mativenga, N. Goffin, W. Liu, Z. Liu, N. Mirhosseini et al., *Energy consumption and performance optimisation of laser cleaning for coating removal*, CIRP J Manuf Sci Technol 37 (2022), pp. 245–257.

[88] X. Zhang, S. Yang, W. Zhang, H. Guo and X. He, *Influence of outer rust layers on corrosion of carbon steel and weathering steel during wet–dry cycles*, Corros Sci 82 (2014), pp. 165–172.

[89] M. Morcillo, I. Díaz, H. Cano, B. Chico and D. de la Fuente, *Atmospheric corrosion of weathering steels. Overview for engineers. Part II: Testing, inspection, maintenance*, Constr Build Mater 222 (2019), pp. 750–765.

[90] M. Morcillo, B. Chico, J. Alcántara, I. Díaz, R. Wolthuis and D. de la Fuente, *SEM/Micro-*

Raman Characterization of the Morphologies of Marine Atmospheric Corrosion Products Formed on Mild Steel, J Electrochem Soc 163 (2016), pp. C426–C439.

[91] Y. Fan, W. Liu, S. Li, T. Chowwanonthapunya, B. Wongpat, Y. Zhao et al., *Evolution of rust layers on carbon steel and weathering steel in high humidity and heat marine atmospheric corrosion*, J Mater Sci Technol 39 (2020), pp. 190–199.

[92] T. Kamimura, S. Hara, H. Miyuki, M. Yamashita and H. Uchida, *Composition and protective ability of rust layer formed on weathering steel exposed to various environments*, Corros Sci 48 (2006), pp. 2799–2812.

[93] J. Calero, J. Alcántara, B. Chico, I. Díaz, J. Simancas, D. de la Fuente et al., *Wet/dry accelerated laboratory test to simulate the formation of multilayered rust on carbon steel in marine atmospheres*, Corrosion Engineering, Science and Technology 52 (2017), pp. 178–187.

[94] T. Nakai, H. Matsushita, N. Yamamoto and H. Arai, *Effect of pitting corrosion on local strength of hold frames of bulk carriers (1st report)*, Marine Structures 17 (2004), pp. 403–432.

[95] Q. WANG, Fundamental Study on The Relationship Between Rust Characteristics and Corrosion Degree of Common Steel, in Proceedings of Constructuretinal Steel 2020, 2020, pp. 222–227.

[96] Y. Ma, Y. Li and F. Wang, *Corrosion of low carbon steel in atmospheric environments of different chloride content*, Corros Sci 51 (2009), pp. 997–1006.

[97] J. Liao, S. Matsui, M. Kushida, T. Shinohara and Y. Fujino, *Atmospheric Corrosion of Structural Steel at Semi-Closed Environment*, Zairyo-to-Kankyo 54 (2005), pp. 383–390.

[98] T. Shimada, Y. Oya, Y. Honkawa, Y. Kojima and I. Muto, *Effects of Deposited Salts on Corrosion Behavior for 1100 Aluminum Alloy during Constant Dew Point Test*, Zairyo-to-Kankyo 62 (2013), pp. 56–60.

[99] Z. Dan, I. Muto and N. Har, *Constant Dew Point Corrosion Tests for Metals*, in *Developments in Corrosion Protection*, InTech, 2014, .

[100] I. Muto and K. Sugimoto, *Modeling of Atmospheric Corrosion Environments and Its Application to Constant Dew-Point Corrosion Test*, Zairyo-to-Kankyo 47 (1998), pp. 519–

527.

[101] Z. Dan, S. Takigawa, I. Muto and N. Hara, *Applicability of constant dew point corrosion tests for evaluating atmospheric corrosion of aluminium alloys*, Corros Sci 53 (2011), pp. 2006–2014.

[102] R. Hashimoto, K. Ochibe, Y. Akita, H. Matsumoto and A. Imai, Capability verification of diamond tools for removing abnormal rust generated on weathering bridges, in 66th Material and Environmental Discussion Meeting, 2019, pp. 369–372.

[103] R. Hashimoto, K. Ochibe, D. Sano and A. Imai, Examination of application of diamond tools for substrate adjustment of bolts and narrow areas, in 73rd Annual Scientific Lecture Meeting of the Japan Society of Civil Engineers, 2018, pp. 59–60.

[104] M. Morcillo, B. Chico, I. Díaz, H. Cano and D. de la Fuente, *Atmospheric corrosion data of weathering steels. A review*, Corros Sci 77 (2013), pp. 6–24.

[105] Japan society of civil engineers (JSCE), *Issues and Countermeasures for Recovering Anticorrosion Performance of Steel Structures in Atmospheric Environment*, Maruzen, 2019.

[106] S. Kainuma and aran Kim, *Fundamental Investigation on Adhering Method for NaCl Particle by Ultrasonic Spray and Its Characteristics*, Rust Prevention & Control 64 (2020), pp. 201–2011.

[107] H. Chu, Z. Xie, Q. Liu, Y. Shao and Z. Mi, Surface-cleanliness inspection apparatus for optical component based on machine vision, in 2010 3rd International Congress on Image and Signal Processing, 2010, pp. 1694–1698.

[108] H. Chu, Z. Xie, Q. Liu, Y. Shao and Z. Mi, Surface-cleanliness inspection apparatus for optical component based on machine vision, in 2010 3rd International Congress on Image and Signal Processing, 2010, pp. 1694–1698.

[109] T. Shi, L. Zhou, C. Wang, G. Mi and P. Jiang, *Machine Vision-Based Real-Time Monitor System for Laser Cleaning Aluminum Alloy*, Chinese Journal of Lasers 46 (2019), pp. 0402007.

[110] K.Y. Choi and S.S. Kim, *Morphological analysis and classification of types of surface corrosion damage by digital image processing*, Corros Sci 47 (2005), pp. 1–15.

[111] R.M. Pidaparti, B. Hinderliter and D. Maskey, *Evaluation of Corrosion Growth on SS304*

Based on Textural and Color Features from Image Analysis, ISRN Corrosion 2013 (2013), pp. 1–7.

[112] F.N.S. Medeiros, G.L.B. Ramalho, M.P. Bento and L.C.L. Medeiros, *On the Evaluation of Texture and Color Features for Nondestructive Corrosion Detection*, EURASIP J Adv Signal Process 2010 (2010), pp. 817473.

[113] M.D. Fairchild and R.S. Berns, *Image color-appearance specification through extension of CIELAB*, Color Res Appl 18 (1993), pp. 178–190.

[114] B. Hill, Th. Roger and F.W. Vorhagen, *Comparative analysis of the quantization of color spaces on the basis of the CIELAB color-difference formula*, ACM Trans Graph 16 (1997), pp. 109–154.

[115] V.L. Zhbanova, Research into methods for determining colour differences in the cielab uniform colour space, in Light & Engineering 2020, 2020, pp. 53–59.

[116] D. Durmus, *CIELAB color space boundaries under theoretical spectra and 99 test color samples*, Color Res Appl 45 (2020), pp. 796–802.

[117] A. Jain, B.K. Pradhan, P. Mahapatra, S.S. Ray, S. Chakravarty and K. Pal, *Development of a low-cost food color monitoring system*, Color Res Appl 46 (2021), pp. 430–445.

[118] T.H. de Almeida, D.H. de Almeida, D. Gonçalves and F.A.R. Lahr, *Color variations in CIELAB coordinates for softwoods and hardwoods under the influence of artificial and natural weathering*, Journal of Building Engineering 35 (2021), pp. 101965.

[119] R. Mazlina, J. Muhd Herman, I. Mohd Ashraf Mohamad, Y. Intan Norsheira, N. Sharan Kumar, Z. Zuraini et al., *Quantitative Weathering Assessment of Rock Slope using CIELAB Color Space and Image Analysis Technique*, Environ Earth Sci (2021), .

[120] B. Hernández Salueña, C. Sáenz Gamasa, J.M. Diñeiro Rubial and C. Alberdi Odriozola, *CIELAB color paths during meat shelf life*, Meat Sci 157 (2019), pp. 107889.

[121] J. Cuadros, M. Sánchez-Marañón, C. Mavris, S. Fiore, J.L. Bishop and M. Melgosa, *Color analysis and detection of Fe minerals in multi-mineral mixtures from acid-alteration environments*, Appl Clay Sci 193 (2020), pp. 105677.

[122] D.N.M. Jedynakiewicz, *Digital colour matching in restorative dentistry*, Br Dent J 199 (2005), pp. 33–33.

[123] D. Shrivastava, K.C. Srivastava, K.K. Ganji, M.K. Alam, I. al Zoubi and M.G. Sghaireen, *Quantitative Assessment of Gingival Inflammation in Patients Undergoing Nonsurgical Periodontal Therapy Using Photometric CIELab Analysis*, Biomed Res Int 2021 (2021), pp. 1–8.

[124] A. Choubey, S.C. Vishwakarma, D.M. Vachhani, R. Singh, P. Misra, R.K. Jain et al., *Study and development of 22kW peak power fiber coupled short pulse Nd:YAG laser for cleaning applications*, Opt Lasers Eng 62 (2014), pp. 69–79.

[125] Z.J. Isherwood, Q. Huynh-Thu, M. Arnison, D. Monaghan, M. Toscani, S. Perry et al., *Surface properties and the perception of color*, J Vis 21 (2021), pp. 7.

[126] H. Zhu, F. Cao, D. Zuo, L. Zhu, D. Jin and K. Yao, *A new hydrothermal blackening technology for Fe3O4 coatings of carbon steel*, Appl Surf Sci 254 (2008), pp. 5905–5909.

[127] Y. Garbatov, S. Saad-Eldeen, C. Guedes Soares, J. Parunov and J. Kodvanj, *Tensile test analysis of corroded cleaned aged steel specimens*, Corrosion Engineering, Science and Technology 54 (2019), pp. 154–162.

[128] D. de la Fuente, J. Alcántara, B. Chico, I. Díaz, J.A. Jiménez and M. Morcillo, *Characterisation of rust surfaces formed on mild steel exposed to marine atmospheres using XRD and SEM/Micro-Raman techniques*, Corros Sci 110 (2016), pp. 253–264.

[129] J. Calero, J. Alcántara, B. Chico, I. Díaz, J. Simancas, D. de la Fuente et al., *Wet/dry accelerated laboratory test to simulate the formation of multilayered rust on carbon steel in marine atmospheres*, Corrosion Engineering, Science and Technology 52 (2017), pp. 178–187.

[130] J. Yin, H. Zhu, L. Ke, W. Lei, C. Dai and D. Zuo, *Simulation of temperature distribution in single metallic powder layer for laser micro-sintering*, Comput Mater Sci 53 (2012), pp. 333–339.

[131] Y. Huang, M.B. Khamesee and E. Toyserkani, *A comprehensive analytical model for laser powder-fed additive manufacturing*, Addit Manuf 12 (2016), pp. 90–99.

[132] W.A. Ayoola, W.J. Suder and S.W. Williams, *Parameters controlling weld bead profile in conduction laser welding*, J Mater Process Technol 249 (2017), pp. 522–530.

[133] J. Ouyang, P.T. Mativenga, Z. Liu and L. Li, *Energy consumption and process*

characteristics of picosecond laser de-coating of cutting tools, J Clean Prod 290 (2021), pp. 125815.

[134] A. Momber, *Colour-based assessment of atmospheric corrosion products, namely of flash rust, on steel*, Materials and Corrosion 63 (2012), pp. 333–342.

[135] A. Bendoumi, N. Makuch, R. Chegroune, M. Kulka, M. Keddam, P. Dziarski et al., *The effect of temperature distribution and cooling rate on microstructure and microhardness of laser re-melted and laser-borided carbon steels with various carbon concentrations*, Surf Coat Technol 387 (2020), pp. 125541.

[136] B. W. Meade, C. Goff, S. Palle and T. Hopwood II, *Chloride Contamination Remediation on Steel Bridges*, 2016.

[137] B. Fotovvati, S.F. Wayne, G. Lewis and E. Asadi, *A Review on Melt-Pool Characteristics in Laser Welding of Metals*, Advances in Materials Science and Engineering 2018 (2018), pp. 1–18.

[138] M.A. Shaheen, A.S.J. Foster, L.S. Cunningham and S. Afshan, *Behaviour of stainless and high strength steel bolt assemblies at elevated temperatures — A review*, Fire Saf J 113 (2020), pp. 102975.

[139] Y. Xing, W. Wang and H. Al-azzani, *Assessment of thermal properties of various types of high-strength steels at elevated temperatures*, Fire Saf J 122 (2021), pp. 103348.

[140] N. Hosoya, T. Niikura, S. Hashimura, I. Kajiwara and F. Giorgio-Serchi, *Axial force measurement of the bolt/nut assemblies based on the bending mode shape frequency of the protruding thread part using ultrasonic modal analysis*, Measurement 162 (2020), pp. 107914.

[141] R. Miao, R. Shen, S. Zhang and S. Xue, *A Review of Bolt Tightening Force Measurement and Loosening Detection*, Sensors 20 (2020), .

[142] S.M.Y. Nikravesh and M. Goudarzi, *A Review Paper on Looseness Detection Methods in Bolted Structures*, Latin American Journal of Solids and Structures 14 (2017), .

[143] K. Hashimoto, T. Tsukiji and K. Sugiura, *Experimental Study on Remaining Strength of High Strength Bolted Joint after Corrosion*, JSCE Proceedings A1 (Structural / Earthquake Engineering) 69 (2013), pp. 159–173.

[144] J. Huang, J. Liu, H. Gong and X. Deng, *A comprehensive review of loosening detection methods for threaded fasteners*, Mech Syst Signal Process 168 (2022), pp. 108652.

[145] Q. Wang, S. Kainuma, S. Zhuang, K. Shimizu and M. Haraguchi, *Laser cleaning on severely corroded steel members: Engineering attempt and cleanliness assessment*, J Clean Prod 376 (2022), pp. 134224.

[146] Q. Wang, S. Kainuma, P. Huo and R. Morikawa, *Quantitative evaluation of surface cleanliness of weathering steel treated by continuous wave laser*, Opt Laser Technol 158 (2023), pp. 108864.

[147] X.-P. Pang, Y. Hu, S.-L. Tang, Z. Xiang, G. Wu, T. Xu et al., *Physical properties of high-strength bolt materials at elevated temperatures*, Results Phys 13 (2019), .

[148] S. Abdus, X. Cheng, Y. Cheng, R. Hu and A. Muhammad, *Dynamic properties of single and multi-bolted composite joints at different bolt-loads and elevated temperature*, Australian Journal of Mechanical Engineering 19 (2021), pp. 406–413.

[149] Z. Guo, N. Lu, F. Zhu and R. Gao, *Effect of preloading in high-strength bolts on bolted-connections exposed to fire*, Fire Saf J 90 (2017), .

[150] S.A. Moeller, *Relaxation in bolted assemblies*, 2016.

[151] Y. Jiang, M. Zhang and C.-H. Lee, *A Study of Early Stage Self-Loosening of Bolted Joints*, Journal of Mechanical Design 125 (2003), pp. 518–526.

[152] K. MINAMI, K. TSUTSUI and H. TAMURA, *A COMPARATIVE STUDY ON CHARACTERISTIC OF BOLT PRETENSION LOSS OF RELAXATION IN HIGH STRENGTH BOLT FRICTION JOINTS*, Journal of Japan Society of Civil Engineers, Ser. A1 (Structural Engineering & Earthquake Engineering (SE/EE)) 78 (2022), pp. 180–189.

[153] Q. Wang, S. Kainuma, S. Zhuang and P. Huo, *Axial Force Behaviors of High-strength Bolt Treated by High Power CW Leaser*, International Journal of Structural and Civil Engineering Research (2022), pp. 75–78.

[154] M. Kvíčala and K. Frydrýšek, *Simulation of temperature gradients and equivalent stress of low- alloyed Cr-Mo based steel*, Mechanical Structures and Foundation Engineering 2010 (2012), .

[155] X.F. Wang, X.D. Lu, G.N. Chen, Sh.G. Hu and Y.P. Su, *Research on the temperature field*

in laser hardening, Opt Laser Technol 38 (2006), pp. 8–13.

[156] I.-T. Kim, J.M. Lee, J. Huh and J.-H. Ahn, *Tensile behaviors of friction bolt connection with bolt head corrosion damage: Experimental research B*, Eng Fail Anal 59 (2016), pp. 526–543.

[157] T. Fukuoka and M. Nomura, *Proposition of Helical Thread Modeling With Accurate Geometry and Finite Element Analysis*, J Press Vessel Technol 130 (2008), .

[158] Y. Li, Z. Liu, Y. Wang, L. Cai and M. Zheng, *Experimental study on behavior of time-related preload relaxation for bolted joints subjected to vibration in different directions*, Tribol Int 142 (2020), pp. 106005.

[159] J. Liu, H. Ouyang, Z. Feng, Z. Cai, X. Liu and M. Zhu, *Study on self-loosening of bolted joints excited by dynamic axial load*, Tribol Int 115 (2017), pp. 432–451.

[160] Z. Liu, M. Zheng, X. Yan, Y. Zhao, Q. Cheng and C. Yang, *Changing behavior of friction coefficient for high strength bolts during repeated tightening*, Tribol Int 151 (2020), pp. 106486.

ACKNOWLEDGEMENT

First of all, I would like to express my highest respect and sincere thanks to my supervisor, Prof. Shigenobu Kainuma for giving me such a good opportunity to join the world's highest research laboratory three years ago, enjoying the best research environment, the most cutting-edge research topics and the most sophisticated experimental machines. Over the past three years, Prof. Kainuma's patient instruction and valuable advice have encouraged me until I finish this dissertation. This is a difficult but happy journey, which will benefit me for my whole life.

I would also like to thank our partner company, TOYOKOH Inc., for all the help they have provided us, especially Mr. Peng Huo for his technical support to my research over the past 2 years. We would also like to thank West Nippon Expressway Highway Co., Ltd. for providing valuable specimens and technical support for my research.

Thanks to all the members of the Structural Design Laboratory, whose help, support and encouragement have been the motivation for me to study and live in Japan. Special thanks to Research assistant professor Muye Yang, Secretary Ms. Reiko Kato and Technical Official Staff Hiroyuki Shibata for their patient support. I will firmly remember the three years in the laboratory, the together experienced laughter and tears are priceless.

I would like to thank the China Scholarship Council for supporting my Ph.D study. The great Chinese government is the strongest backing of every Chinese student. I am proud to be a government-sponsored student.

Thanks to my parents for their support all the time. It has been three and a half years since I left home, and the vast sea cannot stop their relatives from missing me. I would like to dedicate this dissertation to my parents and thank them for their company and protection in my student life.

Thanks to my pet cat Nienie for sticking with me through the most challenging journey of my life so far. I will always love you, always.

Finally, thanks to myself, for not giving up all the time. Thank you!